

AD-A128 569 IMPROVED MATERIALS FOR COMPOSITE AND ADHESIVE JOINTS

1/2

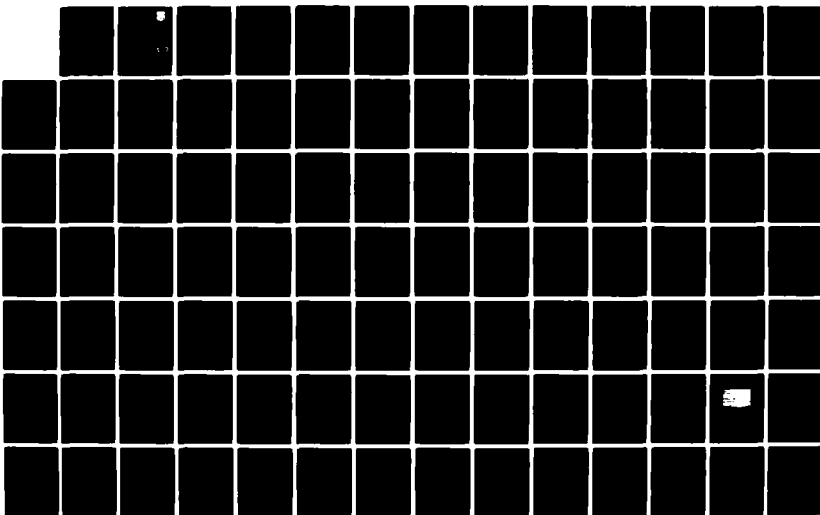
(U) DAYTON UNIV OH RESEARCH INST

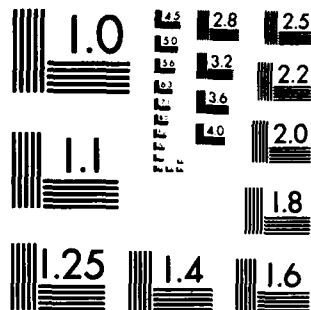
R KIM /W. /CLICK ET AL. JAN 83 UDR-TR-82-118

UNCLASSIFIED AFWAL-TR-82-4182 F33615-81-C-5056

F/G 11/4

NL





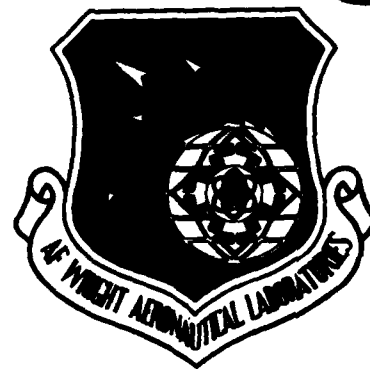
MICROCOPY RESOLUTION TEST CHART
NATIONAL BUREAU OF STANDARDS-1963-A

AFWAL-TR-82-4182

IMPROVED MATERIALS FOR COMPOSITE AND
ADHESIVE JOINTS

University of Dayton
Research Institute
Dayton, Ohio 45469

January 1983



Report for the period 1 Sept. 81 - 31 Aug. 82

Approved for public release; distribution unlimited

AD A 128569

DTIC
ELECTE
S MAY 25 1983 D
B

DTIC FILE COPY

MATERIALS LABORATORY
AIR FORCE WRIGHT AERONAUTICAL LABORATORIES
AIR FORCE SYSTEMS COMMAND
WRIGHT-PATTERSON AIR FORCE BASE, OHIO 45469


83 05 25 010

NOTICE


When Government drawings, specifications, or other data are used for any purpose other than in connection with a definitely related Government procurement operation, the United States Government thereby incurs no responsibility nor any obligation whatsoever; and the fact that the government may have formulated, furnished, or in any way supplied the said drawings, specifications, or other data, is not to be regarded by implication or otherwise as in any manner licensing the holder or any other person or corporation, or conveying any rights or permission to manufacture use, or sell any patented invention that may in any way be related thereto.

This report has been reviewed by the Office of Public Affairs (ASD/PA) and is releasable to the National Technical Information Service (NTIS). At NTIS, it will be available to the general public, including foreign nations.

This technical report has been reviewed and is approved for publication.



J. M. WHITNEY, Project Engineer
Mechanics & Surface Interactions Branch
Nonmetallic Materials Division



S. W. TSAI, Chief
Mechanics & Surface Interactions Branch
Nonmetallic Materials Division

FOR THE COMMANDER:



F. D. CHERRY, Chief
Nonmetallic Materials Division

"If your address has changed, or if you wish to be removed from our mailing list, or if the addressee is no longer employed by your organization, please notify AFWAL/MLBM, WPAFB, OH 45433 to help us maintain a current mailing list."

Copies of this report should not be returned unless return is required by security considerations, contractual obligations, or notice on a specific document.

UNCLASSIFIED

SECURITY CLASSIFICATION OF THIS PAGE (When Data Entered)

REPORT DOCUMENTATION PAGE		READ INSTRUCTIONS BEFORE COMPLETING FORM
1. REPORT NUMBER AFWAL-TR-82-4182	2. GOVT ACCESSION NO. A128 569	3. RECIPIENT'S CATALOG NUMBER
4. TITLE (and Subtitle) IMPROVED MATERIALS FOR COMPOSITE AND ADHESIVE JOINTS		5. TYPE OF REPORT & PERIOD COVERED Annual Report 1 Sept 81 - 31 Aug 82
		6. PERFORMING ORG. REPORT NUMBER UDR-TR-82-118
7. AUTHOR(s) R. Kim, W. Click, J. Hartness, M. Koenig, M. Rich, and S. Soni		8. CONTRACT OR GRANT NUMBER(s) F33615-81-C-5056
9. PERFORMING ORGANIZATION NAME AND ADDRESS University of Dayton Research Institute 300 College Park Avenue Dayton, Ohio 45469		10. PROGRAM ELEMENT, PROJECT, TASK AREA & WORK UNIT NUMBERS 24190323
11. CONTROLLING OFFICE NAME AND ADDRESS Materials Laboratory (AFWAL/MLBM) Air Force Wright Aeronautical Laboratories, AFSC Wright-Patterson Air Force Base, Ohio 45433		12. REPORT DATE January 1983
14. MONITORING AGENCY NAME & ADDRESS (if different from Controlling Office)		13. NUMBER OF PAGES 158
		15. SECURITY CLASS. (of this report) Unclassified
		15a. DECLASSIFICATION/DOWNGRADING SCHEDULE
16. DISTRIBUTION STATEMENT (of this Report) Approved for public release; distribution unlimited.		
17. DISTRIBUTION STATEMENT (of the abstract entered in Block 20, if different from Report)		
18. SUPPLEMENTARY NOTES		
19. KEY WORDS (Continue on reverse side if necessary and identify by block number) Composites Rheology Cure Thermal Analysis Epoxy Adhesives Fatigue Chemical Composition Matrix Interfacial Environmental Interlaminar Stresses Fiber Processing Electrode Fibrous Materials Thermoplastic Formulation Moisture (continued - reverse side)		
20. ABSTRACT (Continue on reverse side if necessary and identify by block number) This report presents a summary of the work performed by the University of Dayton Research Institute under Contract No. F33615-81-C-5056 during the period 1 Sept 1982 through 31 Aug 1982. Research was conducted in the following areas: Processing and Evaluation of Composites, Adhesive Bonded Joints, Interface/Interphase Characterization, and Mechanics of Composites and Adhesive Bonded Joints. The work was performed at the Air Force Wright Aeronautical Laboratories, Materials Laboratory, Wright-Patterson Air Force Base, Ohio, with Dr. J.M. Whitney as project engineer.		

DD FORM 1 JAN 73 1473

EDITION OF 1 NOV 68 IS OBSOLETE

UNCLASSIFIED

SECURITY CLASSIFICATION OF THIS PAGE (When Data Entered)

UNCLASSIFIED

SECURITY CLASSIFICATION OF THIS PAGE(When Data Entered)

19. Key Words: (Concluded)

Acetylene Terminated
Delamination
Life Prediction
Bonded Joint
Failure Analysis
Aging
Adherends
Shear Strength
Photoelastic
Surface Analysis
Photoelectron Spectroscopy
Graphite Fibers
Anodization
Surface Treatment
Adhesive Bonding
Aluminum Alloys
Surface Area

Transverse Crack
Residual Strength
Compact Tension
Composite Fracture
Neat Resin Fracture
Fracture Toughness
Fracture Mechanics
Thermal Effects
Aluminum Oxide
Tensile Strength
Interphase

UNCLASSIFIED

SECURITY CLASSIFICATION OF THIS PAGE(When Data Entered)

FOREWORD

This report was prepared by the University of Dayton Research Institute under Air Force Contract No. F33615-81-C-5056, Project No. 2419, Task No. 241903. The work was administered under the direction of the Nonmetallic Materials Division, Air Force Wright Aeronautical Laboratories, Materials Laboratory, Air Force Systems Command, with Dr. J. J. Whitney (AFWAL/MLBM) as Contract Monitor.

This report was submitted in September 1982 and covers work conducted from 1 Sept. 81 through 31 Aug. 82.

Personnel who contributed to this research are: W. E. Click, J. T. Hartness, R. Y. Kim, M. Koenig, M. J. Rich, and S. R. Soni.



Accession For	
NTIS GRA&I	<input checked="" type="checkbox"/>
DTIC TAB	<input type="checkbox"/>
Unannounced	<input type="checkbox"/>
Justification	
By	
Distribution/	
Availability Codes	
Dist	Avail and/or Special
A	

TABLE OF CONTENTS

SECTION		PAGE
I	PROCESSING AND EVALUATION OF COMPOSITES	1
	1. FAILURE RESISTANT COMPOSITE CONCEPTS	1
	a. Test Methodology	1
	1) Mode I (PEEL) Test	1
	2) Mechanical Testing	2
	3) Composites Fabricated	8
	b. Material Development	13
	1) Polyetheretherketone (PEEK)	13
	2) Polyethersulfone/graphite	23
	3) Resin Sensitivity	26
	4) Composite Fabrication Development	26
	5) Material Development	29
	a) V-378 A	29
	6) Polyimide Development	32
	7) Acetylene Terminated Quinoxaline (BADABA)	32
II	ADHESIVE BONDED JOINTS	39
	1. EXPERIMENTAL ADHESIVES	39
	a. BADABA (an Acetylene Terminated Quinoxaline)	39
	b. BADABA with 1% Cure Initiator	40
	c. ATS (100% oligomer)-an Acetylene Terminated Sulfone from which all of the Monomer had been Removed.	40
	d. ATS (Gulf)	40
	e. Acetylene Terminated Sulfone	40
	f. ATQ, SBQ, BATQ, and BADABA	42
	g. 5208/T300	42
	h. Polyurethane Model Material	43
	i. 5208 Neat Castings	43
	j. PEEK (Polyetheretherketone)	44
	k. Ordered Polymer	44
	2. MISCELLANEOUS POLYMER FRACTURE	44
	a. Thermosets	45
	b. Thermoplastics	45
III	INTERFACE/INTERPHASE CHARACTERIZATION	46
	1. ALUMINUM OXIDE/EPOXY INTERPHASE	46
	a. Experimental	46
	b. Results and Discussion	47
	2. CARBON FIBER/EPOXY INTERPHASE	47
	a. Surface Free Energy of Carbon Fibers	51

TABLE OF CONTENTS (CONTINUED)

SECTION	PAGE
III	INTERFACE/INTERPHASE CHARACTERIZATION (CONCLUDED)
b.	XPS Studies of Carbon Fibers 51
1)	Water Treatment 55
2)	Epoxy-Coated Fibers 55
3)	PVA-Treated 58
4)	AU Fibers 58
5)	Data Analysis 58
c.	Single Filament Tensile Test 61
d.	Critical Length Studies 65
1)	Interphase Shear Strength Measurement 65
2)	Interphase Hygrothermal Response Evaluation 67
3)	Multifilament Coupon 67
IV	MECHANICS OF COMPOSITES AND ADHESIVE BONDED JOINTS 70
1.	GLOBAL LOCAL VARIATIONAL PRINCIPLE FOR ELASTIC RESPONSE OF COMPOSITE LAMINATES 70
a.	Introduction 70
b.	Variational Principle 72
c.	Development of Theory 75
d.	Problem Description 83
2.	EXPERIMENTAL DETERMINATION OF INTERLAMINAR NORMAL STRESS 84
3.	ONSET OF DELAMINATION 93
4.	FATIGUE STUDY 108
	REFERENCES 127
	APPENDIX A 130

LIST OF ILLUSTRATIONS

FIGURE		PAGE
1	Tensile Creep RT	22
2	Load-Displacement Plots for Half-Inch Indentation Specimens [0-90] PEEK/Cloth vs. Epoxy/Cloth	24
3	Tensile Strength as a Function of Length of AS-4 85% ST Fiber	62
4	Representative Plots Illustrating the Relationship Between Tensile Strength and Gauge Length for Type HM Fibers	63
5	Multifilament Coupon Showing the Close Proximity of Fractures in Adjacent Fibers	69
6	Laminate Half Thickness with One Local-Global Interface	73
7	Ply Coordinate Axes and Rotation Notation	76
7a	Laminate Half Thickness Divided into More than One Global Domain with Different Types of Interfaces. I - Local-Global Interface, II - Global-Local Interface, III - Global-Global Interface	81
8	Variation of σ_z at the Free-Edge Obtained from Analysis	86
9	Effect of Strain Gauge Size on the Measurement of ϵ_z	88
10	Transverse Strain vs. Axial Strain	88
11	Transverse Strain ϵ_z vs. Axial Strain ϵ_x for $[\pm 30_2/90_2]_s$ and $[\pm 30_4/90_4]_s$	89
12	Transverse Strain ϵ_z vs. Axial Strain ϵ_x for $[(\pm 30)_2/90]_s$ and $[(\pm 30)_6/90]_s$	89
13	Transverse Strain ϵ_y vs. Axial Strain ϵ_x	91
14	Interlaminar Normal Stress Distribution Along Y-Direction	94
15	Acoustic Emission vs. Applied Stress which Indicates the Onset of Delamination	96
16	Comparison of Prediction and Experiment for Onset of Delamination	98

LIST OF ILLUSTRATIONS (CONCLUDED)

FIGURE		PAGE
17	Comparison of Prediction and Experiment for Onset of Delamination	99
18	" "	100
19	" "	101
20	" "	102
21	" "	103
22	Photomicrographs and C-Scan Pictures Showing Crack and Delamination Under Static Loading for $(0/+45/90_3)_s$	104
23	Photomicrographs and C-Scan Pictures Showing Crack and Delamination Under Static Loading for $(0/+45/90_6)_s$	105
24	Photomicrographs Showing Transverse Crack and Delamination for the $(0/90_3/+45)_s$	107
25	S-N Curve for $[+45/0/90]_s$	113
26	S-N Curve for $[+45/90_2]_s$	115
27	" "	116
28	S-N Curve for $[0/+45/90/-45]_{2s}$	118
29	X-Ray Showing the Damage Incurred at One Million Cycles Under Tension-Tension Fatigue for $[0/45/90/-45]_{2s}$ Laminate	119
30	X-Ray Showing the Damage Incurred at One Million Cycles Under Tension-Tension Fatigue for $[0/45/0/-45]_s$ Laminate	120
31	X-Ray Showing the Damage Incurred at One Million Cycles Under Tension-Tension Fatigue for $[0/45/90/-45]_{2s}$ Laminate	122
32	Weibull Distribution of Fatigue Data	125
33	Temperature Rise as Function of Frequency	126

LIST OF TABLES

TABLE		PAGE
1	MODE I PEEL Test Data	3
2	Neat Resin Peek Chemical Resistance	14
3	Composite Mechanical Properties	16
4	Wet and Dry, Peek/T-300 Bidirectional Cloth, 3-PT-Flexure	17
5	Graphite/Epoxy Cloth Bidirectional [0/90°], HMF- 133-76 (8-Harness Satin) 3-PT Flex Strength, Dry	18
6	4-PT Shear	19
7	Peel/T-300 Cloth (H-Harness Satin) <u>+45</u> In Plane Shear	19
8	HMF-133-76 (Epoxy/T-300) Cloth (H-Harness Satin) <u>+45</u> In Plane Shear	19
9	MODE I PEEL Test for Delamination Resistance	20
10	Polyethersulfone/Graphite Composite 3 PT-Flexure	25
11	Composite #CB4-8-82, 8 Ply, <u>+45°</u>	27
12	Composite #CB4-2-82, 16 Ply, 0°	27
13	Composite #CB4-2-82, 16 Ply, 90° Flex	27
14	Composite #CB4-4-82, 24 Ply, 0°	28
15	Composite #CB4-5-82, 50 Ply, 0°	28
16	Composite Processing Information	30
17	Mechanical Properties, Panel #1 T300/V378 A, 16 Plies, 0° Configuration, 12" x 12" Panel, Composite Specific Gravity - 1.61, Five Specimens per Data Point	31
18	H795 Polybismaleimide/AS-4 Composite Data	33
19	BADABBA	34
20	Freeze-Drying of BADABBA	35
21	Preparation of Dogbones	35

LIST OF TABLES (CONTINUED)

TABLE		PAGE
22	Neat Resin Properties (R.T.)	36
23	Elevated Temperature Properties (Dry)	37
24	Elevated Temperature Properties (Wet)	37
25	Preparation of Composites in Press	37
26	Composite Properties	38
27	Tensile Test, BADABA/1% Initiator Cured 350°F 32 Hrs. in Air	41
28	K_{1C} Values for Acetylene Terminated Quinoxalines psi $\sqrt{\text{in}}$ (mPA $\sqrt{\text{m}}$)	42
29	Effect of Coatings on Al 99.99% Anodic Oxide Interfracture Distance	48
30	Effect of Coatings on 2024-T3 Anodic Oxide Interfracture Distance	48
31	Effect of Coatings on 6061-T6 Anodic Oxide Interfracture Distance	48
32	Hygrothermal Exposure Effects on Al 99.99% Anodic Oxide Interfracture Distance	49
33	Hygrothermal Exposure Effects on 2024 T4 Anodic Oxide Interfracture Distance	49
34	Hygrothermal Exposure Effects on 6061-T3 Anodic Oxide Interfracture Distance	50
35	Key to Fiber Code Abbreviations	52
36	Mean Contact Angle ($\pm \sigma$) of Carbon Fiber	53
37	Polar, Dispersive, and Total Surface Free Energy of Carbon Fiber Surfaces	54
38	Surface Compositions of Fiber Specimens Obtained Using XPS	56
39	Surface Composition of AS Fiber Specimens Obtained Using XPS	57
40	Surface Composition of Fiber Specimens Obtained Using XPS	59

LIST OF TABLES (CONCLUDED)

TABLE		PAGE
41	Surface Composition of AU Fiber Specimens Obtained Using XPS	60
42	Tensile Strength vs. Gauge Length for Carbon Fibers (Tensile Strength $\times 10^3$ psi $\pm \sigma$)	64
43	Fiber-Matrix Interphase Shear Strength of Single Filaments in Epon 828-mPDA Matrix	66
44	σ_z at Midplane of Laminate for Applied Strain of 0.1%	92
45	σ_z at Applied Axial Strain at Onset of Delamination	92
46	Summary of Static Test Result	110
47	Fatigue Data for Gr/Ep [$\pm 45/0/90$] _s	111
48	Fatigue Data for Gr/Ep [$\pm 45/90_2$]	114
49	Fatigue Data for Gr/Ep [0/ $\pm 45/90/-45$] _{2s}	117
50	Summary of Residual Strength Data for [0/45/90/-45] _{2s} at 1×10^6 Cycle	123
51	Summary of Fatigue Results	127

SECTION I
PROCESSING AND EVALUATION OF COMPOSITES

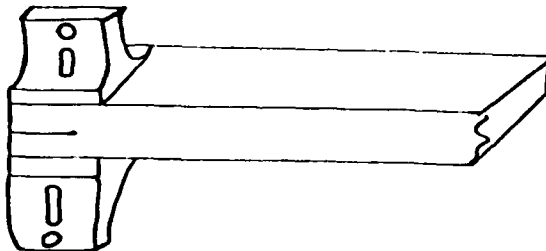
1. FAILURE RESISTANT COMPOSITE CONCEPTS

a. Test Methodology

1) MODE I (PEEL) Test

Work was initiated to develop a test that evaluates the interlaminar fracture of graphite composites. Composites have low interlaminar strengths in comparison to their strengths parallel to the fiber. Often, interlaminar failure initiates from regions of stress concentration such as holes or resin cracks and proceeds by delamination. An increase in the fracture energy of the matrix resin should improve the interlaminar toughness of the composite. In order to effectively accomplish this evaluation, a test was developed. This Mode I (PEEL) test is described below.

A graphite/epoxy composite of some minimum thickness is cut 1" x 9" with a starter crack at one end 1" x 1". The specimen is tabbed with a tee (see drawing).



Some modifications have been made to the initial Mode I test as far as the actual test is run, data reduction, and the equation used to calculate the critical strain energy release rate (G_{IC}). A description of the test is described in the Journal of Reinforced Plastics and Composites yet to be published, entitled, "A Double Cantilever Beam Test for Characterizing Mode I Delamination of Composite Materials" by Whitney, Browning, and Hoogsteden, Air Force Wright Aeronautical Laboratories (AFWAL).

A considerable number of materials have been tested. These include thermoplastics on graphite cloth such as polyphenylenesulfide (PPS) and polyetheretherketone (PEEK) as well as interlaying some rubber toughened epoxy adhesives (AF-163 u) in the center tested ply. Significant improvement was measured with these mentioned systems over the standard graphite/epoxy control. The data generated to date is shown in Table 1.

Additional information and data on angle ply composites are contained in a paper entitled "Determination of G_C in Angle Ply Composites Using a Double Cantilever Beam Test Method", by Nichalls, Gallagher, Whitney, and Browning (AFWAL), yet to be published.

The results of this work now allows us to use this Mode I delamination test as a standard method to evaluate composite interlaminar fracture toughness.

2) Mechanical Testing

Routine mechanical testing was accomplished on supplied composite and neat resin samples that were under development and evaluation. The tests performed on these materials included tensile, four-point strain gaged flexure, four-point shear, mode-one peel, three-point flexure, as well as micro-tensile tests. Specimens were instrumented and tested at ambient and elevated temperatures.

The design and machine work was started on a weldable strain-gage dual bridge extensometer for the testing of micro-tensile specimens at ambient and elevated temperatures.

In this period a special radius supported micro-tensile grip was designed and machined for the testing of compact tension specimens in order to obtain more consistent gage failures in various resin systems that are produced in this laboratory.

A cross-head travel limit alarm system was also built and installed on the TTLC 10,000 pound Instron test machine to prevent damage to the test fixtures and the test machine itself.

TABLE 1
MODE I PEEL TEST DATA

	G _{IC}			G _{IC AVE} (in.lbs/in ²)
	2	3	4	
Debond Length(in)				
*Control: #4	0.822	0.809	0.857	0.829
*OCF				
Glass Mat: #4	1.784	1.454	1.697	1.645
#5	1.238	1.308	0.909	1.152
*Glass Scrim: #4	1.004	1.662	1.599	1.422
Polysulfone/AS-1				
Panel II: #1	5.01	4.19	3.26	4.15
#2	3.51	3.82	3.41	3.58
#3	4.9	4.1	4.02	4.34

*All 3502 + AS1 Composites

TABLE 1
MODE I PEEL TEST DATA (CONTINUED)

	Spec #	G_{IC}					$G_{IC AVE}$ (in. lbs/in ²)
		2	2.5	3	3.5	4	
Control AS-1/3502	#4	0.822	0.877	0.809	0.872	0.857	0.847
	#1 (a)	0.344	0.71	0.618	0.988	0.355	0.603
	#2 (a)	1.214	1.091	0.793	1.087	0.808	0.999
	#1 (b)	.584	.645	.631	.293	.546	.540
	#2 (b)	1.078	.694	.631	-	-	.801
	#3 (b)	.639	.650	.756	.792	.881	.744
AS-1/3502 Mini Panels	#1 (c)	0.909	0.727	0.870	-	-	0.835
	#2 (c)	0.849	1.081	0.899	0.878	0.767	0.895
	#3 (c)	0.709	0.788	0.753	0.779	0.738	0.753
AS-1/3502 OCF Glass Mat	#4	1.784	0.285	1.454	1.715	1.697	1.587
	#5	1.238	0.832	1.308	1.202	0.909	1.098
AS-1/3502 Glass Scrim	#2	1.004	1.466	1.662	1.628	1.599	1.472
AS-1/Polysulfone	#1	5.01	2.70	4.19	3.26	-	3.79
	#2	3.51	2.97	3.82	2.97	3.41	3.34
	#3	4.9	3.32	4.1	4.02	-	4.09
T300/V378-A	#1	.48	.418	.366	.545	.255	.413
	#2	-	.35	.5	.57	.55	.49
T300/PEEK bidir cloth	#1	8.65	13.99	6.3	11.28	12.61	10.57
	#2	9.05	13.74	7.38	9.82	13.26	12.13

TABLE 1
MODE I PEEL TEST DATA (CONTINUED)

	Spec #	G _{IC}			G _{IC AVE}		
		2	2.5	3	3.5	4	(in. lbs/in ²)
T300/PPS Bidir Cloth	#1	2.31	2.12	3.73	1.98	4.40	2.79
	#2	4.72	2.85	3.47	4.18	3.23	3.69
	#3	4.12	4.55	3.23	3.69	4.77	4.07
AS-1/3502 Mini Panel (Matched metal molds)	#1	1.685	2.051	1.461	1.548	-	1.686
	#2	1.073	1.735	0.796	1.195	1.518	1.263
	#3	1.173	1.278	0.675	0.422	0.691	0.848
AS-1/3502 AF-163 U Adhesive Inlay	#1	7.701	6.273	6.313	7.424	6.754	6.893
	#2	-	6.389	7.145	4.353	10.717	7.151
	#3	8.029	7.231	7.800	8.447	7.524	7.806
Control: 3502 & AS2 Post Cured 6 hrs @ 350°F	#1	0.7129	0.5326	0.6312	0.5884	0.6627	0.6256
	#2	0.5846	0.5618	0.5734	0.6234	0.6277	0.5942
	#3	0.6993	0.62004	0.7630	0.59926	0.7464	0.6856
AS1 + 707	#1	0.7855	0.7126	0.6571	0.8316	0.6799	0.7333
	#2	0.9303	0.8625	0.806	0.8146	0.858	0.8543
	#3	0.7503	0.7673	0.5685	0.6940	0.5596	0.6675

TABLE 1
MODE I PEEL TEST DATA (CONTINUED)

	Spec #	G_{IC}				$G_{IC_{AVE}}$	
		2	2.5	3	3.5	4	(in. lbs/in ²)
AS1 + 3502 Kevlar (Dry Paper) Inlay	#1	2.3085	2.6855	2.9098	2.442	1.2179	2.3127
	#2	2.5523	1.9908	2.522	1.9894	2.2887	2.2686
	#3	1.2566	1.9833	3.4497	2.3405	2.3582	2.2763
AS1 + 3502 Preimpregnated Kevlar Paper Inlay	#1	2.6383	2.829	2.7944	2.732	1.825	2.5637
	#2	2.2815	2.6538	2.3513	2.6637	2.3098	2.4520
	#3	2.5795	2.6163	2.7305	2.6787	2.392	2.5994
AS1 + 3502 Preimpregnated Polyester Paper Inlay	#1	2.76	1.7111	2.7675	2.6705	2.3873	2.4593
	#2	2.293	2.969	2.8665	2.3506	2.54	2.6038
	#3	2.1269	2.9012	2.1605	2.552	2.4993	2.4480
V-378A Roll #3 Nonlinear	#1	0.642	0.764	0.595	0.692	0.834	0.7063
	#2	0.3	0.474	0.5088	0.451	0.5095	0.4487
	#3	0.3315	0.3965	0.3597	0.3488	0.4024	0.3678
						$G_{IC_{AVE}} =$	0.5076
V-378A Roll #2 Run #2	#1	0.535	0.613	0.525	0.5815	-	0.5636
	#2	0.5	0.477	0.5035	0.57	0.666	0.5433
	#3	0.327	0.4825	0.4915	0.536	0.5025	0.4479
						$G_{IC_{AVE}} =$	0.5183

TABLE 1
MODE I PEEL TEST DATA (CONCLUDED)

	Spec #	G_{IC}				G_{ICAVE} (in.lbs/in ²)	
		2	2.5	3	3.5		
V-378A Roll #3 Nonlinear	#1	0.4115	0.5166	0.3281	0.401	0.5173	0.4349
	#2	0.3	0.474	0.5088	0.451	0.5095	0.4487
	#3	0.3315	0.3965	0.3597	0.3488	0.4024	0.3678
						$G_{ICAVE} =$	0.4171
V-378A Roll #2 Run #2	#1	0.535	0.613	0.525	0.5815	-	0.5636
	#2	0.5	0.477	0.5035	0.57	0.666	0.5433
	#3	0.327	0.4825	0.4915	0.436	0.5025	0.4479
						$G_{ICAVE} =$	0.5183
AS1 + 3502 Straight (s) & Chevron (c) Starter Crack*	S-1	-	-	-	0.765	0.736	0.7655
	S-2	0.6339	0.8315	0.7015	0.7945	0.76	0.7443
							0.7549
AS1 + 3502 Straight (s) & Chevron (c) Starter Crack	C-1	1.2055	0.5438	0.7869	0.691	0.7594	0.7973
	C-2	0.6928	0.7719	0.6668	0.7741	0.945	0.7701
	C-3	1.0525	1.1932	0.9495	1.1752	1.2171	1.1175
							0.895
AS + 1076E	#1	0.4615	0.584	0.5287	0.476	0.631	0.5362
	#2	0.556	0.444	0.564	0.5305	0.6062	0.5401
	#3	0.49	0.4225	0.4978	0.5223	0.5388	0.49428
							0.5236

*There was a loss of autoclave pressure during final hold.

Electronic repairs were made on the Instron Models 1123, 1115 and TTC test machines to correct electrical malfunctions in order to keep the various test programs in operation.

Special mode-one peel test loading fixtures were machined for the testing of various composite materials to study the effects of crack-growth. In order to do this work a Satec LVDT was modified to measure the deformation of the specimen while it was under load.

An initial computer test program format was started for the automatic data acquisition and reduction system that will be interfaced with Instron test machines.

3) Composites Fabricated

<u>Material</u>	<u>Lay-up Orientation</u>	<u>No. of Plies</u>	<u>Size</u>
T-300/5208	$[\pm 30_2/90_2]_s$	12 ply	10" x 10"
"	$[\pm 30_4/90_4]_s$	24 ply	"
"	$[\pm 30_4/90]_s$	18 ply	"
"	$[\pm 30_6/90]_s$	26 ply	"
AS1-3502	$[0^\circ]_{24T}$	24 ply	12" x 12"
T300/6K/E767	$[0^\circ]_{16T}$	16 ply	6" x 12"
AS1-3502 with mylar at midpoint (1" wide strip) mode #1 test	$[0^\circ]_{24T}$	24 ply	6" x 12"
" w/scrim cloth at midpoint	$[0]_{24T}$	"	"
" OCF glass "	$[0]_{24T}$	"	"
T300/5208	$[0]/\pm 15/90]_s$	8 ply	10" x 10"
"	$[0/\pm 30/90]_s$	8 ply	"
"	$[\pm 45/0/90]_s$	"	"
"	$[\pm 30_2/90]_s$	12 ply	"
"	$[\pm 30/90/\pm 30/90]_s$	"	"

<u>Material</u>	<u>Lay-up Orientation</u>	<u>No. of Plies</u>	<u>Size</u>
T300/5208	[$\pm 30/90/90/\pm 30$] _s	12	10" x 10"
"	[$\pm 30/90_3/\pm 30/90$] _s	16	"
"	[$\pm 30/90/\pm 30_3/90_3$] _s	24	"
"	[$\pm 30_3/90_4/\pm 30$] _s	24	"
"	[$\pm 30/90_4/\pm 30_3$] _s	30	"
"	[$\pm 30/\pm 60$] _s	8	"
"	[$\pm 30_2/\pm 60_2$] _s	16	"
T300/5208	[$0/\pm 45/0/\pm 45/0/\pm 45/90$] _s	20	"
"	[$0/\pm 45/0/\pm 45/0/\pm 45/90_3$] _s	24	"
"	[$0/\pm 45/0/\pm 45/90_2$] _s	16	"
T300/V-378-A	[0°] _{12T}	12	12" x 12"
HMF-133-76	[$0^\circ/90$] cloth	4	6" x 6"
Hy-E 1076 E uni- directional non- autoclave cure (voids & voids)		16	12" x 12"
HyE-1076-E		16	12" x 12"
T300/5208	[$\pm 30_2/90_2$] _s	16	6" x 6"
"	[$\pm 30_4/90_4$] _s	16	"
AS1-E707	[0°]		"
AS1-3502 (post cured)	[0°]	24	12" x 12"
AS1-3502	[90°]		6" x 9"
AS1-E707 (Mode 1 Test)	[0°]	12	"
AS1-3502 (Mode 1 Test w/Kevlar at Midpoint)	[0°]		"
AS1-E707	[$\pm 30_2/90_2$] _s	24	10" x 10"
AS1-3502 (Mode 1 Test, coated Kevlar paper at midpoint)	[0°]		"

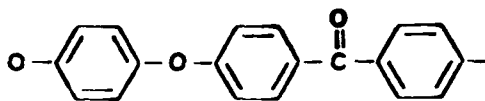
<u>Material</u>	<u>Lay-up Orientation</u>	<u>No. of Plies</u>	<u>Size</u>
AS1-3502 (Mode I Test, coated polyester paper at midpoint	[0°]	24	6" x 9"
T300/5208 Graphite/ Epoxy Alum/Suspension		10	6" x 6"
AS1-3502	[0°]	8	24" x 24"
AS1-3502	[0°] _s	3	10" x 10"
"	"	4	"
"	"	6	"
HMF-133-76	[0°/90] cloth	10	6" x 10"
"	[+45]	4	6" x 6"
T300/5208	[0/90/+45] _s	8	6" x 6"
"	[0 ₂ /90 ₂ /+45] _s	16	"
"	[0 ₃ /90 ₃ /+45 ₃] _s	24	"
"	[0 ₃ /90 ₃]	12	2" x 6"
"	[0 ₃ /90 ₃]	12	2" x 6"
HyE-1076-E non autoclave cure	0°	16	12" x 12"
HMF-133-76	[0/90]	4	6" x 6"
"	[+45]	4	"
" Mode I	[0/90]	10	6" x 10"
U-376-A	[+30/+30/-30/-30/90/90] _s	12	6" x 10"
"	"	12	"
" Mode I	0°	16	"
" "	"	16	"
HME CON 11 non autoclave cure	0°	16	12" x 12"
AS1-3502	[0/+45/90] _s	8	12" x 12"
"	"	"	"
"	"	"	"
"	"	"	"
" Mode I	0°	16	6" x 10"

<u>Material</u>	<u>Lay-up Orientation</u>	<u>No. of Plies</u>	<u>Size</u>
T300/5208	$[0_4/+45_4/90_4]_s$	32	6" x 6"
"	$[(+30)_{10}/90]_s$	42	"
U-378-A	0°	29	6" x 10"
Mode I Rerun Roll #2			
AS1-3502/Alum. Suspension unidirectional	18 panels	3 & 4	3" x 3"
AS1-E707	0°	12	6" x 10"
"	"	16	"
"	"	12	6" x 6"
"	"	24	6" x 6"
"	"	50	4" x 6"
AS1-3502	"	16	9" x 18"
T300/F-178	[0/90] Bidir. cloth	10	12" x 12"
AS1-3502	$[\pm 45/0_8/\pm 45]_s$ Nichols	24	6" x 10"
"	$[\pm 15/0_8/\pm 15]_s$	24	6" x 10"
AS1-E-707	$[+45/90/-45/90/+45/90/-45/90]_s$	15	6" x 10"
"	$[+45_2/-45_2]_s$	8	6" x 10"
AS-1076	0° Mode I	24	10" x 10"
"	0°	16	12" x 12"
AS-3502	0° Mode I	24	10" x 10"
HMP 133-76	[0/90]	4	10" x 10"
HYE 934	$[0_2/+45_2/-45_2/90_2]_s$		24" x 24"
AS-3502	$[\pm 60/0_8/\pm 60]_s$ Mode I	24	6" x 10"
"	$[\pm 75/0_8/\pm 75]_s$ Mode I	24	6" x 10"
1076-E Mode I	0°	24	6" x 14"
AS1-707	0° Rail shear test	16	6" x 6"
HMP-133-76 (2 ea)	$[\pm 45]$	4	12" x 12"
1076-E	0° Mode I precompacted for 3 days		6" x 14"

<u>Material</u>	<u>Lay-up Orientation</u>	<u>No. of Plies</u>	<u>Size</u>
AS4-my720	0°	12	6" x 4"
AS4-828/DDS	0°	7	6" x 10"
T300/976/1076 No bag cure	0°	16	6" x 6"
1076-E, Mode I	0°	24	6" x 14"
HMF 133-76	0/90	4	10" x 10"
" "	± 45 (2 ea)	4	12" x 12"
New material			
AS4-3502 Mode I	0°	24	6" x 10"
AS1-3502	$[\pm 45]_s$	8	6" x 6"
AS1-E707	0° 4" direction	50	4" x 6"
T300/976/1076 precompaction test	0°	16	6" x 6"
U-378A/T300	$[+30_2/-30_2/90]_s$	12	6" x 10"
AS1-E707 re-run	0°	50	4" x 6"
HMF 133-76 cloth Mode I	± 45	10	6" x 10"
" "	$\frac{[0/90/\pm 45/\pm 45/90/10]_t}{1 \quad 2 \quad 3 \quad 4}$	4	12" x 12"
E707		50	6" x 4"
U-378A 90° in 6" direction	$[+30_2/-30_2/90]_s$	12	6" x 10"
T300/976/1076 precompaction & C-scan		16	6" x 6"
"		"	"
1076-E Mode I with polymer film @ midpoint		24	
my720 DDS Mode I	0°	24	6" x 9"
1076-T300 No bag cure	0°	16	6" x 6"
"	"	"	"
AS4-828-DDS	0°	9	3" x 6"
AS4-DDS-828	90° in 6" direction	8	6" x 10"

b. Material Development

1) Polyetheretherketone (PEEK)



Polyetheretherketone
(PEEK)

A new thermoplastic material was received from ICI Great Britain. The material was in the form of 5 mil. amorphous film as well as some injection molded tensile bars. The main objective of this program was to evaluate the material as a matrix resin.

The first stage of the program looked at the neat resin chemical resistance.

Chemical resistance tests were completed after annealing to convert from amorphous to the crystalline. Machined tensile dog bones were loaded to 1000 psi with the gage section enclosed in a wick saturated with the agent of interest. No failures were observed as well as stress crazing. Results are shown in Table 2.

The question of additional chemical resistance tests on composites has not been decided.

A composite fabrication study was started using PEEK film and bidirectional 8 harness satin graphite cloth with UC 307 (thermoplastic) finish. The polymer melts at 630°F but maintains a very high viscosity even at 750°F, (4000-5000 Poise). Isothermal TGA's were run in both N₂ and air at 750°F 1 hr + 800°F for 1 hr. Weight loss was .25% and .50%, respectively for H₂ and air. Because of the inherent high viscosity, the processing temperature investigated with success has been 750°F. One of the major efforts in this study was to look at low pressure processing. The goal was to produce void free composites using 200 psi. A successful processing condition was developed. This processing cycle is not optimized.

TABLE 2
NEAT RESIN PEEK
CHEMICAL RESISTANCE

<u>Chemical</u>	<u>Stress (psi)</u>	<u>Time at Stress</u>
MIL-H-5606C ¹	1000	1 week
Skydrol 500B ²	1000	1 week
JP-4 AF-Fuel	1000	1 week
Dichloro Methane	1000	1 week
MEK	1000	1 week
Acetone	1000	1 week
T-5351 AL ³	1000	1 week

¹Air Force Hydraulic Fluid

²Commercial Aircraft Hydraulic Fluid

³Air Force Paint Stripper

The film and cloth are stacked in alternate layers, and then compression molded as follows:

1. RT \longrightarrow 750°F contact pressure
2. 750°F for 1 hr. at 200 psi
3. cool to 200°F and remove

Composites fabricated using this processing show little or no voids by photomicrographs. Mechanical properties were generated on dry and moisture aged composites. Neat resin tensile specimens were moisture aged under water at 160°F to equilibrium. The moisture gain recorded was 0.30%. Tensile properties were measured on the neat resin with the material maintaining 100% of its 250°F tensile properties.

Mechanical properties were generated on bidirectional graphite cloth and are shown in Table 3. Moisture aging data are included in this table because no drop off was measured in the moisture aged samples. As can be seen the composites picked up very little moisture.

In order to better compare the mechanical properties of graphite cloth/PEEK, a state-of-the art epoxy on graphite cloth prepreg was ordered from Fiberite Corp. The material is designated HMF-133-76. The resin is Fiberite's 976 epoxy on T-300 graphite from Union Carbide.

Additional data has been generated on both PEEK/graphite cloth and epoxy/graphite cloth as a direct comparison. The 350°F wet flexural properties of PEEK were significantly better than the epoxy. See Tables 4 and 5. The four-point shear showed no significant difference in strength but the mode of failure was different. See Table 6. In plane shear data on $\pm 45^\circ$ can be seen in Table 7. In the Mode I Peel test the most significant results can be seen between the two systems. See Table 8. One specimen of unidirectional graphite and PEEK was tested in the Mode I test. (See Table 9.)

A study was initiated to look at the creep properties of PEEK composites and also evaluate epoxy along side. The following describes this ongoing program:

TABLE 3
COMPOSITE MECHANICAL PROPERTIES

<u>Property</u>	<u>Epoxy/Gr Cloth</u>	<u>Peek/Gr Cloth</u>
Flex Strength (KSi)	113	102
250°F (DRY)	108	85
250°F (WET)	71	83
350°F (DRY)	80	59
350°F (WET)	34	60
Moisture Wt. Gain (%)	1.3	0.4
Fiber Volume (%)	62.0	57.3

TABLE 4
WET & DRY
PEEK/T-300 BIDIRECTIONAL CLOTH
3 PT - FLEXURE

Temp.	Strength x 10 ³ psi	Modulus x 10 ⁶ psi
RT	102.10	7.43
250°F	83.42	6.87
350°F	60.00	5.99

Moisture Aged 160°F uw

Fiber Vol. 57.32%

Equilibrium Moisture Gain 0.42%

TABLE 5
GRAPHITE/EPOXY CLOTH BIDIRECTIONAL [0/90°]
HMF-133-76 (8-HARNESS SATIN)
3-PT FLEX STRENGTH
DRY

<u>Temp</u>	<u>Strength KSi/GPa</u>	<u>Modulus MSi/GPa</u>
RT	113.3 (.781)	7.85 (54.09)
250°F (121°C)	107.6 (.741)	7.64 (52.64)
350°F (177°C)	80.2 (.552)	7.88 (54.29)

WET*

		<u>% of Dry Strength</u>
RT	120.1 (.827)	106
250°F (121°C)	71.4 (.492)	66
350°F (177°C)	5.78 (39.82)	42.5

Moisture Aged 160°F (71°C) UW
*Equilibrium Moisture Gain = 1.34%
F.V. = 62%

TABLE 6
4 - PT SHEAR

Material	Ult. Strength KSi/GPa	Span-to-Depth	Mode of Failure	Fiber Volume %
PEEK/Cloth	5.71(0.39)	16/1	Tensile	60
Epoxy/Cloth	6.36(.044)	16/1	Shear	55

TABLE 7

PEEL/T-300 CLOTH (H-HARNES SATIN)
+45 IN PLANE SHEAR

Tensile Strength KSi/GPa	Tensile Modulus MSi/GPa	Shear Stress Ult. KSi/GPa	Shear Strain Ult. %	Poisson's Ratio
26.46(.182)	3.41(23.49)	13.23(.091)	7.38	.606

% F.V. = 57.38

TABLE 8

HMF-133-76 (EPOXY/T-300) CLOTH (H-HARNES SATIN)
+45 IN PLANE SHEAR

Tensile Strength KSi/GPa	Tensile Modulus MSi/GPa	Shear Stress Ult. KSi/GPa	Shear Strain Ult. %	Poisson's Ratio
26.25(.180)	2.24(15.43)	13.13(.090)	3.27	.773

% F.V. = 62.0

TABLE 9
MODE I PEEL TEST FOR
DELAMINATION RESISTANCE

<u>Material</u>	<u>Critical Strain Energy Release Rate, G_{IC} (IN-LBS/IN²)</u>
Epoxy/Gr Cloth	1.34
PEEK/Gr Cloth	11.35
Epoxy/Unidirectional GR	0.8
*PEEK/Unidirectional GR	8.0

*One specimen tested

Creep Summary

Objective: To compare test results of epoxy/graphite cloth and tape with PEEK/graphite cloth to determine differences in creep strain between thermosets and thermoplastics. The tests were conducted on panels with a $\pm 45^\circ$ lay-up orientation. This allowed the test samples to be more resin dominated and, thus, more susceptible to creep. The materials used include:

+45° PEEK/cloth	4 ply panel
+45° EPOXY/cloth	4 ply panel
+45° EPOXY/tape	8 ply panel
1/4" strain gages	
creep frames	

Procedure: The panels were cut into 3/4" x 6" strips and two strain gages were mounted on each specimen, one longitudinally, and one transversely. The specimens were loaded into a creep frame and a predetermined load was applied. All tests were conducted at ambient temperatures.

The PEEK/graphite cloth specimens were separated into two groups each containing three samples. The first group was tested at 30% ultimate strain for 500 hrs. and then terminated. The second group was tested at 70% ultimate strain for 1500 hrs. and then allowed to recover to determine any damage. After recovery the samples were polished and checked for cracks. The epoxy specimens, both cloth and tape, were tested at 70% ultimate strain and then allowed to recover. These specimens will also be checked for cracks.

Comparative results: (See Figure 1).

<u>Specimen</u>	<u>% ult. strain</u>	<u>time (hrs)</u>	<u>creep strain(μin/in)</u>	<u>% creep</u>
PEEK/cloth	30	800	3500	.35
PEEK/cloth	70	800	15000	1.5
EPOXY/cloth	70	800	20000	2.0
EPOXY/tape	70	800	23000	2.3

The results show a slightly higher creep strain for epoxy/cloth and tape when compared to PEEK/cloth. The results are not conclusive, however, and are still being explored. The

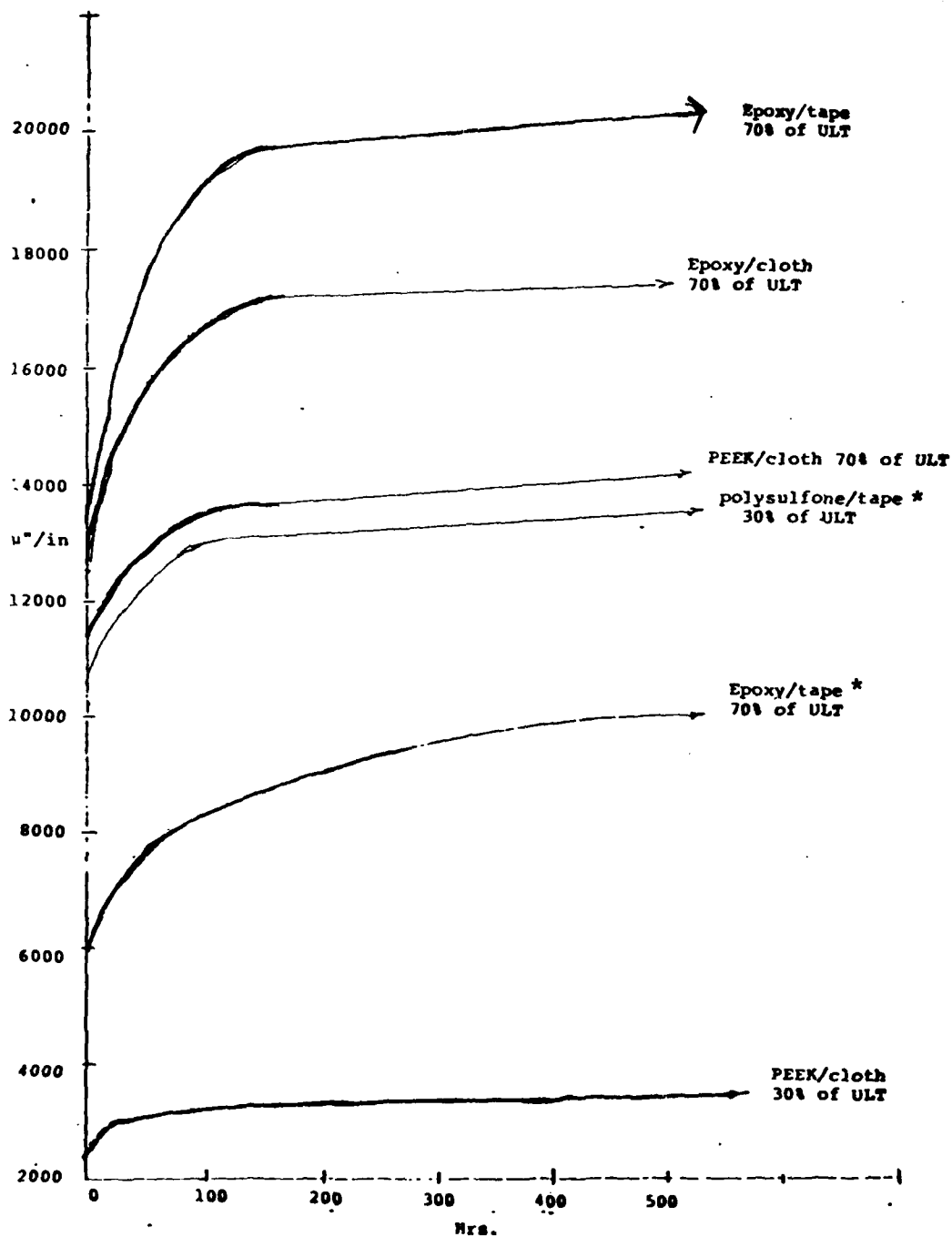


Figure 1. Tensile Creep RT.

epoxy/tape results obtained are significantly different from previously published results found in the Technical Report AFML-TR-77-151, Sept. 1977. One possible explanation could be the void content of the panels or cracks in the area of the strain gages. The PEEK/cloth samples which have been polished did not reveal any cracks. The epoxy/cloth and tape samples have yet to be checked.

In the future, PEEK/tape will be tested under the previously used conditions and compared to the present data. The comparison will be continued by testing both PEEK and epoxy samples at elevated temperatures (250°F and 350°F) and observing their recovery.

A preliminary study was initiated to look at the impact properties of PEEK/cloth versus epoxy/cloth. Static tests were run at NASA Langley on the two systems with actual impact yet to be completed. The static tests show good correlation with actual impact. Load versus displacement was plotted for the two systems with PEEK showing greater load carrying and delamination resistance. A plot of the reduced data is shown in Figure 2.

A program was initiated to evaluate the fatigue properties of PEEK/graphite cloth versus epoxy/graphite cloth. This program is ongoing. The data generated on the two systems is undergoing analysis.

2) Polyethersulfone/graphite

An evaluation was carried out on a panel supplied from ICI Americas. This material was a polyethersulfone/graphite material. The composite was tested in 3-pt. flexure dry and wet. As was suspected the moisture aged specimens lost significant properties at elevated temperatures. The data is shown in Table 10.

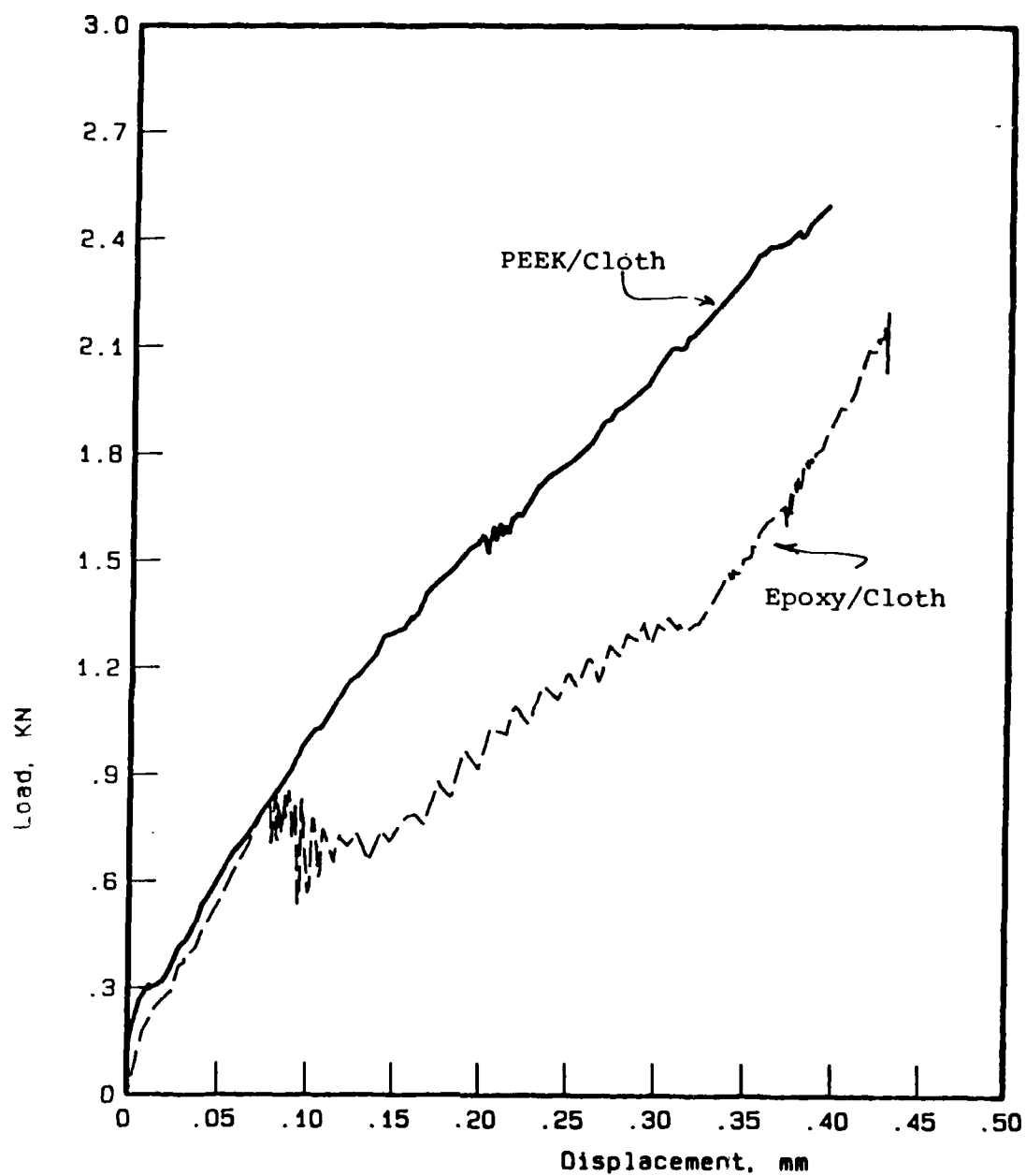


Figure 2. Load-Displacement Plots for Half-Inch Indentation Specimens, [0-90] PEEK/cloth versus Epoxy/cloth.

TABLE 10

POLYETHERSULFONE/GRAPHITE COMPOSITE*
3 PT - FLEXURE

DRY

25

*Fabric: Code G827 - 98.5% Tied Unidirectional

Weight : 11 Tex "E" Glass

****Wet : Moisture Aging 160°F Underwater**

Moisture Gain to Equilibrium = 0.97 (140 days)

3) Resin Sensitivity

The data below represents the initial phase of a program to study the resin matrix sensitivity of AS-1/E707.

The resin for this system was developed in the laboratory. The formulation was supplied to U.S. Polymeric who in turn made the prepreg for us according to our specifications.

A total of four AS-1/E707 composites were prepared using our standard epoxy composite cure cycle.

None of these panels were postcured.

<u>Composite No.</u>	<u>No. of Plies</u>	<u>Composite Size</u>	<u>Orientation</u>
CB4-8-82	8	6" x 10"	+45°
CB4-2-82	16	6" x 10"	0°
CB4-4-82	24	6" x 6"	0°
CB4-5-82	50	4" x 6"	0°

All of the above composites had average specific gravity measurements of 1.63 gm/cc. Photomicrographs showed all composite panels to be void-free except CB4-5-82, the 50-ply composite. This panel contains numerous elongated voids running through the center of the composite. Because of the thickness of this composite, the cure cycle may have to be altered. Because no decision has been made to redo this composite, the data is included in Tables 11-15.

All tests were conducted at room temperature. The data reported represents averages of five specimens per data point.

An additional evaluation of this resin is ongoing in the lab. The basic resin system is MY-720/DDS.

Tapes are being wound and composites fabricated. Analysis of the mechanical properties is still in process.

4) Composite Fabrication Development

An effort is underway to duplicate data compiled by General Dynamics. This involves the precompaction of the laminate before continuing the cure cycle. Using 1076 C prepreg,

TABLE 11
COMPOSITE #CB4-8-82
8 PLY, +45°

<u>Tensile Strength</u> KSi	<u>Tensile Modulus</u> MSi	<u>Shear Strength Ult.</u> KSi	<u>Poisson's</u> <u>Ratio</u>
21.56	2.93	.0231	.718

TABLE 12
COMPOSITE #CB4-2-82
16 PLY, 0°

<u>3 pt Flex Strength</u> KSi	<u>Modulus</u> MSi	<u>Failure Mode</u>
259.48	17.09	Ten/Shear
<u>Short Beam Shear</u> <u>4/1 Span to depth, Compression</u> <u>Failure</u>		<u>Short Beam Shear</u> <u>6/1 Span to depth shear</u> <u>Failure</u>
17.43 KSi		13.87 KSi

TABLE 13
COMPOSITE #CB4-2-82
16 PLY, 0°, 90° FLEX

<u>UTS</u> <u>KSi</u>	<u>Modulus E</u> <u>MSi</u>	<u>Strain to</u> <u>Failure</u>	<u>Mode of</u> <u>Failure</u>
12.95	1.59	00.84	Tensile

TABLE 14
COMPOSITE #CB4-4-82
24 PLY, 0°

4 Pt. Shear
UTS KSi

13.11

Short Beam Shear
6/1 Span to Depth, Shear Failure

14.80 KSi

TABLE 15
COMPOSITE #CB4-5-82
50 PLY, 0°

Short Beam Shear KSi
4/1 Span to Depth

10.50

a 24 ply, 0° laminate was prepared with a 1" teflon spacer placed on the 12th ply edge so Mode I tests could be conducted on the cured composite. The laminate was precompacted in the autoclave for three days at room temperature and 100 psi before continuing the cure. At this time the Mode I tests show no improvements in mechanical properties. The theory behind this method is not fully understood at this time.

5) Material Development

a) V-378 A

A new work effort was initiated to evaluate a new polyimide from U.S. Polymeric. V-378 A is a new modified bis maleimide matrix resin. This resin is said to exhibit significant advantages over previously available bis maleimides and 350°F curing epoxy resins. V-378 A can be cured under standard low autoclave pressure of 100 psi and temperatures of 350°F similar to current 350°F curing epoxy systems. Unrestrained post cure at temperatures of 475-500°F are required to maximize elevated temperature strength retention.

Prepreg was received from U.S. Polymeric and composite processing was initiated. See Table 16. Basic mechanical properties were generated, and a moisture aging program was also initiated. The processing conditions used and mechanical properties are listed in Table 17. There is some indication that the composite fiber volume is on the high side, thus causing less than desirable properties in some of the matrix dominated tests such as the Mode I Peel test and the angle ply composites.

After the initial evaluation of several lots of prepreg, both of which contained lower than acceptable resin contents, additional prepreg was received.

The evaluation of a higher resin content prepreg resulted in only slightly higher Mode I values and a continued macrocracking in the delamination specimens. The delamination specimens consist of a 12 ply (+30₂, -30₂, 90₂)_s. The cracking was

TABLE 16
COMPOSITE PROCESSING INFORMATION

Material System - V378 A

Fiber T300 w/epoxy size

Matrix - V378 A

Maximum Rated Temperature 450°F

Prepreg by - U.S. Polymeric

Cure Schedule: 1. Full vac & 85 psi
autoclave cured 2. Heat to 175°F (@ 5°F/min), Hold 1/2 hr.
 3. Vacuum off, raise pressure to 100 psi
 4. Heat to 355°F
 5. Hold @ 355°F/100 psi/no vacuum for 4 hrs.
 6. Reduce pressure to 10 psi and cool to
 150°F before removing

Post cure schedule: 1. Heat to 475°F @ 3-5°F/min
 Hold 4 hrs. @ 475°F
 Cool @ 3-5°F/min.

TABLE 17
MECHANICAL PROPERTIES

PANEL #1 T300/V378 A
16 PLIES 0° CONFIGURATION 12" x 12" PANEL
COMPOSITE SPECIFIC GRAVITY-1.61
FIVE SPECIMENS PER DATA POINT

	<u>3-pt. Flex Strength</u> <u>x10³ psi</u>	<u>Modulus</u> <u>x10⁶ psi</u>	<u>Failure</u> <u>Mode</u>	<u>Strain to</u> <u>Failure</u>
Room Temp.	240.76	17.54	Ten&Shear	
350°F(177°C)	184.93	17.56	Compression	
450°F	170.45	17.60	"	
	<u>4-pt. Shear Strength</u> <u>x10³ psi</u>			
	11.14		Shear	
350°F(177°C)	9.25		"	
450°F(232°C)	6.55		"	
	<u>90°-4 pt. Flex Strength</u> <u>x10³ psi</u>			
	14.03	2.71	Tensile	.0059
	<u>Short Beam Shear</u> <u>x10³ psi</u>			
	15.41		Compression	
350°F	10.87		"	
450°F	9.09		"	

noticed in the 90's and is the result of thermal stresses on a brittle matrix resin. The work on this project has been planned for the future.

6) Polyimide Development

Material development has been concentrated on a polybismaleimide resin, namely H795. This resin is a proprietary thermosetting heat curable maleimide type supplied by Technochem, an overseas firm. Formulation work has been done to improve the tack and drape of the prepreg. Two different formulations were used to make two prepreg tapes using the hot melt prepregger. A total of three, 4" x 4", 8-ply composites were made from these two tapes. The first two composites were made using the same resin formulation and cure cycle. The resin formulation contained 50 gms of H795 resin and 25 gms of Ebecryl (Ebe) hardener. A different resin formulation was used for the third composite. It contained 50 gms of H795, 25 gms Ebe and 2.5 gms of M751. The M751, also a polybismaleimide, was added to improve toughness. AS-4 graphite fiber was used for all the tapes. Specific gravities of about 1.59 gm/cc were obtained on all three panels. Photomicrographs also indicate void-free panels. The data below includes all mechanical properties obtained from the three panels (see Table 18). Additional work is planned for the future.

7) Acetylene Terminated Quinoxaline (BADABA)

Work is ongoing with the "one pound" evaluation of an acetylene terminated quinoxaline (BADABA). Tensile specimens have been prepared from freeze drying and mechanical properties determined at room and elevated temperatures both dry and humid aged. Composites have been prepared from solvent winding and processed in the press using matched die molding. Some composite properties have been generated. Although this material is not considered a candidate material, much valuable experience is being gathered on this project. Shown below are the supporting Tables 18-26 for this work.

TABLE 18
H795 POLYBISMALEIMIDE/AS-4 COMPOSITE DATA

<u>Material</u>	<u>Condition of Test</u>	<u>Short Beam Shear x10³ PSI</u>	<u>3 pt. Flex UTS 10³ PSI</u>	<u>Modulus x10⁶ PSI</u>	<u>Mode of Failure</u>
H795/Ebe/M751 Composite #1 Tape #1	R.T.	11.63	216.77	15.09	SBS/comp. 3 pt. flex. ten & comp.
H795/Ebe Composite #2 Tape #1	Dry 350°F	7.35	127.08	14.80	SBS/comp. 3 pt. flex comp.
	Wet 350°F	4.48	89.01	14.80	SBS/comp. 3 pt. flex/comp.
H795/Ebe Composite #1 Tape #1	R.T.	12.68	220.59	15.73	SBS/comp. 3 pt. flex/ten & comp.

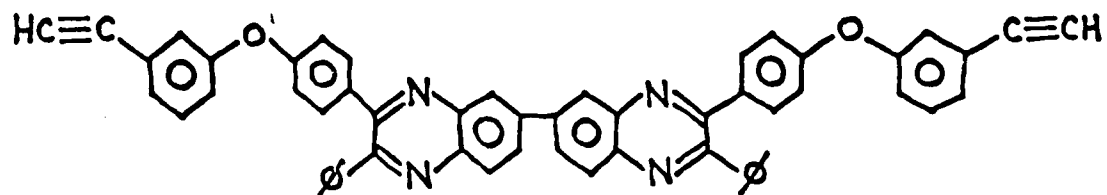
TABLE 19

BADABA

BA = Benzil Acetylene

DAB = Diaminobenzidine

BA = Benzil Acetylene



M.W. = 794

TABLE 20
FREEZE-DRYING OF BADABA

- Dissolved 2 g. of Badaba in 225 ml. of benzene
- Immersed flask in bath of dry ice & acetone
- Rotated constantly for approx. 12 min.
- Placed flask on freeze-drier cooled to -60°F
- Left on for minimum of 48 hrs.

TABLE 21
PREPARATION OF DOGBONES

- B - staged 55 min at 340°F
- Mold preheated to 400°F
- Badaba B stage placed in mold
- 200 lbs pressure applied
- Held $1/2$ hr at 400°F

TABLE 22
NEAT RESIN PROPERTIES (R.T.)

<u>Cure Cycle</u>	<u>UTSx10³(psi)</u>	<u>% Strain</u>	<u>Ex 10⁵ (psi)</u>
B+½hr/450°F/air+2hrs/700°F/air	3.8	.89	4.6
B+½hr/450°F/press+2hrs/700°F/N ₂	5.4	1.2	5.3
B+½hr/450°F/air+2hrs/700°F/vac	6.0	1.3	5.6
B 16hrs/525°F/air	5.8	1.1	5.9
B ½hr/450°F/press	3.4	.69	5.2
B 15½hrs/400°F/air	5.4	1.0	5.9
B 4hrs/482°F/air	3.7	.73	5.1
B 16hrs/400°F/air+4hrs/482/air	4.7	1.0	5.2

TABLE 23
ELEVATED TEMPERATURE PROPERTIES (DRY)

<u>Temperature</u>	<u>UTSx10³(psi)</u>	<u>% Strain</u>	<u>Ex10³(psi)</u>
RT	5.8	1.1	5.9
300°F	5.7	1.5	-
500°F	4.6	1.9	4.1
600°F	2.5	2.6	2.7

TABLE 24
ELEVATED TEMPERATURE PROPERTIES (WET)

<u>Temperature</u>	<u>UTSx10³(psi)</u>	<u>% Strain</u>	<u>Ex10³(psi)</u>
RT	5.8	1.2	6.5
300°F	6.0	1.6	5.4
500°F	5.0	2.2	3.3

TABLE 25
PREPARATION OF COMPOSITES IN PRESS

- Mixed equal parts of Badaba and THF
- Wound prepreg
- Dried 3 hrs
- Heat at 5°F/min to 375°F
- Apply 125 lbs pressure
- Heat at 5°F/min to 400°F
- Hold 1/2 hr

TABLE 26
COMPOSITE PROPERTIES

<u>Cure Cycle</u>	<u>Test</u>	<u>USx10³(psi)</u>
B 16 hrs 400°F	SBS	8.6
B 16 hrs 525°F	SBS	11.2
B 16 hrs 400°F	4 point shear	7.4
B 16 hrs 525°F	4 point shear	8.3

SECTION II
ADHESIVE BONDED JOINTS

1. EXPERIMENTAL ADHESIVES

a. BADABA (an Acetylene Terminated Quinoxaline)

BADABA material that had been synthesized by MRI (Midwest Research Institute) was molded into 1/2" x 0.1" x 3" (1.27 cm x 0.25 cm x 7.62 cm) beam specimens. After molding, the beams were separated into four groups. Each group was cured at a selected temperature and all four groups were cured in N₂.

The cure conditions were:

- A. 16 hrs. at 240°C in N₂
- B. 16 hrs. at 300°C in N₂
- C. 16 hrs. at 340°C in N₂
- D. 16 hrs. at 371°C in N₂

After cure one bar from each condition was tested for dynamic modulus in a Rheometrics machine up to the cure temperature. All the beams were then machined into CT (compact tension) specimens (approx. four specimens from each beam). There were 20 beams and five beams to each cure group.

The CT specimens were tested in that mode at R.T. and selected elevated temperatures.

	R.T.	200°C	240°C*	250°C	300°C
Group A	x	x	x		
Group B	x	x		x	x
Group C	x	x		x	x
Group D	x	x		x	x

*240°C was the cure temperature for Group A and testing above that temperature would not have been informative for those specimens.

Two specimens were tested per data point.

b. BADABA with 1% Cure Initiator

Tensile dogbone and beam specimens were molded from purified MRI BADABA that had 1% cure initiator added. Processing techniques were determined for that material.

Compression molded dogbone specimens of BADABA were tested in tensile at RT, 200°F, 300°F & 350°F using an extensometer to measure strain. Data is reported in Table 27.

c. ATS (100% Oligomer) an Acetylene Terminated Sulfone from Which all of the Monomer had been Removed

Tensile dogbone and beam specimens were molded from ATS (100% oligomer). Two 1/2" x 0.1" x 3" beams and five dogbone specimens were fabricated from 9 g of material.

The purpose of the investigation was to determine the effect of higher molecular weight ATS on the mechanical properties of the cured polymer. The results of the tests were somewhat clouded by the discovery of elemental Palladium in the sample which could have caused an undetermined specie and erroneous conclusions.

d. ATS (Gulf)

ATS (Gulf) dogbone and beam moldings were fabricated and then cured in an N₂ atmosphere. This sample of ATS contained approximately 24% oligomer and 76% monomer.

It was hoped that the higher molecular weight material in the polymer, along with the monomer, would have a favorable influence on elongation and fracture toughness properties of the ATS.

The dogbone specimens were tested in tensile and the beams were machined into CT specimens and tested for fracture characteristics in the MTS machine.

e. Acetylene Terminated Sulfone (ATS)

Midwest Research Institute ATS polymer was cast into beam configuration. Dynamic modulus was determined on the

TABLE 27

TENSILE TEST
BADABA/1% INITIATOR CURED-350°F 32 HRS. IN AIR

	Cond. of Test	Ult. Strength ($\times 10^3$)	(%) Elong.	Mod. of Elast. ($\times 10^3$)
BA-1	R.T. Dry	9.1	1.7	524
2	"	10.5	2.0	528
3	R.T. Wet	5.8	1.0	583
4	"	4.9	1.0	512
5	200°F Dry	5.3	1.1	486
6	"	6.5	1.4	464
7	200°F Wet	5.6	1.2	468
8	"	4.7	1.03	454
9	300°F Dry	10.7	3.0	360
10	"	4.0	1.0	400
11	300°F Wet	9.3	3.2	294
12	"	10.3	4.1	248
13	350°F Dry	9.3	3.4	270
14	"	8.7	2.8	311
15	350°F Wet	7.8	3.0	264
16	"	8.8	4.2	210

Rheometrics machine, beams were machined into nominal .5" (12.7mm) CT specimens, and fracture evaluation was done. Data is being reduced.

f. ATQ, SBQ, BATQ and BADABA

ATQ, SBQ, BATQ, and BADABA were molded into beams and cut into compact tension (CT) specimens for fracture characterization. Testing was done at R.T., 200°C, 250°C, and one material, BADABA "D" at 300°C.

Data are reported in Table 28.

TABLE 28

K_{IC} VALUES FOR ACETYLENE
TERMINATED QUINOXALINES
psi \sqrt{in} (mPA \sqrt{m})

	20°C	200°C	250°C	300°C
SBQ	620 (.68)	550 (.603)	-	-
BADABA "D"	650 (.71)	590 (.65)	540 (.59)	560 (.615)
ATQ	920 (1.01)	1350 (1.48)	2450 (2.69)	-
BATQ	950 (1.043)	1350 (1.48)	2500 (2.75)	-

Data are from two specimens at each condition.

g. 5208/T300

Fracture specimens in compact tension configuration (CT) were previously machined and are currently being tested. Sets of those composite specimens have been tested during the past year. A set consists of two fracture specimens and two compliance specimens. The compliance specimens are useful in analysis of the fracture characteristics of the composite fracture specimens fabricated of the same materials.

In the CT fracture test the crack front cannot be readily identified, if at all; therefore, crack displacements cannot be associated with load peaks during evaluation which makes K_{IC} values impossible to accurately calculate. When employing a compliance measurement, predetermined crack lengths may be cut into a specimen and the displacement per unit load may be measured. An initial crack of nominal length is generally cut into the compliance specimen, and the specimen is then loaded and the stress/strain slope recorded. The crack is then cut longer in about one mm increments and loaded after each cut. The slopes are measured for each crack length.

Conversely, when a CT fracture specimen is loaded, the slope of the curves produced may be correlated to the compliance curves, thereby determining the crack length per unit load of the fracture CT specimen.

Compliance and fracture tests have been completed on 5208/T300 at 130°C, 150°C, 177°C, 190°C, and 200°C. Additional evaluation must be done at lower temperatures and also at the same conditions after humid aging to complete the spectrum.

h. Polyurethane Model Material

Five polyurethane, low Tg materials, each being a different molecular weight, were machined into 1" CT specimens. Those materials were tested on the MTS test machine at various temperatures and load rates strictly to observe models of various characteristics of plastics of the same family type but of different molecular weights.

i. 5208 Neat Castings

Neat resin castings were made from 5208. The castings were 0.10" (2.54mm), 0.20" (5.08mm), and 0.50" (12.7mm) in thickness. The 0.1" castings were machined in 0.5" (12.7mm) x 0.5" (12.7mm) compact tension (CT) specimens and 1" (25.4mm) x 1" (25.4mm) CT specimens. The 0.20" castings were machined into 1" x 1" and 2" x 2" (50.8mm x 50.8mm) CT specimens, and the 0.5" thick CT specimens were machined into 2" x 2" CT specimens.

Those specimens were used as standards for fracture calculations and for test method reliability. Approximately 80 specimens total were prepared.

In addition, an experiment was run to determine the quantity of adsorbed or absorbed moisture present on or in the material as cured. Several 1" x 1" x .2" specimens were dried in a desiccator and an additional group was dried in a vacuum oven at R.T. for 70 days each. The group in the vacuum oven lost 0.4% compared to 0.075% weight loss for the group in the desiccator.

j. PEEK (Polyetheretherketone)

PEEK/AS-4 composites were machined into 0.5" (12.7mm) x .78" (19.8mm) x ~ 0.1 (2.54mm) thick compact tension specimens and compliance calibrations were run for K_Q baseline data.

k. Ordered Polymer

Processing techniques for an ordered polymer were explored. Material was extruded through various shaped dies to form either a ribbon-shaped or fiber-shaped specimen as it was extruded and wound on a mandrel. A winding machine was modified for that purpose.

A tensile loading device was designed and machined to be employed on the x-ray diffraction equipment primarily for measurement of loading effects of high modulus ordered polymer fibers, although the device could be used with any fiber.

The device also has the capability of X/Y positioning of the fiber and is instrumented and calibrated for variable load from 0-15 lbs. total force.

2. MISCELLANEOUS POLYMER FRACTURE

Compact tension specimens were machined and tested for fracture characteristics from the following materials:

a. Thermosets

- 1) 828/DDS
- 2) MY 720/DDS
- 3) 5208

b. Thermoplastics

- 1) P-1800 Polysulfone
- 2) Polyetheretherketone (PEEK)
- 3) Radel

Methods for data reduction are being studied.

The following specimens were machined in the laboratory and are ready for future fracture characterization or have been tested.

(42)	3501 epoxy	1"
(63)	T-300/5208	1/2" x .78"
(15)	T-300/5208	1/2" x 1/2"
(4)	5208	1"
(20)	5208	1/2"
(2)	BADABA "C"	1/2"
(2)	BADABA "D"	1/2"
(20)	43-A Polyurethane	1"
(12)	42 "	1/2"
(12)	43 "	1/2"
(12)	44 "	1/2"
(7)	ATQ	1/2"
(4)	SBQ	1/2"
(5)	BATQ	1/2"

A special tensile specimen was hand machined 5 1/4" long x 1/4" thick with a 2" gage section.

SECTION III

INTERFACE/INTERPHASE CHARACTERIZATION

1. ALUMINUM OXIDE/EPOXY INTERPHASE

Aluminum adhesive bonding technology is based upon the formation of a stable oxide layer on the aluminum substrate. In this study attempts have been made to characterize the substrate-oxide-matrix interphase using the single filament coupon technique. This approach involves uniaxially embedding a 5 mil phosphoric acid anodized aluminum wire in a polymeric test coupon. Application of tensile forces to the specimen induces circumferential cracks in the oxide which can be viewed in a reflected light microscope. Measurement of the intercrack distance is indicative of the oxide/matrix shear adhesion strength. A detailed account of this procedure can be found elsewhere.¹

Work to date has centered on establishing baseline data for three systems, namely Al-99.99%, Al-2024T4, and Al-6061T3 5 mil wires tested in Epon 828 epoxy resin cured with 14.5 phr meta-phenylenediamine (mPDA). Subsequent experimentation has focused on the effects of coatings and hygrothermal exposures on interphase properties.

a. Experimental

The procedure for wire preparation and anodization has been reported previously.¹ Anodization time and voltage were held constant at 60 volts for 20 minutes.

Coatings were applied to the oxide surface by submersing the anodized wire for 30 minutes in solutions containing resins and/or curing agents dissolved in methyl ethyl ketone (MEK) and then permitted to air dry for 24 hours prior to sample fabrication. Four coatings have been evaluated to date: 1) resin rich coating of 5 wt.% Epon 828 in MEK; 2) curing agent rich coating of 5 wt.% mPDA in MEK; 3) 5 wt.% Epon 1009F, a higher molecular weight homologue of Epon 828, in MEK; and 4) Epon 1009F + 0.9 phr mPDA in MEK.

Hygrothermal exposures were conducted by suspending either the anodized wires or test coupons above distilled water in a sealed container. Coupon weight was monitored for establishment of equilibrium to indicate complete water sorption by the test specimen.

b. Results and Discussion

The effects of anodic oxide coatings on interfracture distance as determined by the single filament coupon technique are reported in Tables 29-31. In the Al 99.99% system, each of the coatings has resulted in a decrease in the mean oxide interfracture distance. The reverse trend is observed in the two other systems studied, Al 2024T4 and Al 6061T3. The precise reason for this difference is not fully understood but may be attributable to differences in oxide chemistry and tensile strength.

Moisture at the oxide/matrix interphase also influences the oxide intercrack distance (see Tables 32-34). Anodized wires subjected to 100% relative humidity for 72 hours at either 70°C or 125°C exhibit significant reductions in the mean oxide interfracture distance. Test coupons exposed to 100% RH at 125°C show a similar trend but of lesser magnitude.

Because the tensile strength of the anodic oxides has not been determined, comparison of oxide/matrix shear strengths is not valid for the three systems studied. Work in progress is directed at measurement of the anodic tensile strength. However, results are insufficient to report at this time.

2. CARBON FIBER/EPOXY INTERPHASE

Adhesion between fiber and matrix is a crucial element contributing to composite performance. In this study factors governing interactions occurring at the carbon fiber-epoxy interphase were evaluated and correlated to an average shear adhesion strength. Fiber surface free energy, surface chemistry,

TABLE 29
EFFECT OF COATINGS ON Al 99.99% ANODIC OXIDE
INTERFRACTURE DISTANCE

<u>Coating Solution</u>	<u>Oxide Interfracture Distance</u> <u>(in. + $\sigma \times 10^{-3}$)</u>
None: Fabricated per usual	1.63 \pm 0.38
5% Epon 828 in MEK	1.56 \pm 0.08
5% mPDA in MEK	1.49 \pm 0.11
4.5% Epon 1009F in MEK	1.18 \pm 0.12

TABLE 30
EFFECT OF COATINGS ON 2024-T3 ANODIC OXIDE
INTERFRACTURE DISTANCE

<u>Coating Solution</u>	<u>Oxide Interfracture Distance</u> <u>(in. + $\sigma \times 10^{-4}$)</u>
None: Fabricated per usual	4.62 \pm 0.89
5% Epon 828 in MEK	5.18 \pm 0.13
5% mPDA in MEK	5.38 \pm 0.17
4% Epon 1009F in MEK	5.51 \pm 0.18
4% Epon 1009F + 0.9 phr mPDA in MEK	5.71 \pm 0.10

TABLE 31
EFFECT OF COATINGS ON 6061-T6 ANODIC
OXIDE INTERFRACTURE DISTANCE

<u>Coating Solution</u>	<u>Oxide Interfracture Distance</u> <u>(in. + $\sigma \times 10^{-4}$)</u>
None: Fabricated per usual	5.21 \pm 0.50
5% Epon 828 in MEK	5.35 \pm 0.52
5% mPDA in MEK	5.43 \pm 0.31
4% Epon 100F in MEK	5.40 \pm 0.45
4% Epon 100F + 0.9 phr mPDA in MEK	5.55 \pm 0.37

TABLE 32
HYGROTHERMAL EXPOSURE EFFECTS ON Al 99.99%
ANODIC OXIDE INTERFRACTURE DISTANCE

<u>Hygrothermal Exposure</u>	<u>Oxide Interfracture Distance (in + σ)</u>
None: Fabricated per usual	$1.63 \pm 0.38 \times 10^{-3}$
Anodized wire at 100% RH - 70°C - 72 hrs prior to coupon fabrication	$7.73 \pm 0.82 \times 10^{-4}$
Anodized wire at 100% RH - 125°C - 72 hrs prior to coupon fabrication	$3.60 \pm 0.35 \times 10^{-4}$
Test coupon at 100% RH - 70°C till saturated	
Test coupon at 100 RH - 125°C till saturated	$1.55 \pm 0.13 \times 10^{-3}$

TABLE 33
HYGROTHERMAL EXPOSURE EFFECTS ON 2024T4
ANODIC OXIDE INTERFRACTURE DISTANCE

<u>Hygrothermal Exposure</u>	<u>Oxide Interfracture Distance (in. + $\sigma \times 10^{-4}$)</u>
None: Fabricated per usual	4.62 ± 0.89
Anodized wire at 100% RH - 70°C - 72 hrs prior to coupon fabrication	3.65 ± 0.23
Anodized wire at 100% RH - 125°C - 72 hrs	1.78 ± 0.18
Test coupon at 100% RH - 70°C till saturated	
Test coupon at 100% RH - 125°C till saturated	4.38 ± 0.09

TABLE 34
HYGROTHERMAL EXPOSURE EFFECTS ON 6061 - T3
ANODIC OXIDE INTERFRACTURE DISTANCE

<u>Hygrothermal Exposure</u>	<u>Oxide Interfracture Distance</u> <u>(in. + $\sigma \times 10^{-4}$)</u>
None: Fabricated per usual	5.21 \pm 0.50
Anodized wire at 100% RH - 70°C - 72 hrs prior to coupon fabrication	3.70 \pm 0.22
Anodized wire at 100% RH - 125°C - 72 hrs prior to coupon fabrication	2.00 \pm 0.04
Test coupon at 100% RH - 70°C till saturated	
Test coupon at 100% RH - 70°C till saturated	4.72 \pm 0.35

tensile strength, and critical transfer length were measured and are discussed in the following sections. A key to the fiber code abbreviations used is given in Table 35.

a. Surface Free Energy of Carbon Fibers

Surface energetic measurements are an important thermodynamic parameter used to predict wetting of a solid surface by a liquid phase. Knowledge of the dispersive and polar components of the surface free energy can provide insight to the type and degree of solid-liquid interfacial interactions. The dispersive, polar, and total surface free energy of a variety of carbon fibers were determined using a micro-Wilhelmy technique on single filaments. A detailed description of this technique can be found in Reference 4. Approximately six to twelve filaments were tested in each of eight liquids having a wide range of dispersive to polar ratios of surface free energy. To preclude cross contamination each filament was tested once in a fresh aliquot of the high purity liquids used in this study.

Recent instrument recalibrations necessitated retesting some previously reported work. Hence, the data reported herein supersedes that contained in the quarterly progress reports of this contract.⁵ The mean fiber contact angle and the calculated surface energetic parameters are provided in Tables 36 and 37, respectively.

b. XPS Studies of Carbon Fibers

Carbon fiber specimens which have undergone various surface treatments have been examined using x-ray photoelectron spectroscopy (XPS). These analyses will be discussed in the sections below. Two types of fibers have been characterized by XPS. These two types, A and HM, are polyacrylonitrile fibers which have been graphitized at $\approx 1500^{\circ}\text{C}$ and $\approx 2600^{\circ}\text{C}$, respectively. These fibers are further labeled with an S or U, indicating whether the fibers have undergone an oxidizing surface treatment by the manufacturer or are untreated. The main constituents of the fibers (carbon, oxygen, and nitrogen), along with the two

TABLE 35
KEY TO FIBER CODE ABBREVIATIONS

<u>Code</u>	<u>Designation</u>
AU	Hercules' PAN precursor Type II fiber, similar to AU1 ²
AS	Surface treated AU fiber
AU1	Hercules' PAN precursor Type II fiber
AS1	Surface treated AU1 fiber
AU4	Hercules' pitch precursor Type II fiber
AS4	Surface treated AU4 fiber
HMU	Hercules' PAN precursor Type I fiber
HMS	Surface treated HMU fiber
C	Coating of pure diglycidylether of Bisphenol A (DER 330) applied to fiber (eg., AS1-C)
% ST	Refers to the percentage of normal surface treatment given to fiber tow (eg., AS4-70% ST)
VT	Thermal treatment given in vacuo to fiber tow
Allyl	Flash cured allyl coating applied by Ashland Chemical Co. ³
Acet	Flash cured acetylene coating applied by Ashland Chemical Co.
Epoxy	Flash cured epoxy coating applied by Ashland Chemical Co.

TABLE 36
MEAN CONTACT ANGLE ($\pm \sigma$) OF CARBON FIBERS

Liquid	Fiber Type							
	AS4-70% ST	AS4-85% ST	AS4-100% ST	AS4-120% ST	AS1-ACET	AS1-Allyl	AS1-Epoxy	
Hexadecane	0	0	0	0	23.5±6.5	26.7±4.6	27.3±10.6	
Polypropylene Glycol	11.2±2.3	6.8±8.3	7.7±8.0	5.9±8.9	8.2±9.3	11.5±11.3	10.7±8.4	
Bromonaphthalene	28.7±2.6	28.7±3.8	30.5±6.8	28.2±2.4	0 ± 0	0 ± 0	0 ± 0	
Ethylene Glycol	18.2 ±4.8	17.3±5.8	11.7±9.8	16.3±2.6	23.9±3.6	20.7±3.6	22.0±2.6	
Methylene Iodide	36.3±1.1	39.0±1.5	40.5±1.2	39.3±2.5	4.4±7.1	2.0±5.1	10.1±8.6	
Formamide	13.5±10.3	25.2±10.7	24.1±6.3	9.5±10.3	0.9±2.6	0 ± 0	3.1±6.1	
Glycerol	39.9±6.0	45.7±3.2	43.7±5.0	40.1±6.0	1.4±3.9	1.7±3.6	4.1±8.2	
Water	50.4±5.0	48.2±3.0	51.7±2.9	53.0±6.7	36.0±2.9	41.4±5.8	38.6±7.0	

TABLE 37
POLAR, DISPERSIVE, AND TOTAL SURFACE
FREE ENERGY OF CARBON FIBER SURFACES

<u>Fiber</u>	<u>Surface Free Energy</u>		
	γ_S^P (mJ/m ²)	γ_S^D (mJ/m ²)	γ_S^T (mJ/m ²)
AS4-70% ST	21.1	28.9	50.0
AS4-85% ST	21.3	28.0	49.3
AS4-100% ST	20.4	28.5	48.9
AS4-120% ST	20.3	29.2	49.5
AS1-Acet	27.4	29.4	56.8
AS1-Allyl	25.6	30.0	55.6
AS1-Epoxy	26.8	29.4	56.2

major impurities due to manufacturing processes (sodium and sulfur), were the peaks of interest for these analyses. All specimens were analyzed using $MgK\alpha$ radiation ($h\nu = 1253.6$ eV), and the energy scale was calibrated by assigning the C_{1s} peak of graphite the value 284.6 eV binding energy.

1) Water Treatment

Specimens F054 and F055 are HMS fibers which have been heated in water at 125°C for several days. A listing of the percent surface compositions as determined by XPS can be found in Table 38. Comparison with specimen F057, which is a HMS fiber that has not been subjected to water treatment, shows that the fibers F054 and F055 have undergone no major chemical changes in surface composition, but the amounts of sodium, sulfur, and nitrogen present on the fiber surfaces have decreased. This agrees with previous analyses of water treated fibers, indicating that the sodium, sulfur, and nitrogen are present mainly in water soluble forms.

2) Epoxy-Coated Fibers

Two similar types of fibers, AS-1 and AS-4, underwent the same surface treatments. Analyzed using XPS were: AS-1 (F073) and AS-4 (F071) samples as received from the manufacturer, AS-1 and AS-4 samples which were coated with DER 330 by the manufacturer (labeled AS-1C (F072) and AS-4C (F070)), and specimens F074, F056, and F075 which are AS-1C and AS-4C fibers that had been soaked in methylethyl ketone (MEK) to attempt to remove the DER 330 epoxy coating.

From Table 39 it can be seen that the coated fibers are easily distinguishable from the uncoated fibers due to the absence of nitrogen, sulfur, and sodium peaks. After soaking in MEK, the fibers return almost to the same condition as the uncoated fibers, except that the soaked fibers have a slightly more oxidized surface (about 15% more oxygen). By examining the carbon 1s peaks from these two surfaces, it is seen that the more oxidized MEK soaked fibers have larger peak intensities due

TABLE 38
SURFACE COMPOSITIONS OF FIBER SPECIMENS OBTAINED USING XPS

Specimen	Photoelectron Peak	Peak Area (arb. units)	Surface Concentration (atomic percent)	Concentration from Previous Analysis+
F054 (HMS + H ₂ O)	C _{1s}	3.6 x 10 ⁶	95	94
	O _{1s}	4.6 x 10 ⁵	3.6	4.0
	N _{1s}	4.4 x 10 ⁴	0.6	1.0
	S _{2p}	1.2 x 10 ⁴	< 0.2	< 0.5
	Na _{KLL}	4.7 x 10 ⁴	0.6	1.0
F055 (HMS + H ₂ O)	C _{1s}	3.5 x 10 ⁶	95	
	O _{1s}	4.3 x 10 ⁵	3.5	
	N _{1s}	3.3 x 10 ⁴	0.5	
	S _{2p}	1.2 x 10 ⁴	< 0.2	
	Na _{KLL}	4.9 x 10 ⁴	0.7	
F057 (HMS)	C _{1s}	3.3 x 10 ⁶	94	95
	O _{1s}	4.3 x 10 ⁵	3.8	3.5
	N _{1s}	6.7 x 10 ⁴	1.0	1.3
	S _{2p}	2.5 x 10 ⁴	< 0.5	< 0.2
	Na _{KLL}	4.5 x 10 ⁴	0.7	0.5

TABLE 39
SURFACE COMPOSITION OF AS FIBER SPECIMENS OBTAINED USING XPS

Specimen	Photoelectron Peak	Peak Area	Surface Concentration (atomic percent)	Specimen	Photoelectron Peak	Peak Area	Surface Concentration (atomic percent)
F073 (AS-1)	C _{1s}	2.1×10^6	84	F071 (AS-4)	C _{1s}	1.9×10^6	83
	O _{1s}	9.1×10^5	11		O _{1s}	9.0×10^5	12
	N _{1s}	2.1×10^5	4.3		N _{1s}	1.8×10^5	4.0
	S _{2p}	9.3×10^3	< 0.2		S _{2p}	9.4×10^3	0.2
	Na _{KLL}	4.8×10^4	1.0		Na _{KLL}	3.0×10^4	0.7
F072 (AS-1C)	C _{1s}	2.2×10^6	88	F070 (AS-4C)	C _{1s}	2.7×10^6	87
	O _{1s}	9.5×10^5	11		O _{1s}	1.3×10^6	12
	N _{1s}	2.0×10^4	0.4		N _{1s}	2.1×10^4	0.4
	S _{2p}		-		S _{2p}	-	-
	Na _{KLL}	3.1×10^4	0.6		Na _{KLL}	3.9×10^4	0.6
F074 (AS-1C + MEK Extract)	C _{1s}	2.2×10^6	82	F075 (AS-4C + MEK Extract)	C _{1s}	2.2×10^6	83
	O _{1s}	1.2×10^6	13		O _{1s}	1.2×10^6	14
	N _{1s}	1.5×10^5	3.0		N _{1s}	1.3×10^5	2.6
	S _{2p}	9.9×10^3	0.2		S _{2p}	8.8×10^3	0.2
	Na _{KLL}	5.2×10^4	1.0		Na _{KLL}	5.1×10^4	1.0
F056 (AS-1C + MEK Extract)	C _{1s}	2.2×10^6	83				
	O _{1s}	1.1×10^6	13				
	N _{1s}	1.5×10^5	3.0				
	S _{2p}	1.3×10^4	< 0.5				
	Na _{KLL}	5.0×10^4	1.0				

to carbonyl-type carbon atoms. The reason why the surface appears more oxidized could be either due to residual epoxy coating or MEK remaining on the fibers, or the processes involved in applying and removing the epoxy coating could have left the surface more oxidized.

3) PVA-Treated

Specimens F058 and F059 are HM type fibers which have been exposed to a polyvinyl alcohol (PVA) containing solution and then heated to leave only the adsorbed PVA on the fiber surface. Although the surface concentrations, as seen from Table 40, are not that close to the one previous analysis of these fibers, F058 is still measured to contain more oxygen than F059.

4) AU Fibers

The first three specimens listed in Table 41 (F063, F062, and F060) are AU fibers from three separate lots. Each of these specimens are fairly representative of their lots, judging from past analyses of similar fibers. The remaining AU fibers listed in the table have undergone varying amounts of an oxidative surface treatment and are designated AS4-70, 85, 100, or 120% ST, 100% being that treatment usually used to manufacture AS fibers. We should, therefore, observe a transition from five-eight atom % oxygen as seen on the AU fibers to 10-12% oxygen as seen on the AS fibers. The actual results show no such trend. In fact, these results show no effect from the surface treatment at all. The reason for this discrepancy is being investigated.

5) Data Analysis

Several computer programs are being developed to aid in the interpretation of this data. A deconvolution routine has already been written and debugged, which will be used to enhance the resolution of the acquired data. Also, a curve-fitting routine is being written to estimate more quantitatively the relative percentages of different chemical species present on the fiber surface. Finally, a smoothing routine is being adapted for use with the above two programs, which will improve their accuracy.

TABLE 40
SURFACE COMPOSITIONS OF FIBER SPECIMENS OBTAINED USING XPS

Specimen	Photoelectron Peak	Peak Area (arb. units)	Surface Concentration (atomic percent)	Concentration from Previous Analysis ⁺
F058 (HM + PVA)	C _{1s}	2.6×10^6	86	83
	O _{1s}	1.1×10^6	12	14
	N _{1s}	2.7×10^4	0.5	1.0
	S _{2p}	2.0×10^4	< 0.5	< 0.2
	Na _{KLL}	9.4×10^4	1.6	1.5
F059 (HM + PVA)	C _{1s}	2.3×10^6	91	88
	O _{1s}	5.8×10^5	7	11
	N _{1s}	1.8×10^4	< 0.5	1.0
	S _{2p}	1.6×10^4	< 0.5	< 0.2
	Na _{KLL}	4.7×10^4	1.0	< 1.0

⁺ These concentrations were obtained from specimens of the same fiber type and lot, and were analyzed during the previous contract.

TABLE 41
SURFACE COMPOSITION OF AU FIBER SPECIMENS OBTAINED USING XPS

Specimen	Photoelectron Peak	Peak Area	Surface Concentration (atomic percent)	Specimen	Photoelectron Peak	Peak Area	Surface Concentration (atomic percent)
F063 (AU)	C _{1s}	2.2 x 10 ⁶	8.3	F064 (AS-4 70%)	C _{1s}	5.5 x 10 ⁶	90
	O _{1s}	7.3 x 10 ⁵	8.3		O _{1s}	1.3 x 10 ⁶	6.4
	N _{1s}	7.3 x 10 ⁴	1.5		N _{1s}	3.4 x 10 ⁵	3.0
	S _{2p}	5.3 x 10 ⁴	1.0		S _{2p}	1.5 x 10 ⁴	< 0.2
	NaKLL	3.3 x 10 ⁵	6.3		NaKLL	9.3 x 10 ⁴	0.8
F062 (AU-1)	C _{1s}	2.2 x 10 ⁶	89	F067 (AS-4 85%)	C _{1s}	3.2 x 10 ⁶	90
	O _{1s}	5.4 x 10 ⁵	6.5		O _{1s}	7.6 x 10 ⁵	6.5
	N _{1s}	1.1 x 10 ⁵	2.3		N _{1s}	2.1 x 10 ⁵	3.1
	S _{2p}	2.5 x 10 ⁴	0.5		S _{2p}	6.6 x 10 ³	< 0.2
	NaKLL	6.3 x 10 ⁴	1.3		NaKLL	5.1 x 10 ⁴	0.7
F060 (AU-4)	C _{1s}	2.3 x 10 ⁶	91	F066 (AS-4 100%)	C _{1s}	2.4 x 10 ⁶	99
	O _{1s}	5.0 x 10 ⁵	6.1		O _{1s}	6.3 x 10 ⁵	7.1
	N _{1s}	7.8 x 10 ⁴	1.7		N _{1s}	1.8 x 10 ⁵	3.5
	S _{2p}	1.8 x 10 ⁴	< 0.5		S _{2p}	8.4 x 10 ³	< 0.2
	NaKLL	4.7 x 10 ⁴	1.0		NaKLL	4.1 x 10 ⁴	0.8
F061 (AU-4 70%)	C _{1s}	2.2 x 10 ⁶	82	F065 (AS-4 120%)	C _{1s}	2.7 x 10 ⁶	90
	O _{1s}	7.0 x 10 ⁵	8.0		O _{1s}	6.2 x 10 ⁵	6.3
	N _{1s}	1.3 x 10 ⁵	2.6		N _{1s}	1.8 x 10 ⁵	3.2
	S _{2p}	1.9 x 10 ⁴	< 0.5		S _{2p}	7.0 x 10 ³	< 0.2
	NaKLL	3.8 x 10 ⁵	7.2		NaKLL	4.8 x 10 ⁴	0.8
F077 (AS-4 70%)	C _{1s}	2.3 x 10 ⁶	87	F078 (AS-4 120%)	C _{1s}	1.1 x 10 ⁶	86
	O _{1s}	7.1 x 10 ⁵	8.2		O _{1s}	4.0 x 10 ⁵	9.6
	N _{1s}	1.6 x 10 ⁵	3.2		N _{1s}	6.7 x 10 ⁴	2.8
	S _{2p}	1.5 x 10 ⁴	< 0.5		S _{2p}	1.2 x 10 ⁴	< 0.5
	NaKLL	9.1 x 10 ⁴	1.7		NaKLL	2.7 x 10 ⁴	1.1

c. Single Filament Tensile Tests

Knowledge of fiber tensile strength is necessary to accurately determine interfacial shear strengths. Since the measured tensile strength of these brittle fibers is greatly influenced by the presence of flaws, the tensile strength increases as the gauge length decreases. Usually, fiber strength is estimated at the "critical length" by extrapolation along a log-log curve using data derived at much longer lengths. However, in this study the use of a Tecam micro-tensile tester⁶ allowed the determination of strength at gauge lengths as short as 0.3 mm (0.012 in.). The actual critical length can therefore be bracketed with tests at several gauge lengths, allowing a more accurate estimate of strength than extrapolation.

The first group of samples tested was a series of experimental surface treated AS-4. The strongest fiber, AS4-85% surface treatment, was chosen for an extensive gauge length series (see Figure 3). At a gauge length of approximately 2 mm (0.08 in.), the graph shows a discontinuity of the type theorized by Hitchon and Phillips⁷ to exist as a result of a bimodal distribution of large and small flaws. This is further emphasized by the striking change in the coefficient of variation as the transition length is crossed. This effect may or may not be universal, may occur in the unimportant region shorter than the critical length, or may be too subtle to easily detect on other fibers.

Fiber diameters were measured with an image shearing microscope, and ten filaments were tested at each gauge length in the region of interest. As a result of this relatively small set size, some of the data points appear slightly erratic. Typical test results are plotted in Figure 4. Included are tensile values for 25.4 mm (1.0 in.) gauge length for use as a reference to aid in estimating actual critical length strength. However, it should be noted that there are no documented values for the intermediate lengths. Data from the individual tests have been previously reported.⁽⁵⁾ A summary of these results is given in Table 42.

AS-4 85%ST

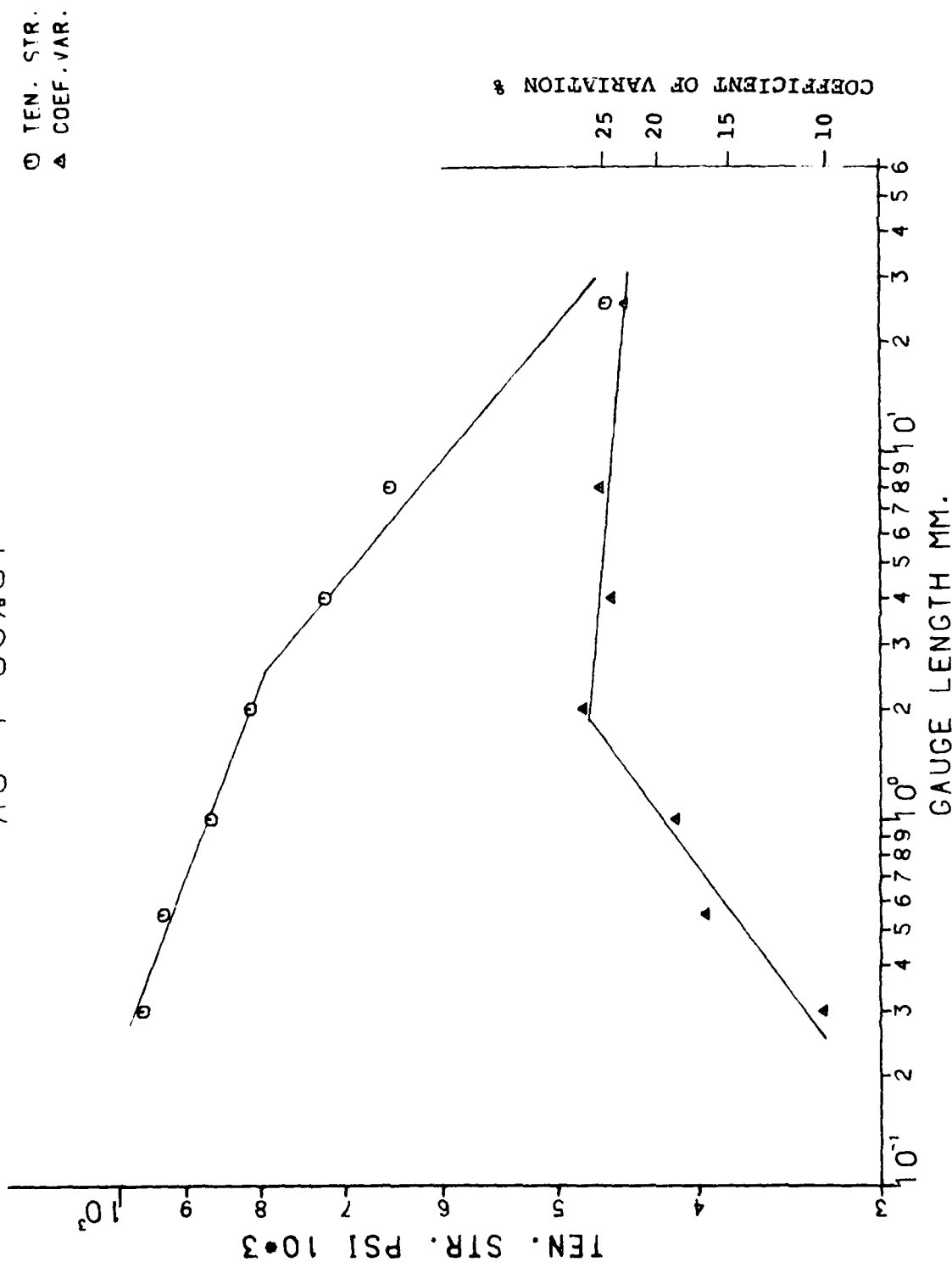


Figure 3. Tensile Strength as a Function of Length of AS-4 85% ST Fiber.

TABLE 42
TENSILE STRENGTH VS. GAUGE LENGTH FOR CARBON FIBERS
(TENSILE STRENGTH X 10^3 PSI + σ)

Sample Type:	AU	AS	AS-300°VHT	AS-600°VHT	AS-750°/H ₂	AU-1	AU-1C	AS-1	AS-1C	AS1-Epoxy	AS1-Allyl	AS1-Acst
Gauge Length (mm.)												
0.30	678±87	725±117	588±89	609±73	630±80	604±91	648±94	674±94	820±114	616±128	863±63	
0.40		656±49										
0.55	625±64	643±41	597±85	526±138	629±54	687±85	619±73		768±135	494±110	721±103	
1.0	569±102	613±57	640±70	527±113	530±78	599±47	590±115		710±110	470±127	700±108	
25.4	391±89	405±51	424±56	350±50	373±35		390±30	387±43	353±75	221±30	417±52	
Sample Type:												
	AU-4	AD-4C	AS-4	AS-4C	AS-4	AS-4	AS-4	AS-4	AS-4	HMU	HMS	HMS-300°VHT
Gauge Length (mm.)												
0.30	904±81											
0.35				757±105		962±97				599±82	580±75	588±68
0.55		759±113	739±151			842±133	932±154	818±144	863±114	479±69	526±78	534±68
0.80	864±132					792±213	864±162	766±251	821±177	482±77	518±92	597±63
1.0		726±99					811±225			452±98	495±90	445±94
2.0							721±177					
4.0							650±167					
8.0												
25.4	538±140		393±72	426±77	429±186	462±107	466±140	502±119	364±43	360±44	325±41	

d. Critical Length Studies

Loading in tension of a polymeric coupon containing a single carbon filament causes the fiber to fail in situ. With continued application of stress the fiber is further fragmented till the critical transfer length, ℓ_c , is attained. This value can be correlated to an average interphase shear strength (τ) by the relationship

$$\tau = \frac{\sigma_f}{2 \frac{\ell_c}{d}} \Gamma \left(1 - \frac{1}{\alpha}\right) \quad 1$$

where σ_f is the fiber tensile strength, d is the fiber diameter, Γ is the gamma function, and α is the Weibull shape parameter of the $\frac{\ell_c}{d}$ probability density function distribution. A detailed analysis of this technique can be found elsewhere.⁽⁸⁾

Work has proceeded in three areas: 1) evaluation of single filament interphase shear strength, 2) interphase response to hygrothermal exposure, 3) fabrication and testing of multi-filament (2-5) tensile coupons.

1) Interphase Shear Strength Measurement

Fiber tensile strength at the critical length is a required variable needed to calculate τ . One inch gauge length fiber tensile strengths previously used in calculating τ can now be replaced by σ_f measured at ℓ_c . These values are reported in Table 43. Using the fiber fracture strength at ℓ_c does not alter the relative ranking of fiber-matrix shear strengths. It does, however, increase the magnitude of τ .

A homologous series of fibers, such as AS4 70, 85, 100, and 120% ST, would be expected to exhibit the same tensile strength at a given length. However, deviations from this expectation are observed due to the large scatter in the data which typically has a coefficient of variation of 15%. Because of this scatter, tensile strengths for a homologous fiber series are averaged together to obtain the 'best' approximation of σ_f at ℓ_c .

TABLE 43
FIBER-MATRIX INTERPHASE SHEAR STRENGTH OF
SINGLE FILAMENTS IN EPON 828-mpDA MATRIX

Fiber	Weibull β	α	Tensile Strength at ϵ_c ($\cdot 10^3$ psi)	($\cdot 10^3$ psi)
AU1	70.14	2.6	670	6.9
AS1	38.77	3.5	650	10.7
AU1C	50.84	3.2	650	8.4
AS1C	26.56	3.9	700	16.2
AU4	99.49	3.3	860	5.5
AS4	57.24	3.1	760	8.9
AU4C	75.82	3.8	760	6.2
AS4C	43.77	4.1	760	10.5
AS-300°C VT	43.60	2.8	645	10.4
AS-600°C VT	37.31	3.6	580	9.9
AS-750°C VT	46.12	2.7	630	9.5
HMU	142.95	3.7	468	2.0
HMS	117.94	3.2	522	2.9
HMS-300°C VT	122.11	3.3	535	2.9
AS4-70% ST	70.85	3.0	865	8.1
AS4-85% ST	69.00	2.9	865	8.3
AS4-100% ST	68.89	2.7	865	8.8
AS4-120% ST	68.24	3.3	865	8.2
AS-100% RH-RT	85.10	3.3	640	4.9

2) Interphase Hygrothermal Response Evaluation

Interphase response to hygrothermal exposure is being evaluated using the single filament coupon technique. AS fibers embedded in Epon 828-mpDA matrix are being subjected to 100% relative humidity (RH) at either room temperature, 70°C, or 125°C until sample weight reaches a maximum. Measurements have been completed on the 100% RH at room temperature regime (AS-100% RH RT) tested in the hydrated condition.

After 202 days of exposure sample weight and length increases an average of 2.51% and 0.64% respectively. No fiber fractures or gross anomalies could be detected at the interphase using optical microscopy.

The critical length for these specimens is over 2X larger than the same fiber-matrix system not subjected to the high humidity environment. This loss in interphase adhesion may be attributed to a combination of bulk polymer and/or interphase deterioration. Further testing in this area is ongoing.

3) Multifilament Coupon

Efforts have been directed at fabricating and testing coupons containing two-five filaments aligned within a fiber diameter of each other, in order to study the processes of reinforcement. Only a few specimens of high integrity have been successfully fabricated to date primarily due to the difficult lay-up process. However, some general observations can be made regarding the performance of the multifilament coupons.

Two coupons each having two AS filaments aligned in close proximity were fabricated. In specimen "A" the fibers were within a diameter of each other whereas in specimen "B" the filaments were separated by three-four fiber diameters (~ 25 μ m). In "A" both filaments failed in concert, i.e., when one fiber fractured, the other would fail at the same position along the fiber axis. Nearly all breaks were located across from one another. Furthermore, the critical length for these two fibers was

measured to be ~ 20% greater than that of single filament coupons of the same materials. In "B" both fibers were observed to perform independently, and both achieved the expected value of single filament coupons.

In another sample a coupon containing five filaments with variable interfiber spacings was fabricated and tested. As load was applied to the coupon, the outermost fibers fractured first followed by the inner fibers. Again the fractures all occurred in close proximity to those in the adjacent filament as seen in Figure 5. The critical lengths measured for all five fibers are ~ 20% larger than the single filament coupon ℓ_c .



Figure 5. Multifilament Coupon Showing the Close Proximity of Fractures in Adjacent Fibers.

SECTION IV
MECHANICS OF COMPOSITES AND ADHESIVE
BONDED JOINTS

1. GLOBAL LOCAL VARIATIONAL PRINCIPLE FOR ELASTIC RESPONSE
OF COMPOSITE LAMINATES

a. Introduction

The principal problem of interest in the present investigation is the same as that treated in Ref. 9, i.e., the stress analysis of a composite laminate built of anisotropic elastic layers of uniform thickness and subjected to prescribed tractions and/or displacements on its boundary surfaces. The body is bounded by a cylindrical edge surface and upper and lower faces that are parallel to the interfacial planes. This assumption is made only for convenience in writing the governing equations. There is no difficulty in extending the model to include laminates of variable thickness.

In practical applications, numerous layers may be present (use of 100 layers in aircraft structures is not unusual). Contemporary models are incapable of providing precise resolution of the local stress fields in the vicinity of stress raisers under such conditions. Global models, which follow from an assumed, usually elementary, displacement field, lead to the definition of effective (or smeared) laminate moduli and are not sufficiently accurate for stress field computation.⁹ On the other hand, local models, in which each layer is represented as a homogeneous, anisotropic continuum, become intractable as the number of layers result in technical/economic barriers to accurate stress resolution. In this work we blend these concepts into a self-consistent model which can define detailed response functions in a particular, predetermined region of interest (local), while representing the remainder of the domain by effective properties (global). Such dual representations are not without precedent in solid mechanics. For example, Gurtin¹⁰ discussed this approach with reference to the solution of crack-tip stress field problems. Wang and

Crossman⁽¹¹⁾ used an effective modulus representation of regions of a laminate; however, only the extensional response of the regions were considered, i.e., the flexural and flexural-extension coupling characteristics of laminated bodies were ignored. Hence, that approach fails to provide correct solutions to certain elementary laminate problems for which exact solutions are available. Stanton et. al.⁽¹²⁾ used a global representation based upon a three dimensional laminate model developed by Pagano⁽¹³⁾ which is based upon the assumption that the stress field is only a function of one space coordinate. This is a generalization and improvement of the material model given in Ref. 11; however, this approach is not convenient for coupling with the model presented earlier.⁽⁹⁾ Furthermore, it is desirable to retain the model⁽¹⁴⁾ as a special degenerate case of a global model since that result was shown to produce very good agreement with a known elasticity solution for transverse normal stress σ_z .⁽¹⁵⁾

There have been several investigations of the interlaminar stress fields in laminated composites. Pagano⁽⁹⁾ has given a detailed description of the relevant literature in this field. A recent review article⁽¹⁶⁾ by Solomon presents an up-to-date literature survey in related topics as of 1980. In the present paper, reference will be made of only those publications which are not covered by Ref. 9 and 16. Spilker and Ting⁽¹⁷⁾ have conducted the static and dynamic analysis of composite laminates using hybrid stress finite elements. Raju et. al.⁽¹⁸⁾ have investigated the free edge stresses in layered plates using eight node isoparametric elements. In both these publications, the laminate idealization for a reasonably accurate finite element analysis had to be very fine, i.e. a quarter of the laminate was divided into about 600 elements. No more than four layers were considered for numerical calculations. For moderately large number of plies (say 10), these approaches will lead to computer storage/economic difficulties.

Blumberg et. al.⁽¹⁹⁾ studied the edge effects and stress concentrations in composite laminates made of glass sheets

bonded with polymer adhesive. The governing equations employed were similar in nature to those given in Ref. 9, however, not as general. For example, only isotropic layers were considered with the stiff layers being represented by the Kirchhoff-Love theory. Furthermore, the implied edge boundary conditions are not sufficient to satisfy the principle of "layer equilibrium".⁽⁹⁾ The differential equations were solved by perturbation technique defining the dependent variables at three different regions along the width of the laminate. This division of the width has enabled the authors to overcome computation overflow/underflow difficulties.

Finally, Partveskii⁽²⁰⁾ has presented an approximate treatment of a free edge problem. This model combines the treatment of Ref. 21 with a model based upon a layer on an elastic foundation in order to define the distribution of interlaminar normal stress.

b. Variational Principle

The laminate considered in the present investigation is shown in Figure 6. The laminate thickness comprising of $N + M$ layers is divided into two parts viz; (i) local region (ℓ) and (ii) global region (g). N is the number of layers in the local region and M is the number of layers in the global region. In this work, we shall assume that the interface between g and ℓ is a plane $z = \text{constant}$, although less restrictive assumptions are possible. A variational principle as described below has been used to derive the set of field equations and boundary conditions. Different variational functionals in two different regions of the laminate are used such that

$$\delta \left\{ \int_{V_g} \tilde{w} dv + \int_{V_\ell} \left[\frac{1}{2} \sigma_{ij} (u_{i,j} + u_{j,i}) - w \right] dv - \int_{S'} \tilde{T}_i u_i ds \right\} = 0 \quad (1)$$

where $\tilde{w} = \tilde{w}(u_i, e_{ij})$, $w = w(\sigma_{ij}, e_{ij})$ and body forces are neglected. (2)

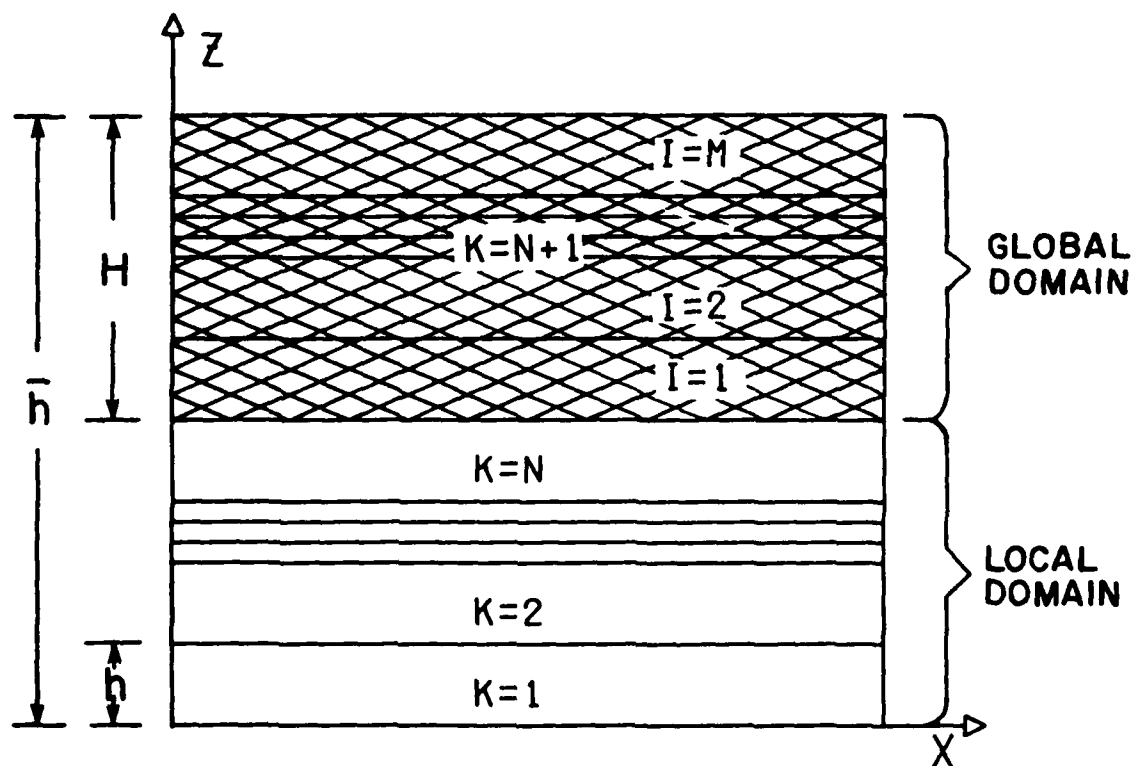


Figure 6. Laminate Half Thickness with One Local-Global Interface.

In equation (1), the first term represents the potential energy for the global region, the second term is the Reissner variational functional for layers in the local region and the third term is the potential energy of the prescribed surface tractions. The notation used here is the same as that of Reference 9, with the exception that the subscripts 'l' and 'g' denote, respectively, the local and global regions. In equation (2), \tilde{w} and w are strain energy density functions, the first in terms of displacements u_i and e_{ij} , the expansional strain components, and the second in terms of stresses σ_{ij} and e_{ij} .

For a layered continuum in the local region, equation (1) can be rewritten as

$$\delta \left\{ \sum_{k=1}^N \int_{V_k} \left[\frac{1}{2} \sigma_{ij} (u_{i,j} + u_{j,i}) - w \right]^{(k)} dv_k - \int_{S'} \tilde{\tau}_i u_i ds + \int_{V_g} \tilde{w} dv \right\} = 0. \quad (3)$$

where the superscript (k) attached to the bracket signifies that each variable within the bracket is associated with the kth layer. The use of Green-Gauss theorem and some mathematical manipulations in equation (3) yield the following equation,

$$\sum_{k=1}^N \int_{V_k} \left[\left(\frac{u_{i,j} + u_{j,i}}{2} - \frac{\partial w}{\partial \sigma_{ij}} \right) \delta \sigma_{ij} - \sigma_{ij,j} \delta u_i \right]^{(k)} dv_k + \int_{S'_l} (\tau_i - \tilde{\tau}_i) \delta u_i ds + \int_{S''_l} \tau_i \delta u_i ds + \sum_{k=1}^{N-1} \int_{I_k} (\tau_i^{(k)} \delta u_i^{(k)} + \tau_i^{(k+1)} \delta u_i^{(k+1)}) ds = 0 \quad (4)$$

$$\begin{aligned} & \tau_i^{(k+1)} \delta u_i^{(k+1)} dI_k - \int_{V_g} \sigma_{ij,j} \delta u_i dv + \int_{S'_g} (\tau_i - \tau'_i) \delta u_i ds + \int_{S''_g} \tau_i \delta u_i ds \\ & + \int_{\bar{S}} (\tau_i^{(l)} + \tau_i^{(g)}) \delta u_i ds = 0. \end{aligned}$$

where V_k is the volume of k th layer, S'_l and S''_l represent the outer surfaces bounding the local region, the former representing the portion with prescribed tractions and the latter with prescribed displacements. I_k'' represents the interlaminar surface between k th and $(k+1)$ th layers in local region that does not belong to S' or S'' , S'_g and S''_g represent the bounding surfaces for the global domain with prescribed traction and prescribed displacement conditions, respectively. \bar{S} represents the surface common to the local domain and the global domain. A superscript/subscript l denotes the local region and g denotes the global region. Clearly, as shown by equation (4), the governing equations of elasticity can be obtained as a consequence of variational equation (1). Equation (4) will be used to derive the field equations and boundary conditions for the two regions of the laminate.

c. Development of Theory

For each layer in the local domain, the theory developed in Ref. 9 has been used. The details of the derivation of equilibrium equations and continuity and boundary conditions for this domain are not repeated in this report. For the sake of continuity, only relevant equations are provided. Figure 7 shows the coordinate axes and thickness of a single layer in the laminate. The interlaminar stresses σ_z , τ_{xz} , and τ_{yz} at the top of the layer are denoted by p_2 , t_2 and s_2 , respectively, while the corresponding stresses at the bottom of the layer are designated as p_1 , t_1 , and s_1 . In the local domain the inplane stress components are assumed to vary linearly through the thickness of each ply. The substitution of these stress components in the differential equations of equilibrium⁽⁹⁾ yields the interlaminar stress components in

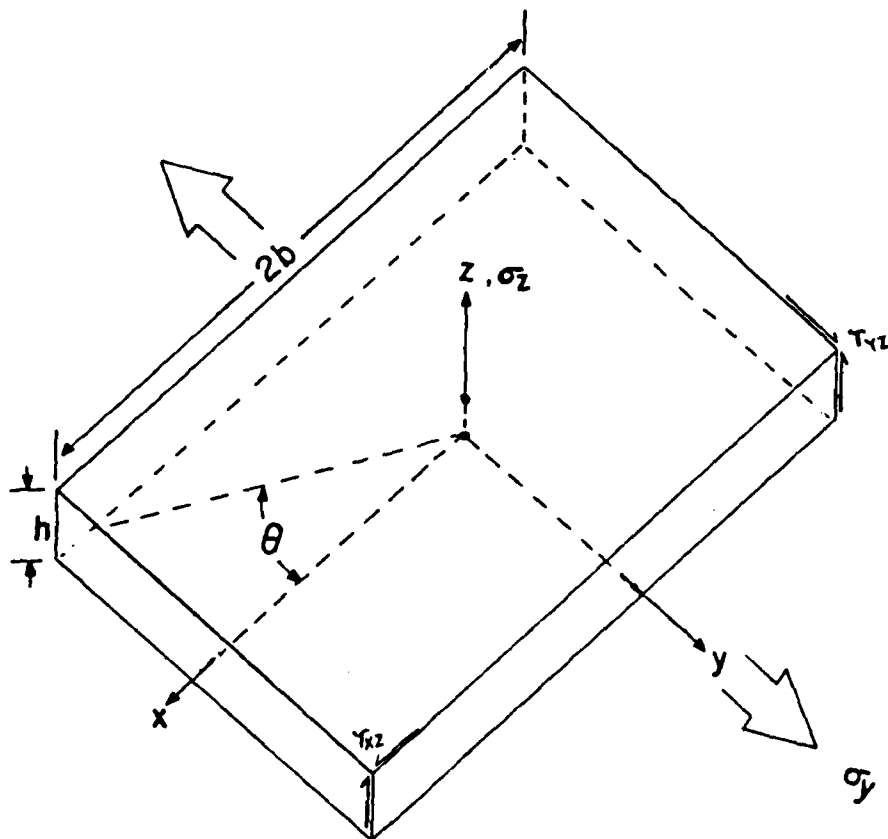


Figure 7. Ply Coordinate Axes and Rotation Notation.

terms of tractions p_i , t_i , s_i ($i = 1, 2$) and force and moment resultants. These stress-stress resultant relations have been used in equation (4) in local domain integrals. In the global domain, an assumed continuous thickness distribution of the displacement field is used. On the basis of these facts, the field equations, interfacial boundary conditions, and edge conditions within the local continuum remain the same as derived in Reference 9. The development of the required relations for the global domain and global/local interface follows. We assume that the global domain is composed of layers, each possessing a single plane of elastic symmetry, $z = \text{constant}$. In this domain, the displacements are assumed to be of the form

$$\begin{aligned} u &= u^0(x, y) + z\psi_x(x, y) \\ v &= v^0(x, y) + z\psi_y(x, y) \\ w &= w^0(x, y) + z\psi_z(x, y) + \frac{z^2}{2}\phi(x, y) \end{aligned} \quad (5)$$

where u , v and w are the displacement components in the x , y and z directions, respectively. It can be seen that the number of displacement functions agrees with that given by the variational principle for each layer in the local domain. The substitution of the displacement functions (5) into the strain displacement relations of elasticity leads to the following stress-strain relations

$$\begin{aligned} \sigma_i &= C_{ij} (\epsilon_j^0 + z\kappa_j - e_j) \quad (i, j = 1, 2, 3, 6) \\ \sigma_i &= C_{ij} (\epsilon_j^0 + z\kappa_j + \frac{z^2}{2}\beta_j) \quad (i, j = 4, 5) \end{aligned} \quad (6)$$

in standard contracted notation, where C_{ij} are the components of the anisotropic stiffness matrix, e_j are engineering expansional strain components and ϵ_i^0 , κ_i and β_i are defined by

$$\begin{aligned} \epsilon_1^0 &= \frac{\partial u^0}{\partial x}, \quad \epsilon_2^0 = \frac{\partial v^0}{\partial y}, \quad \epsilon_3^0 = \psi_z \\ \epsilon_4^0 &= \psi_y + \frac{\partial w^0}{\partial y}, \quad \epsilon_5^0 = \psi_x + \frac{\partial w^0}{\partial x}, \quad \epsilon_6^0 = \frac{\partial u^0}{\partial y} + \frac{\partial v^0}{\partial x} \\ \kappa_1 &= \frac{\partial \psi_x}{\partial x}, \quad \kappa_2 = \frac{\partial \psi_y}{\partial y}, \quad \kappa_3 = \phi \\ \kappa_4 &= \frac{\partial \psi_z}{\partial y}, \quad \kappa_5 = \frac{\partial \psi_z}{\partial x}, \quad \kappa_6 = \frac{\partial \psi_x}{\partial y} + \frac{\partial \psi_y}{\partial x} \\ \beta_4 &= \frac{\partial \phi}{\partial y}, \quad \beta_5 = \frac{\partial \phi}{\partial x} \end{aligned} \quad (7)$$

The stress components $\sigma_1, \sigma_2, \sigma_3, \sigma_4, \sigma_5, \sigma_6$ stand for $\sigma_x, \sigma_y, \sigma_z, \tau_{yz}, \tau_{xz}, \tau_{xy}$, respectively, while ϵ_i^0 ($i = 1, 2, \dots, 6$) represent corresponding engineering inplane strain components. We introduce the following stress and moment resultants

$$\begin{aligned} N_i &= \int_{-H/2}^{H/2} \sigma_i dz & (i = 1, 2, 3, 6) \\ M_i &= \int_{-H/2}^{H/2} \sigma_i z dz \end{aligned} \quad (8)$$

where H is the thickness of the global region and N_3 and M_3 are mathematical, not physical, quantities.

Substituting equations (6) into (8) and conducting the integration, we obtain the following constitutive relations for the global domain

$$\begin{aligned} N_\alpha &= \tilde{A}_{\alpha\beta} \epsilon_\beta^0 + \tilde{B}_{\alpha\beta} \kappa_\beta - \bar{P}_\alpha \\ M_\alpha &= \tilde{B}_{\alpha\beta} \epsilon_\beta^0 + D_{\alpha\beta} \kappa_\beta - \bar{Q}_\alpha & (\alpha, \beta = 1, 2, 3, 6) \\ V_i &= \tilde{A}_{ij} \epsilon_j^0 + \tilde{B}_{ij} \kappa_j + \frac{1}{2} D_{ij} \beta_j \\ R_i &= \tilde{B}_{ij} \epsilon_j^0 + D_{ij} \kappa_j + \frac{1}{2} F_{ij} \beta_j & (i, j = 4, 5) \\ S_i &= \frac{1}{2} D_{ij} \epsilon_j^0 + \frac{1}{2} F_{ij} \kappa_j + \frac{1}{4} H_{ij} \beta_j \end{aligned} \quad (9)$$

where

$$\begin{aligned} (\tilde{A}_{ij}, \tilde{B}_{ij}, D_{ij}, F_{ij}, H_{ij}) &= \int_{-H/2}^{H/2} (1, z, z^2, z^3, z^4) C_{ij} dz & (i, j = 1, 2, \dots, 6) \\ \bar{P}_\alpha &= \int_{-H/2}^{H/2} C_{\alpha\beta} e_\beta dz \\ \bar{Q}_\alpha &= \int_{-H/2}^{H/2} z C_{\alpha\beta} e_\beta dz & (\alpha, \beta = 1, 2, 3, 6) \\ (V_i, R_i, S_i) &= \int_{-H/2}^{H/2} \sigma_i (1, z, z^2) dz & (i = 4, 5) \end{aligned}$$

With the knowledge of the distribution of elastic properties C_{ij} and expansional strains, one can obtain the values of effective stiffness matrices \tilde{A} , \tilde{B} , D , F and H ; and effective "nonmechanical" stress and moment resultants, \bar{P}_i and \bar{Q}_i .

As in Ref. 9, we make the following definitions

$$(\bar{f}, f^*, \hat{f}) = \int_{-H/2}^{H/2} f(1, \frac{2z}{H}, \frac{4z^2}{H^2}) \frac{2dz}{H} \quad (10)$$

where f may represent any of the displacement variables u , v and w . Through the use of relations (5) and (10), the functions involved in the displacements for the global domain can be expressed as

$$u^o = \frac{1}{2} \bar{u}$$

$$v^o = \frac{1}{2} \bar{v}$$

$$w^o = \frac{9}{8} \bar{w} - \frac{15}{8} \hat{w}$$

$$\psi_x = \frac{3}{H} u^*$$

$$\psi_y = \frac{3}{H} v^*$$

$$\psi_z = \frac{3}{H} w^*$$

$$\phi = \frac{45}{H^2} (\hat{w} - \frac{\bar{w}}{3}).$$

(11)

With these relationships, one can express the constitutive relations for the global domain in terms of the same displacement parameters as those for the local domain. This simplifies the definition of the required continuity conditions.

With the use of the assumed stress field in the local region and displacement fields in the global region in equation (4), the required field equations, continuity and boundary conditions can be obtained. For the local region the equilibrium equations, constitutive relations, edge conditions and interfacial continuity conditions are given in Ref. 9. For the global region the equilibrium equations, which follow from substituting (5) into (4), become

$$\begin{aligned}
N_{1,x} + N_{6,y} + t_2 - t_1 &= 0 \\
N_{6,x} + N_{2,y} + s_2 - s_1 &= 0 \\
-N_3 + R_{4,y} + R_{5,x} + \frac{H}{2} (p_1 + p_2) &= 0 \\
M_{1,x} + M_{6,y} - V_5 + \frac{H}{2} (t_2 + t_1) &= 0 \\
M_{6,x} + M_{2,y} - V_4 + \frac{H}{2} (s_2 + s_1) &= 0 \\
V_{5,x} + V_{4,y} + p_2 - p_1 &= 0 \\
-M_3 + S_{4,y} + S_{5,x} + \frac{H^2}{8} (p_2 - p_1) &= 0
\end{aligned} \tag{12}$$

where the symbols t_i , s_i , and p_i ($i = 1, 2$) retain the same meaning as defined earlier for the local domain. Assuming perfect continuity of tractions and displacements at the g-l interface, the local-global interfacial conditions are given by the previous substitution into (4), as

$$\begin{aligned}
t_2^{(k)} &= t_1^{(k+1)} \\
s_2^{(k)} &= s_1^{(k+1)} \\
p_2^{(k)} &= p_1^{(k+1)}
\end{aligned} \tag{13}$$

and (a) local-global (interface I of Figure 7a).

$$\begin{aligned}
[\beta_5 - S_{45}T_4 - S_{55}T_5]^{(k)} &= [-u^\circ + \frac{H}{2} \psi_x]^{(k+1)} \\
[\beta_4 - S_{44}T_4 - S_{45}T_5]^{(k)} &= [-v^\circ + \frac{H}{2} \psi_y]^{(k+1)} \\
[\gamma_2 - S_{33}R_2]^{(k)} &= [-w^\circ + \frac{H}{2} \psi_z - \frac{H^2}{8} \phi]^{(k+1)}
\end{aligned} \tag{13a}$$

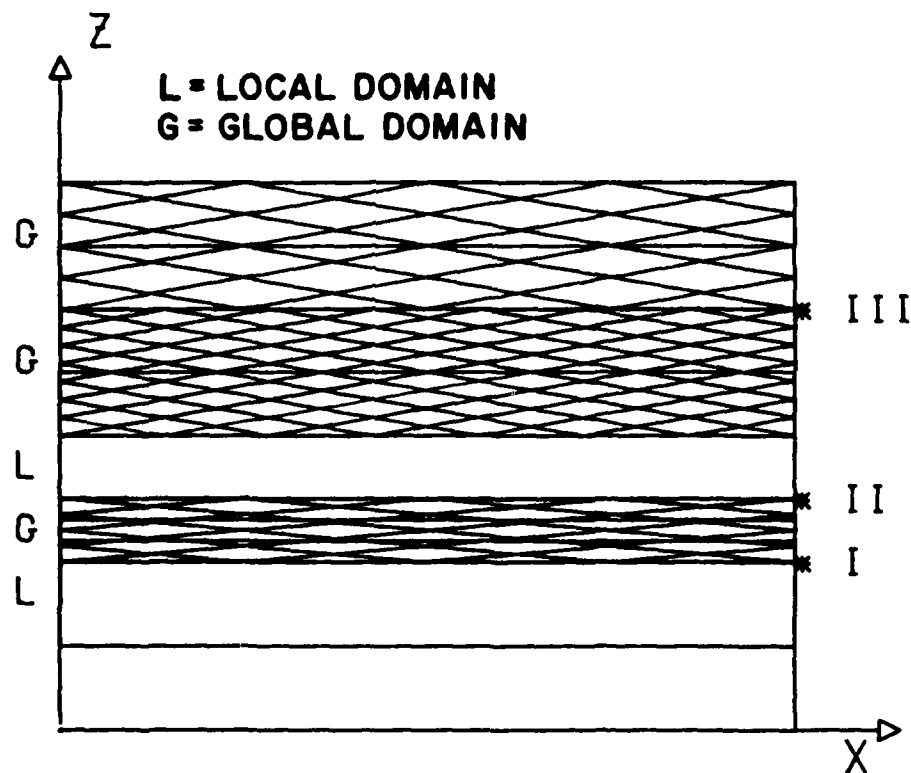


Figure 7a. Laminate Half Thickness Divided into more than One Global Domain with Different Types of Interfaces. I - Local-Global Interface, II - Global-Local Interface, III - Global-Global Interface.

It can be shown that if we consider more than one global region, the following interfacial conditions are required:

(b) global-local (interface II of Figure 7a)

$$\begin{aligned} [u^\circ + \frac{H}{2}\psi_x]^{(k)} &= [\alpha_5 - S_{45}Q_4 - S_{55}Q_5]^{(k+1)} \\ [v^\circ + \frac{H}{2}\psi_y]^{(k)} &= [\alpha_4 - S_{44}Q_4 - S_{45}Q_5]^{(k+1)} \\ [w^\circ + \frac{H}{2}\psi_z + \frac{H^2}{8}\phi]^{(k)} &= [\gamma_1 - S_{33}R_1]^{(k+1)} \end{aligned} \quad (13b)$$

(c) global-global (interface III of Figure 7a)

$$\begin{aligned} [u^\circ + \frac{H}{2}\psi_x]^{(k)} &= [u^\circ - \frac{H}{2}\psi_x]^{(k+1)} \\ [v^\circ + \frac{H}{2}\psi_y]^{(k)} &= [v^\circ - \frac{H}{2}\psi_y]^{(k+1)} \\ [w^\circ + \frac{H}{2}\psi_z + \frac{H^2}{8}\phi]^{(k)} &= [w^\circ - \frac{H}{2}\psi_z + \frac{H^2}{8}\phi]^{(k+1)} \end{aligned} \quad (13c)$$

where the parameters with superscript 'k+1' represent those for the layer above the kth layer. The parameters on the left-hand side of equations (13a) and right-hand side of equations (13b) are defined in Reference 9. In the expression for R_2 of Ref. 9 the roles of p_1 and p_2 were interchanged by mistake whereas R_1 was correct. The correct expression for R_2 is

$$R_2 = \frac{(6p_2 + p_1)h^2 - 7hN_z - 30M_z}{70h} \quad (14)$$

For the edge surface of the global domain, one term each of the following products must be prescribed:

$$N_n u_n^\circ, N_{ns} u_s^\circ, M_n \psi_n, M_{ns} \psi_s, V_n w^\circ, R_n \psi_z, S_n \phi. \quad (15)$$

The boundary conditions at the top surface are given by

$$\begin{aligned} t_2^{(N+1)} &= \hat{t}_2^{(N+1)} \quad \text{or} \quad u^\circ + \frac{H}{2}\psi_x = \hat{U} \\ s_2^{(N+1)} &= \hat{s}_2^{(N+1)} \quad \text{or} \quad v^\circ + \frac{H}{2}\psi_y = \hat{V} \\ p_2^{(N+1)} &= \hat{p}_2^{(N+1)} \quad \text{or} \quad w^\circ + \frac{H}{2}\psi_z + \frac{H^2}{8}\phi = \hat{W} \end{aligned} \quad (16)$$

where the right hand sides in the aforementioned equations (16) represent the prescribed external tractions or displacements. The boundary conditions at the bottom surface remain the same as those explained in Reference 9. This completes the development of the present theory. We observe that the governing equations for the global continuum, equations (9), (12-13), combined with the governing equations for the local continuum, equations (25-28) of Ref. 9, and boundary conditions at the bottom and the top surfaces constitute a set of $23N + 27$ equations in terms of like number of unknowns. This system can be reduced to $13(N+1)$ equations by eliminating the force and moment resultants from the set of governing equations. Relations (15) show that seven edge conditions are required for the global domain, while 7N edge conditions are required for the local domain, equations (29) of Ref. 9.

d. Problem Description

The present model has been used to conduct the free edge stress analysis in a symmetric laminate consisting of $2(N+M)$ perfectly bonded layers (see Figure 6). The laminate is subjected to forces applied only on the ends $y = \text{const.}$ such that a constant axial strain $\epsilon_y = \epsilon_0$ is imposed. Because of the symmetry in ply orientation of the laminate about the midplane, the deformation is symmetric with respect to x and z . Only the z symmetry will be employed in the specific problem treated, so that half of the laminate thickness has been considered. The lower N layers form the local region, whereas the remaining M layers constitute the global region. The stress field in this class of problems is a function of x and z alone, and consequently the force and moment resultants and the interlaminar stresses depend on x only.

The theory derived herein has been employed for solving the edge delamination class of boundary value problems. The governing equations have been solved for the determination of stress distribution in the laminate, for a large number of laminates. The derivation of equations for this particular class of boundary value problems is given in Reference 22. These equations

have been solved for various laminates and the numerical results thus obtained are used for the understanding of edge delamination of composite laminates. (Reference 23, 24)

The research and rationale leading to the development of the global-local model to examine the detailed elastic response of composite laminates is reviewed. The accuracy of the global-local model for elastic stress field analysis of composite laminates is examined by comparison of solutions with this model to those given by purely local models developed in previous work. Emphasis is placed on free-edge laminates under interlaminar normal stresses of small magnitude since they present the most severe challenge to the model. This leads to a good understanding of the range of validity of the model. The global-local model is used in conjunction with experimental data to examine a proposed failure criterion for delamination and to define the range where significant influence of the interlaminar stresses on free-edge laminate failure response is present. (Reference 25)

2. EXPERIMENTAL DETERMINATION OF INTERLAMINAR NORMAL STRESS

To determine the σ_z experimentally, strain in thickness direction was measured at the free edge by employing a miniature strain gauge and calculating the normal stress from three-dimensional constitutive relations in conjunction with axial and transverse strain.

The immediate problem encountered was the selection of a suitable strain gauge size to measure the strain with a reasonable accuracy at the point where a large stress gradient is expected. To resolve this problem, the distribution of the interlaminar normal stress at the region of the midplane of several laminates is obtained from the analysis (50) and presented in Figure 8. The analytical result indicates that σ_z is fairly uniform at the immediate region of midplane. The flat region of σ_z varies depending upon the center layer thickness as well as the laminate thickness. Figure 8 clearly indicates that the strain gauge size

AD-A128 569 IMPROVED MATERIALS FOR COMPOSITE AND ADHESIVE JOINTS

2/2

R KIM /W. /CLICK ET AL. JAN 83 UDR-TR-82-118

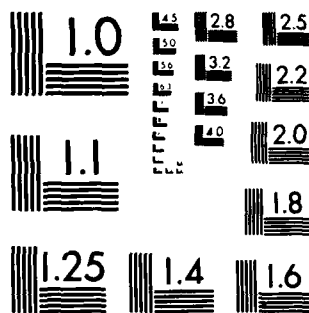
UNCLASSIFIED AFWAL-TR-82-4182 F33615-81-C-5056

AFWAL-TR-82-4182 F33615-81-C-5056

F/G 11/4

NL

END
DATE
FILMED
1 1962
DTIC



MICROCOPY RESOLUTION TEST CHART
NATIONAL BUREAU OF STANDARDS 1963-A

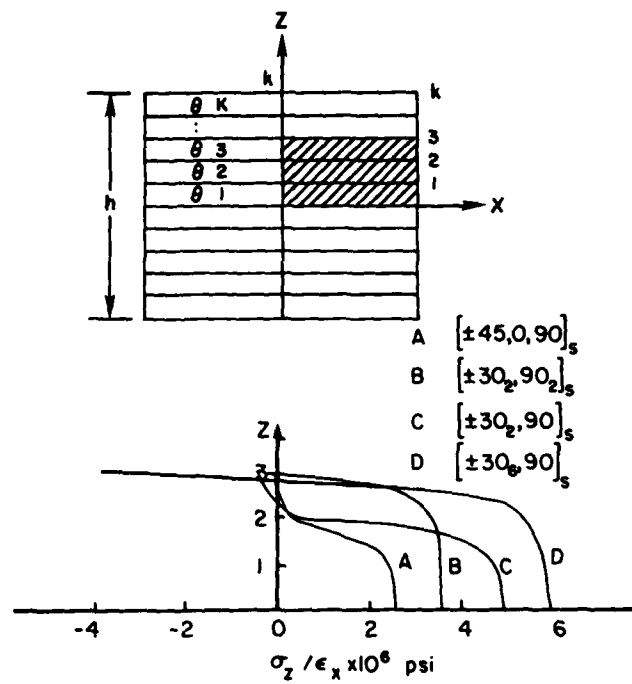


Figure 8. Variation of σ_z at the Free-Edge Obtained from Analysis.

will significantly influence the result of measurement since the strain measured by a strain gauge is the average strain of the gauge length used. The experimental result of strain gauge size effect is shown in Figure 9. This is obtained from three sizes of strain gauges mounted on a free edge of the $[\pm 30_2/90_2]_s$ laminate. Based on analytical and experimental results, a strain gauge with a gauge length of 0.008 in. was chosen to measure ϵ_z supplied by Micromasurement, Inc.

A preliminary test was conducted to insure the validity of such a small strain gauge for measurement of strain in composite laminates. For this purpose, three strain gauges were mounted on a unidirectional laminate, $[0]_{8T}$, one in each x, y, and z direction. Strain gauges in x and y directions were mounted on a free surface of the specimen. Figure 10 shows ϵ_y and ϵ_z vs. the axial strain, ϵ_x , with the location of the strain gauges. The longitudinal modulus is determined to be 20.3×10^6 psi. The Poisson's ratios, ν_{xy} and ν_{xz} , were found to be identical and determined to be 0.29. These elastic constants are practically identical for those of the material system.

To calculate the magnitude of the interlaminar normal stress using the analysis developed in Section 1 and measured strains, the following material properties (T300/5208 Gr/Ep) were used.

$$\begin{aligned} E_{xx} &= 20 \times 10^6 \text{ psi} & E_{yy} &= E_{zz} = 1.4 \times 10^6 \text{ psi} \\ G_{xy} &= G_{xz} = 0.8 \times 10^6 \text{ psi} & G_{yz} &= 0.55 \times 10^6 \text{ psi} \\ \nu_{xy} &= 0.3 & \nu_{yz} &= 0.5 & \nu_{yx} &= 0.021 \end{aligned}$$

where E is the Young's modulus, ν is the Poisson's ratio, and G is the shear modulus. Poisson's ratio ν_{yz} was obtained from Reference 26. Figures 11 and 12 show the experimentally measured ϵ_z plotted against applied axial strain for $[\pm 30_n/90_n]$ and $[(\pm 30)_n/90]_s$ laminates, respectively. The data point indicated with solid symbol for respective laminates represents onset of

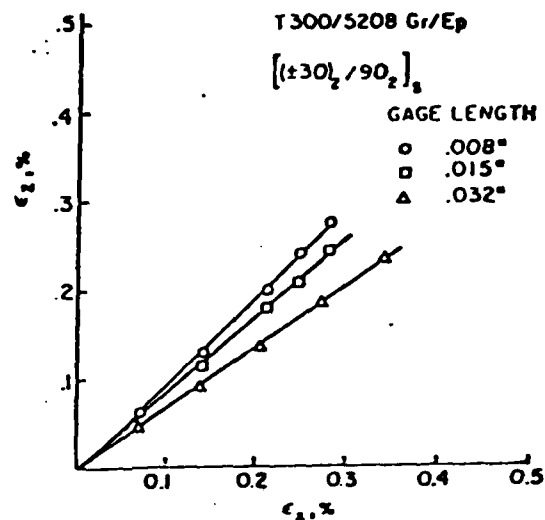


Figure 9. Effect of Strain Gauge Size on the Measurement of ϵ_z .

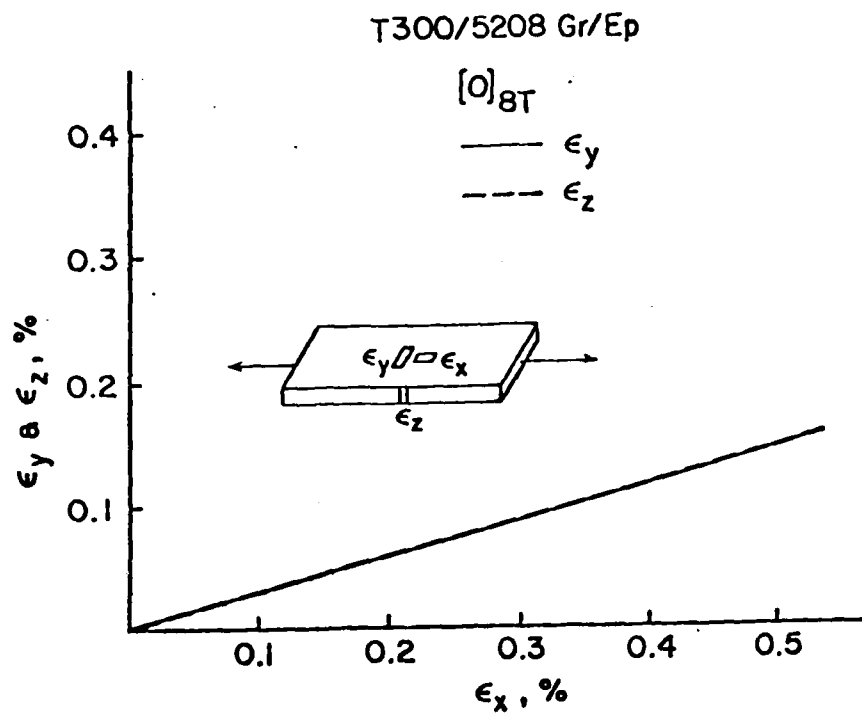


Figure 10. Transverse Strain vs. Axial Strain.

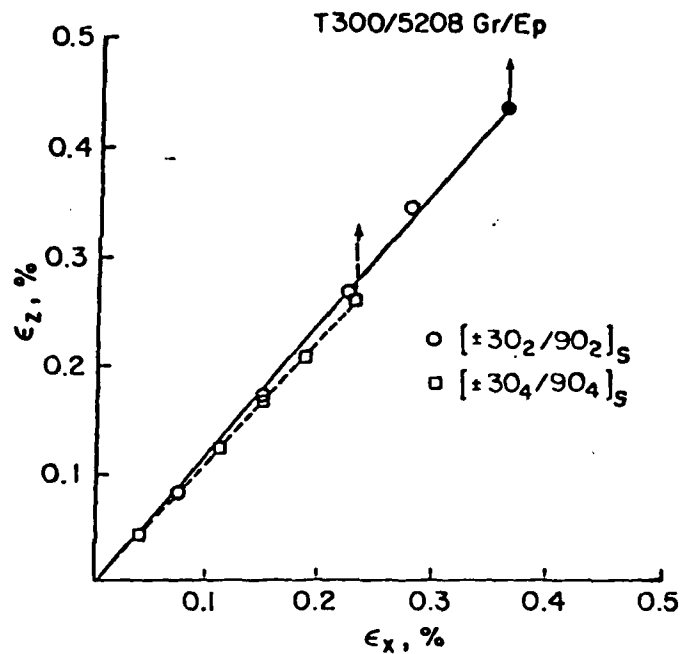


Figure 11. Transverse Strain ϵ_z vs. Axial Strain ϵ_x for $[\pm 30_2/90_2]_S$ and $[\pm 30_4/90_4]_S$.

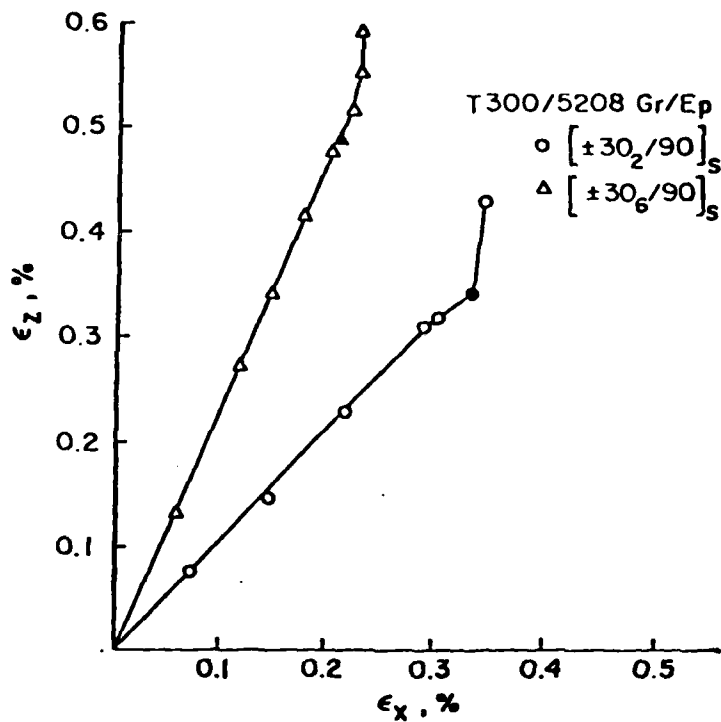


Figure 12. Transverse Strain ϵ_z vs. Axial Strain ϵ_x for $[(\pm 30)_2/90]_S$ and $[(\pm 30)_6/90]_S$.

delamination observed by acoustic emission. In all cases, ϵ_z is linearly related with applied axial strain, ϵ_x , up to onset of delamination and thereafter either increases nonlinearly or indicates overflow. In some other specimens, ϵ_z shows a finite jump prior to onset of delamination and increases with approximately the same initial slope until delamination. This finite jump is believed to be due to a transverse crack which occurred under the strain gauge. The measured values of ϵ_z for both $[\pm 30_2/90_2]_s$ and $[\pm 30_4/90_4]_s$ are practically equal as predicted by analysis (see Figure 11). The experimentally measured transverse strain, ϵ_y , is also plotted against axial strain, ϵ_x , in Figure 13. The variation of ϵ_y obtained by analysis is also indicated in Figure 13. Although the experimentally obtained ϵ_y cannot make a direct comparison with analytical strain because of high strain gradient in the region of strain gauge, the experimental result appears to be enough to support the analysis. It should be noted that the Poisson's ratio measured at the center of the surface was .31 which is close to .304 predicted by laminated plate theory.

Because of the difficulty to the instrument a transverse strain gauge (y direction) at the midplane, calculated ϵ_y was used in conjunction with the measured strains of ϵ_x and ϵ_y to determine σ_z . The stress component σ_z in material coordinate system for a monoclinic material with $z = 0$ as the plane of symmetry is given by Reference 27,

$$\sigma_3 = C_{13}e_1 + C_{23}e_2 + C_{33}e_3 + C_{36}e_6 \quad (17)$$

where C_{ij} are the elements of stiffness matrix and can be obtained from engineering constants of the material system. Equation (17) is employed to calculate σ_z from measured strains except ϵ_y after the required transformation of the stiffness matrix.

The experimental results for all the laminates tested are presented along with the analytical calculation in Table 44.

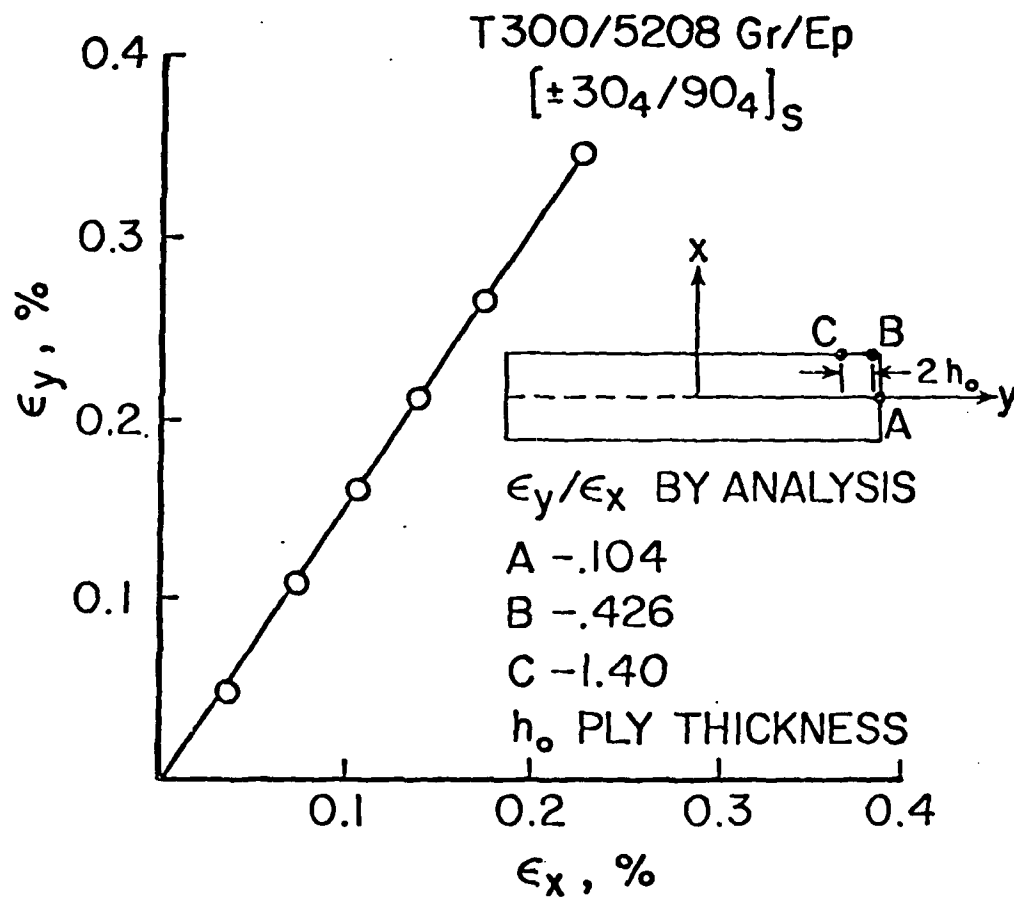


Figure 13. Transverse Strain ϵ_y vs. Axial Strain ϵ_x .

TABLE 44
 σ_z AT MIDPLANE OF LAMINATE FOR APPLIED
 AXIAL STRAIN OF 0.1%

Laminate	σ_z , psi		
	*Analysis	Experiment	No. of Specimens
$[\pm 30_2/90_2]_s$	3,120	2,870	3
$[\pm 30_4/90_4]_s$	3,120	3,060	3
$[(\pm 30)_2/90]_s$	4,320	3,110	2
$[(\pm 30)_4/90]_s$	4,600	4,360	2
$[(\pm 30)_6/90]_s$	4,800	4,640	3

*Without presence of curing residual stress

The experimentally determined σ_z compares very well with the analytical result for all laminates except for $[(\pm 30)_2/90]_s$.

Table 45 shows the experimentally determined σ_z at the onset of delamination.

TABLE 45
 σ_z AND APPLIED AXIAL STRAIN AT ONSET OF DELAMINATION

Laminate	Axial Strain, ϵ	σ_z , ksi
$[\pm 30_2/90_2]_s$.35	10.05
$[\pm 30_4/90_4]_s$.22	6.73
$[(\pm 30)_2/90]_s$.30	9.33
$[(\pm 30)_4/90]_s$.23	9.85
$[(\pm 30)_6/90]_s$.21	9.75

The magnitude of σ_z at the onset of delamination is almost identical for all laminates except for $[\pm 30_4/90_6]_s$. The average of σ_z excluding $[\pm 30_4/90_4]_s$ is determined to be 9.78 ksi which is considerably greater than the transverse strength (7.5 ksi) of the material system.

3. ONSET OF DELAMINATION

An effort has been made to develop a methodology to predict onset of free-edge delamination based on the stress and failure analysis considering effect of transverse crack. In previous sections it was indicated that the calculated interlaminar normal stress at onset of delamination was found to be approximately 30 percent greater than the transverse strength of the material system. This discrepancy could be due to the large gradient of the σ_z along the y-direction which is indicated in Figure 14. This problem is similar to the hole size effect discussed in Ref. 28. The explanation of hole size effect was based simply on the difference that exists in the normal stress distribution ahead of a hole for different sized holes. It is known that, although all sized holes have the same stress concentration factor, the normal stress perturbation from a uniform stress state is considerably more concentrated near the larger hole boundary than in the case of the smaller hole. Thus, intuitively, one might expect the plate containing the smaller hole to be the stronger of the two.

Two types of failure criteria have been considered in conjunction with the σ_z distribution obtained from the analytical work in Section 1. The first failure criterion referred to as the "maximum point stress criterion," assumes failure to occur when σ_z at the free edge reaches the interlaminar tensile strength of the material, S_I , that is, when

$$\sigma_z(y, 0) \Big|_{y=h} = S_I \quad (18)$$

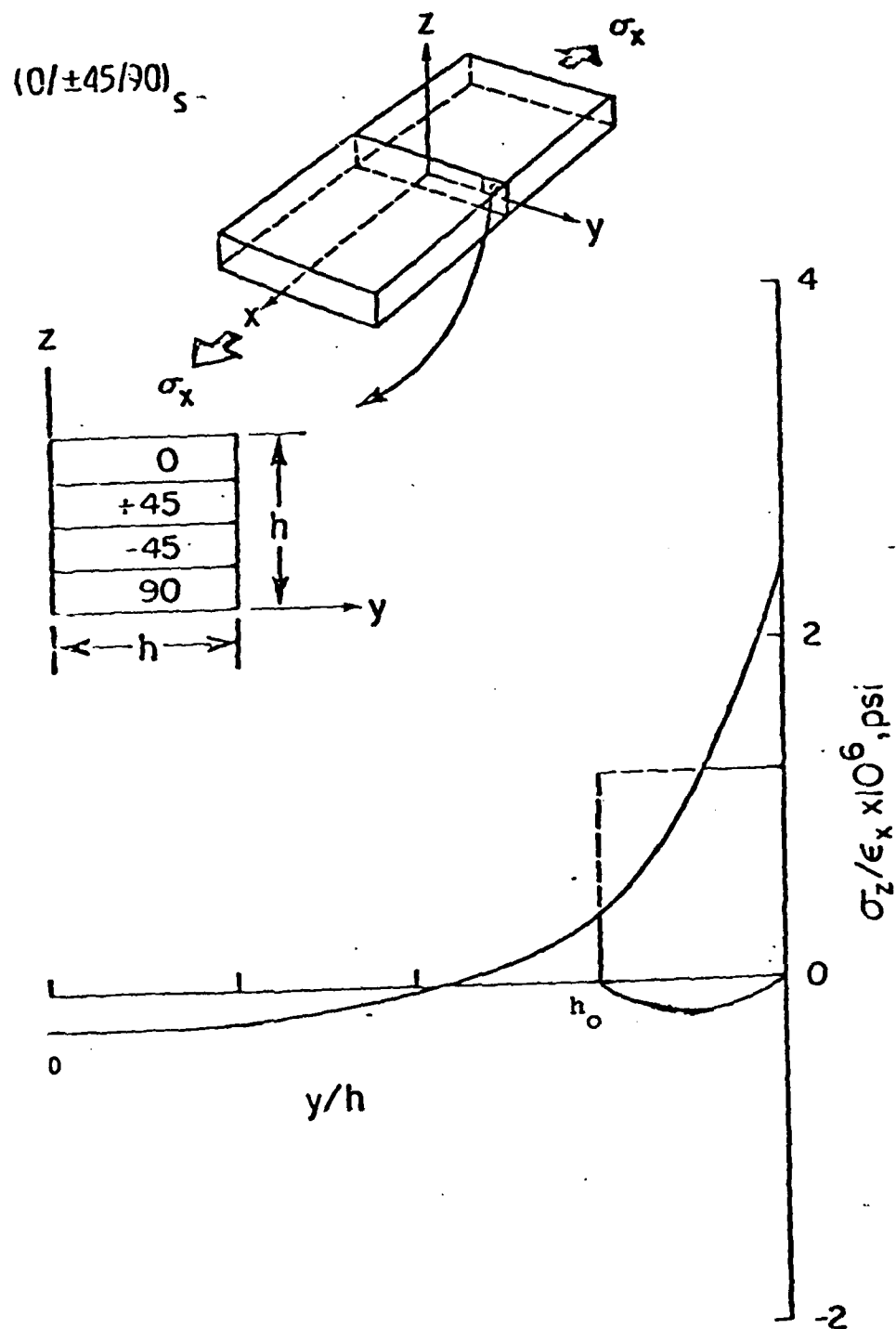


Figure 14. Interlaminar Normal Stress Distribution Along Y-Direction.

The second alternative failure criterion referred to as the "average stress criterion", assumes failure to occur when the average value of σ_z over some fixed distance, h_o , ahead of the free edge reaches the S_I , that is, when

$$\frac{1}{h_o} \int_{h-h_o}^{h_o} \sigma_z(y,0) dy = S_I. \quad (19)$$

The critical length, h_o , was taken as the one ply thickness for all cases. Because of experimental difficulty to determine the interlaminar tensile strength (S_I) of composite laminate, the interlaminar tensile strength assumed to be equal to the transverse strength of the material. The transverse strength of the T300/5208 graphite/epoxy is 7.5 ksi. The stress level at onset of delamination was determined by using acoustic emission. Sudden jump of acoustic signal indicates the initiation of delamination as shown in Figure 15.

The type of laminates studied in this program are as follows:

Under Uniaxial Tension

$[(+30)_n/90]_s$	$n = 1, 2, 4, 6, \text{ and } 10$
$[+30_n/90_n]_s$	$n = 1, 2, \text{ and } 4$
$[0/+45/90_n]_s$	$n = 1, 3, \text{ and } 6$
$[0_n/+45_n/90_n]_s$	$n = 1, 2, \text{ and } 3$

Under Uniaxial Compression

$[0/90_n/+45]_s$	$n = 1, 3, \text{ and } 6$
$[0_n/90_n/+45_n]_s$	$n = 1, 2, \text{ and } 3$

The first four families of laminates show the tensile σ_z at midplane of free edge under applied uniaxial tension, while the last two families of laminates show the tensile σ_z under applied

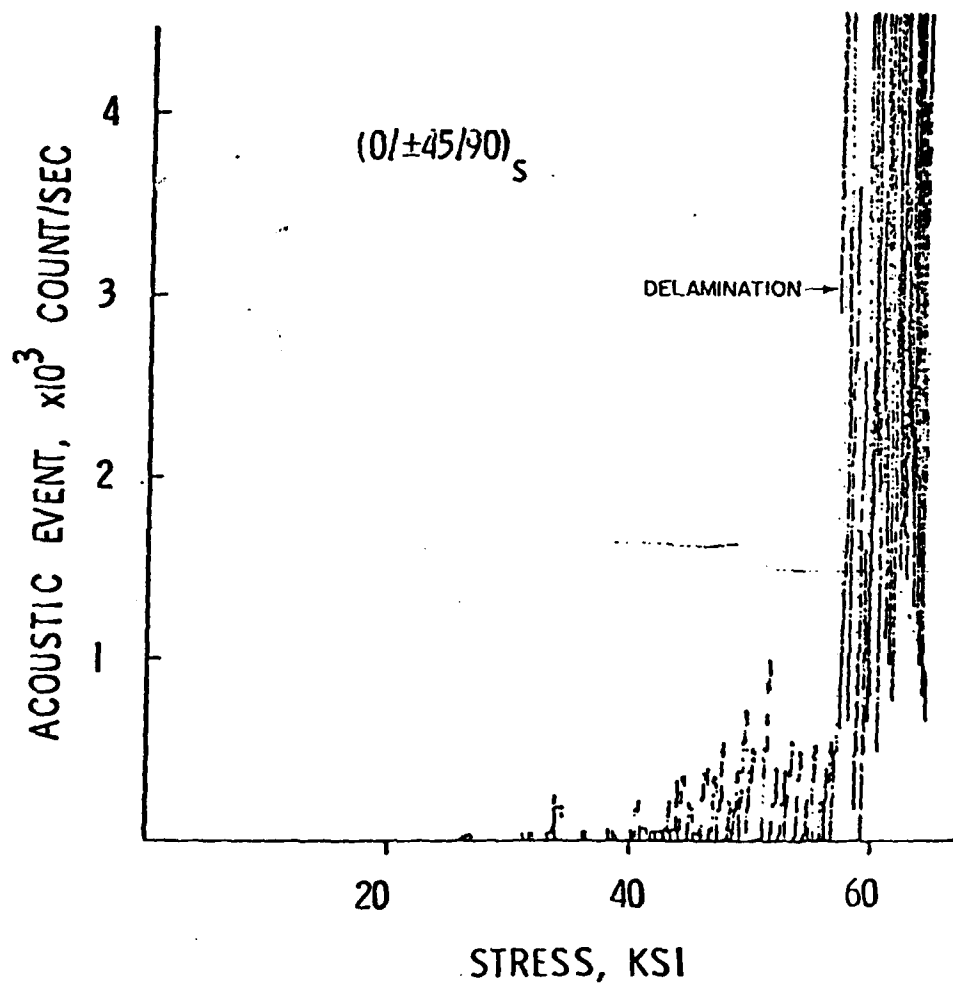


Figure 15. Acoustic Emission vs. Applied Stress Which Indicates the Onset of Delamination.

unaxial compression. Figures 16 to 21 show the comparison between prediction and experiment. The solid line and dotted line indicate the predicted value obtained from the average stress criterion and maximum point stress criterion, respectively. Experimental results are indicated as a circle for the various values of n for each family of the laminate. Each data point indicates the average of four to seven specimens. The experiment except for the $[0/_{\pm}45/90_6]_s$ laminate, is compared very well with the predicted value using the average stress criterion. The maximum point stress appears to be underestimated in most cases, and fails in accounting for the laminate thickness in the case of $[0_n/_{\pm}45_n/90_n]_s$ of which σ_z at the free-edge is independent of r .

Although the transverse cracks in the first four families of laminates occur prior to delamination under the tension, the influence of these cracks appear to be minimal on the onset of delamination as indicated in Figures 16 to 19. However, there is a large discrepancy between experiment and prediction for the $[0/_{\pm}45/90_6]_s$ laminate as shown in Figure 18.

Typical microphotographs and ultrasonic C-scan pictures of the delamination pattern under static loading for the $(0/_{\pm}45/90_3)_s$ and $(0/_{\pm}45/90_6)_s$ laminates are presented in Figures 22 and 23, respectively. Each figure shows delamination patterns of two progressively increased loadings. The pictures of Figures 22a and 23a were taken at the moment delamination occurred. Photomicrograph and C-scan pictures indicate an edge view (free edge) and a plane view (surface), respectively. The two bold-face lines in the C-scan picture correspond to the boundary region of the intact specimen and the white region represents the delaminated area. It appears that delamination is initiated at the central plane for $n=1, 3$ and at $90/_{\pm}45$ interface for $n=6$. Under static loading, the formation of the delamination in all laminates except for the $[0/_{\pm}45/90_6]_s$ occurs in the following manner. Upon a further increase in applied load after transverse cracking, several delaminations in the form of axial

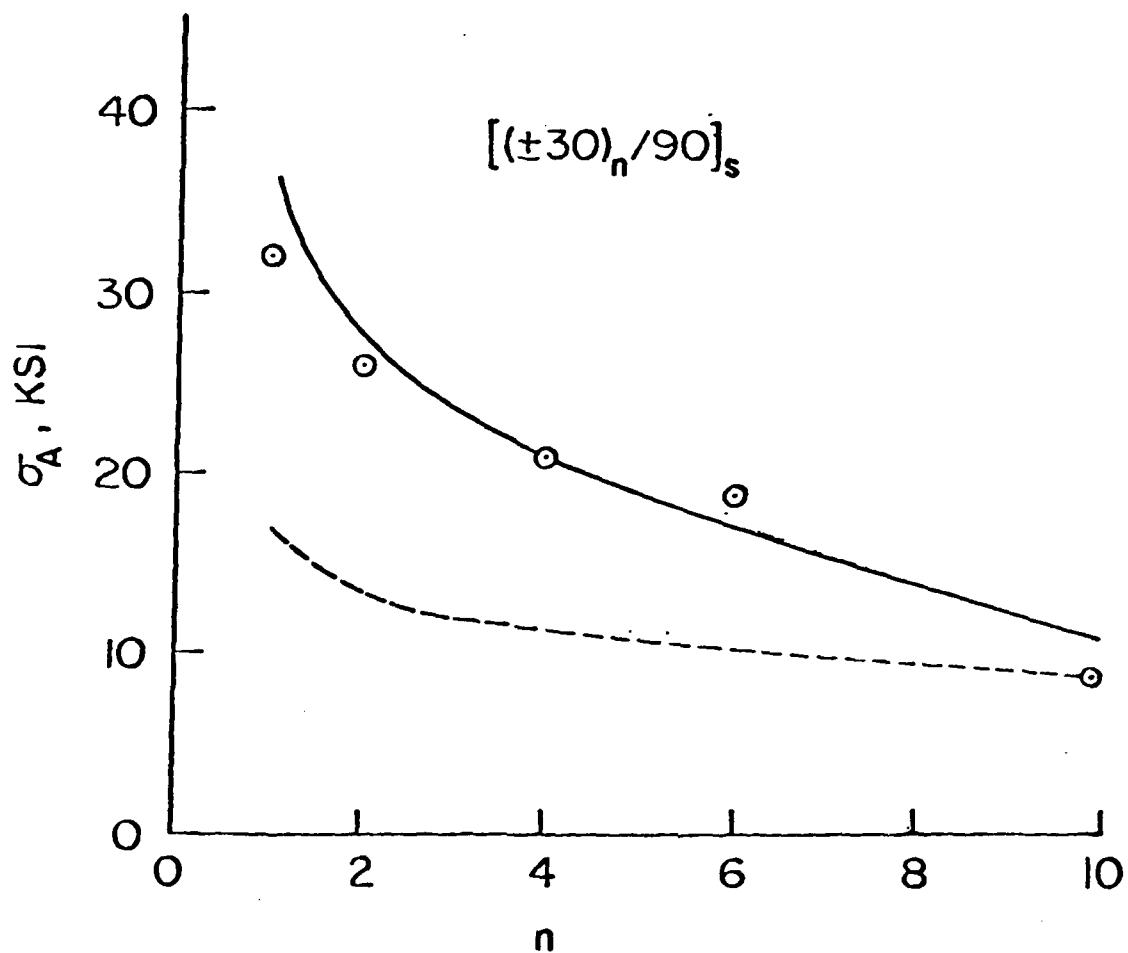


Figure 16. Comparison of Prediction and Experiment for Onset of Delamination.

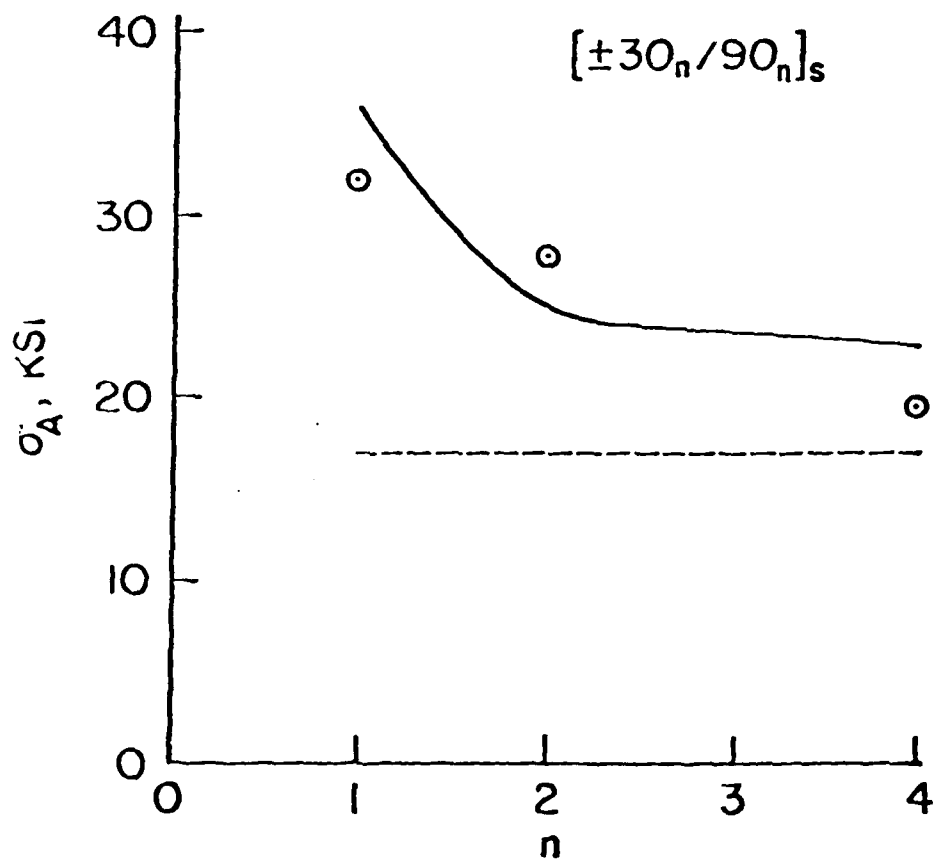


Figure 17. Comparison of Prediction and Experiment for Onset of Delamination.

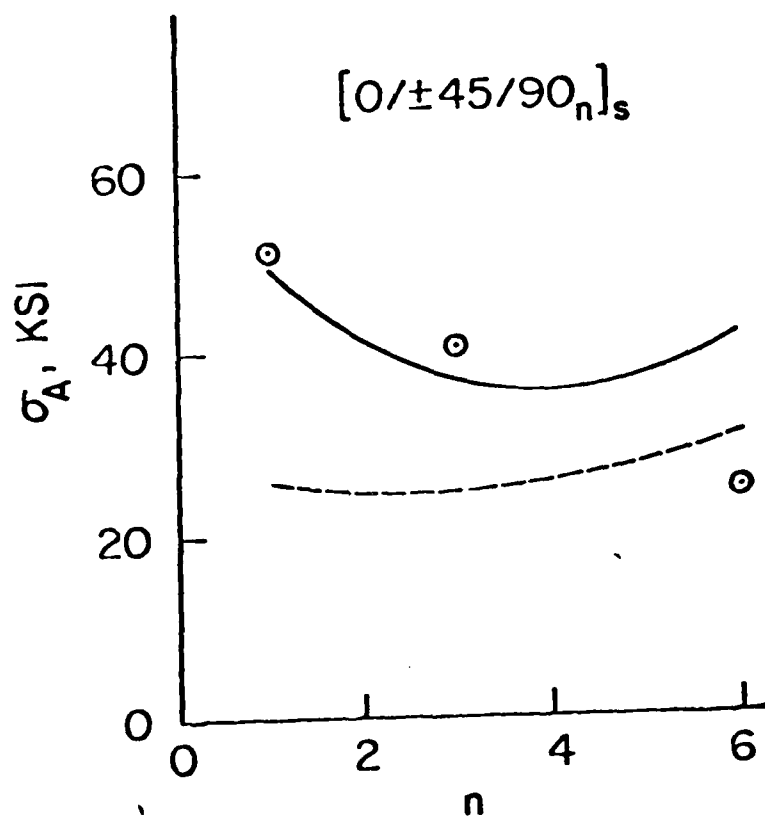


Figure 18. Comparison of Prediction and Experiment for Onset of Delamination.

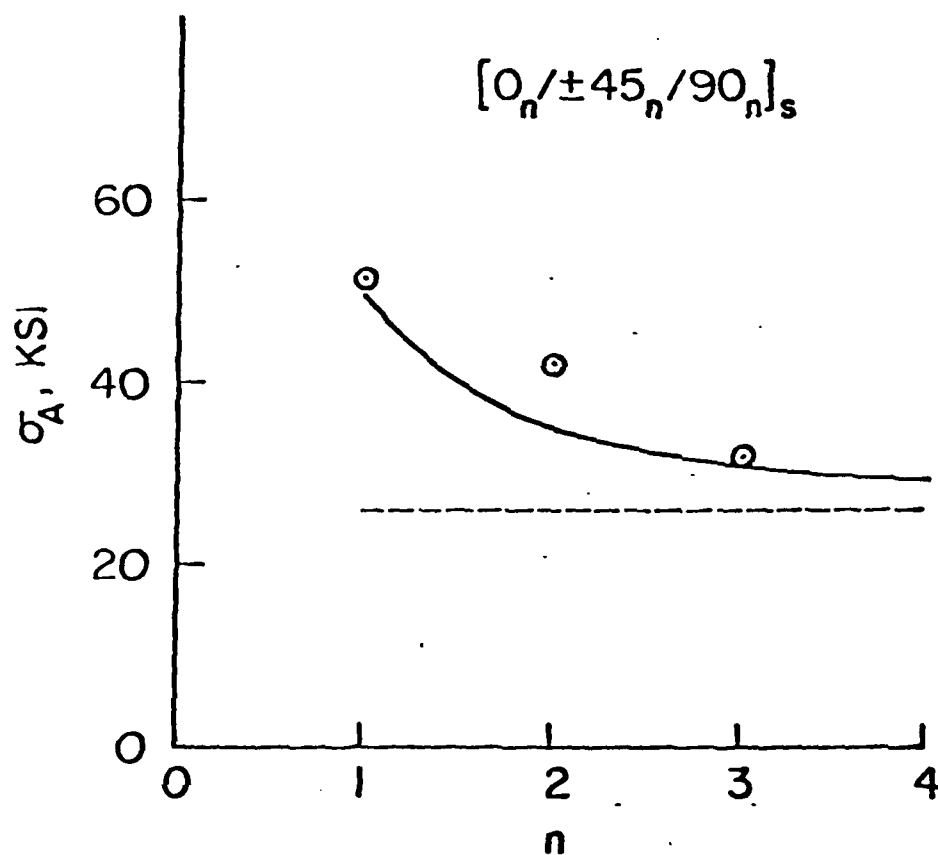


Figure 19. Comparison of Prediction and Experiment for Onset of Delamination.

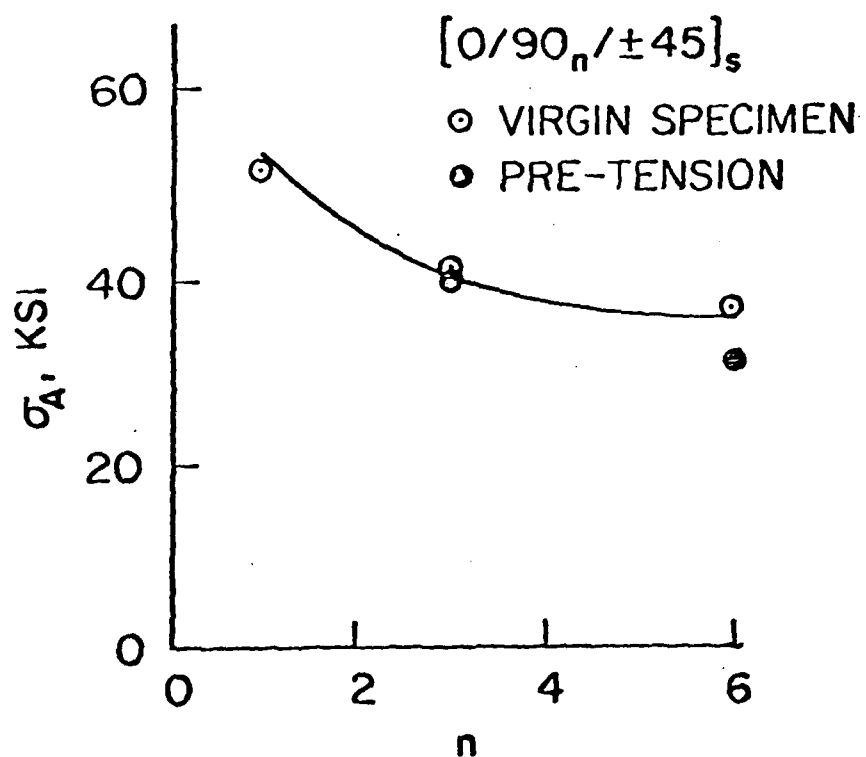


Figure 20. Comparison of Prediction and Experiment for Onset of Delamination.

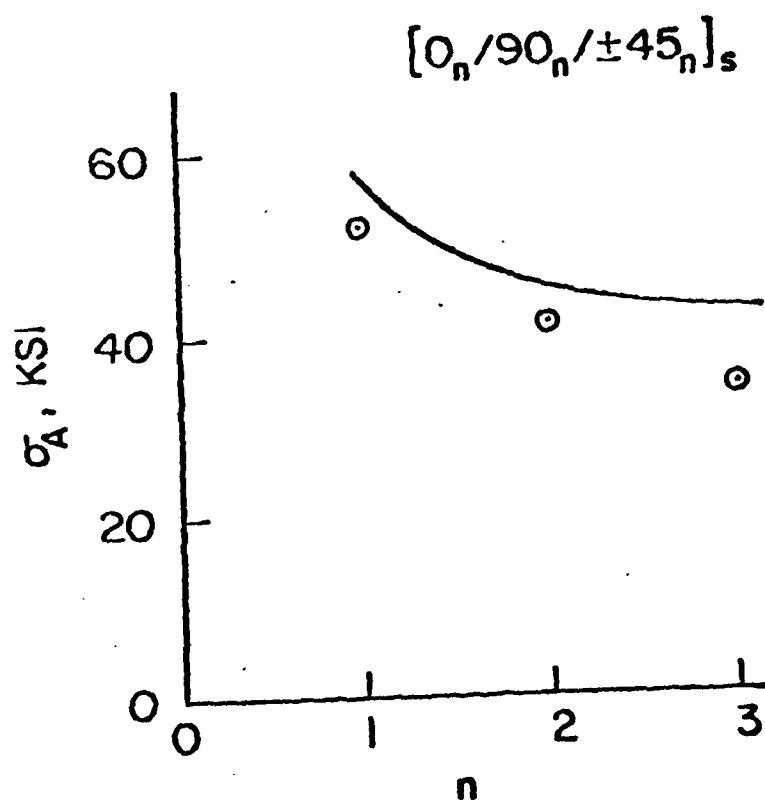
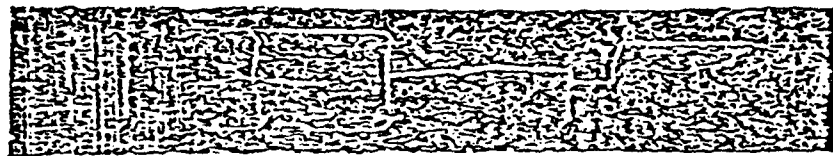
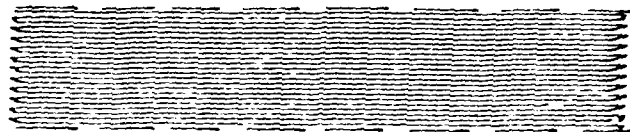


Figure 21. Comparison of Prediction and Experiment for Onset of Delamination.

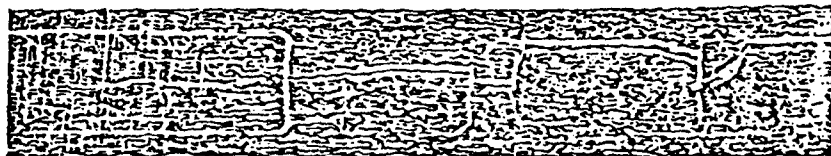


12X

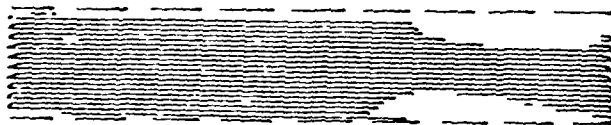


1X

(a) 267 MPa



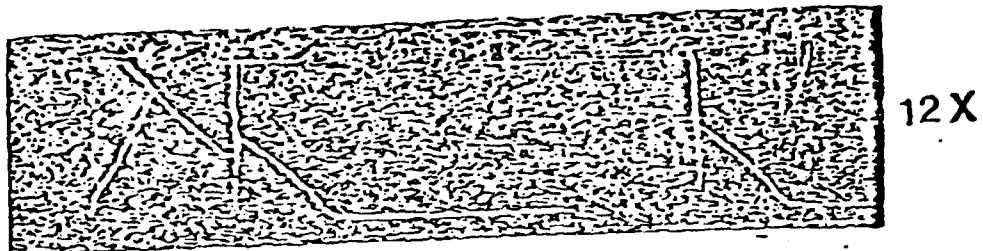
12X



1X

(b) 293 MPa

Figure 22. Photomicrographs and C-Scan Pictures Showing Crack and Delamination Under Static Loading for $(0/+45/90_3)_s$.

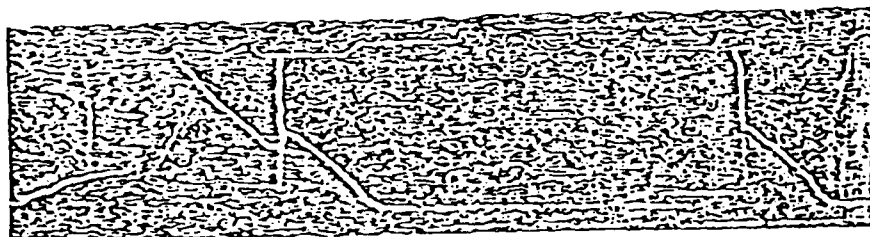


12X



1X

(a) 24.4 ksi



12X



1X

(b) 29.3 ksi

Figure 23. Photomicrographs and C-Scan Pictures Showing Crack and Delamination Under Static Loading for $(0/+45/90)_6$ s.

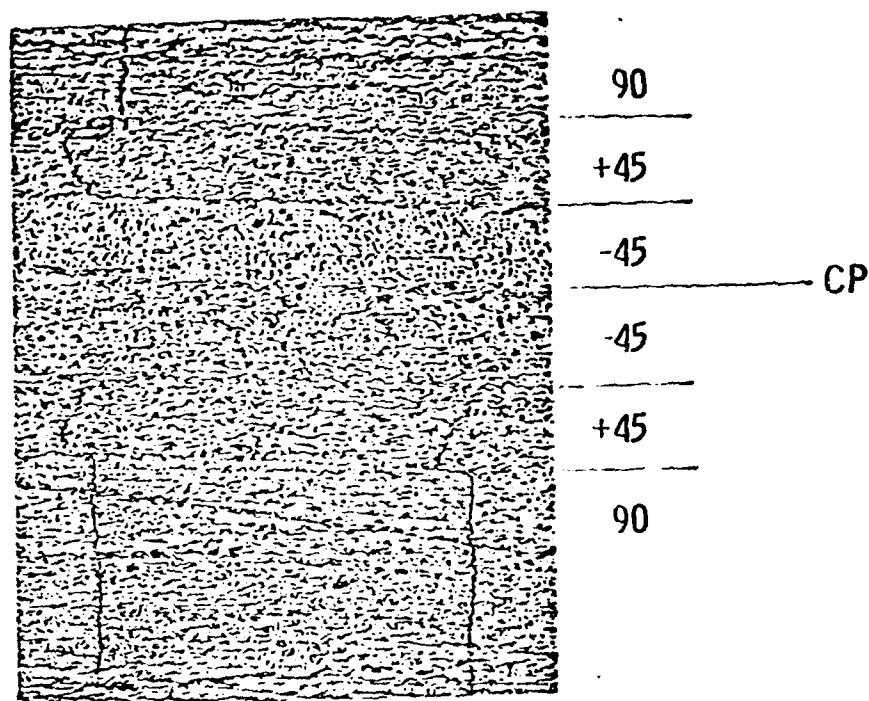
cracks form at or near the midplane. However, the major delamination appears to occur at the midplane as shown in Figure 22a. At this stage, delamination hardly propagates toward the middle of the specimen as shown in the C-scan picture in Figure 22a. As load increases further, the delamination opens up further and either continues to run along the same interface or changes to other interfaces normally at transverse crack. At this time the delamination also propagates rapidly toward the middle of the specimen as shown in the C-scan picture in Figure 22b. The interlaminar tensile stress appears to be responsible for the rapid propagation. Unlike these laminates, in the $(0/+45/90^6)_s$ laminate all the delaminations in the form of axial cracks occur at the tip of the transverse crack at the applied stress below the expected stress, and failure occurs without revealing any appreciable growth of delamination as shown in Figure 23a and b. This premature delamination appears to be mainly influenced by size of transverse crack which occurred prior to delamination. To demonstrate further the size effect of transverse crack, specimens of the $[0/90_3/+45]_s$ and $[0/90_6/+45]_s$ laminates were subjected to tensile fatigue load to form transverse cracks since no transverse crack occurred prior to delamination under uniaxial compression. Figure 24a shows the transverse crack in the $[0/90_3/+45]_s$ laminate after fatigue. This specimen is then tested under compression to observe delamination. Figure 24b shows the microphotograph of delamination occurred under static compression. The major delamination at this time occurred at the interface between $+45/-45$ where transverse cracks are presented. However, the stress level at onset of delamination is virtually unchanged in the case of $[0/90_3/+45]_s$ and is slightly decreased in the case of $[0/90_6/+45]_s$ as indicated with a solid circle in Figure 20. These are an average of four specimens of each laminate.

The result indicates that the methodology used in this work is very promising to predict the stress level onset of delamination. The influence of the size of transverse crack appears to be minimal on the onset of delamination when the crack size is small.

(a) T-T FATIGUE

$N = 10,000$ CYCLES

$S_{max} = 35$ KSI



(b) STATIC COMPRESSION

$\sigma_D = 39.6$ KSI

(σ_D delamination
threshold stress)

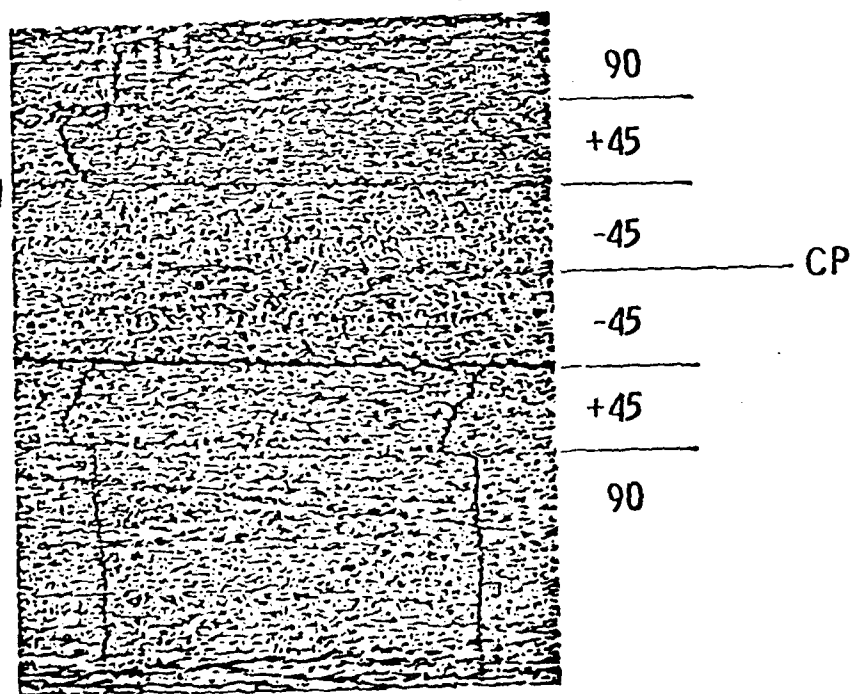


Figure 24. Photomicrographs Showing Transverse Crack and Delamination for the $(0/90_3/+45)_s$.

4. FATIGUE STUDY

An extensive fatigue test program has been initiated to study the fatigue damage processes and to generate fatigue life data under various fatigue loads. The fatigue life data will be compared with the analytical life prediction model which accounts for the competing failure modes developed in Reference 9. The material system used in this program was AS/3501 graphite/epoxy supplied by Fiberite Corp. Three types of laminates $[\pm 45/90_2]_s$, $[\pm 45/0/90]_s$, and $[0/45/90/-45]_{2s}$ were fabricated in an autoclave. Three types of fatigue loads considered in this program are tension-tension (T-T), compression-compression (C-C), and tension-compression (T-C). All specimens are straight-sided coupon, 3/4" wide. The specimen length in gauge section was 5" for T-T fatigue and 2.5" for C-C and T-C fatigue. All specimens for C-C and T-C fatigue were tested using a plexi-glass side support device to prevent specimen buckling. A fatigue test was conducted using constant-amplitude sinusoidal load cycles with stress ratio $R=1/10$ (T-T and C-C fatigue) and a frequency 10 hz under a laboratory environment. A number of stress ratios were employed in the T-C fatigue test. Three to five stress levels were considered to obtain an S-N curve in the T-T and C-C fatigue test. Fatigue test is terminated for those specimens which did not fail at 5×10^6 cycle for the $[\pm 45/90_2]_s$ and 1×10^6 cycle for the $[0/45/90/-45]_{2s}$.

The $[\pm 45/0/90]_s$ laminate exhibits an extensive delamination in both static and fatigue load due to the presence of tensile interlaminar normal stress at free-edge region under applied uniaxial tension. The effect of delamination on fatigue life has been investigated using the $[\pm 45/0/90]_s$ laminate. The freeedges of a half of the $[\pm 45/0/90]_s$ specimens were reinforced with fiber-glass shim cloth to prevent delamination during static and fatigue test.

A microscope and an x-ray were employed to examine the damage related to matrix cracking and delamination developed in the course of the fatigue cycle. Specimens were initially fatigued

to a predetermined cycle, unloaded and then removed from the loading frame to examine the damage. This procedure was repeated with incremental fatigue cycle until final fatigue failure. The transverse cracks developed in the respective off-axis layer were listed using a microscope, and the delamination was identified using an x-ray.

During the current reporting period, a total of 190 specimens were tested. The data presented in this report are rather incomplete since this test is being continued. All experimental data obtained so far were analyzed using two-parameter Weibull distribution. A data pooling scheme was used to determine a single value of the shape parameter whenever applicable.

Table 46 presents the summary of static test data for all three laminates. The $[\pm 45/90]_s$ and $[0/45/90/-45]_{2s}$ laminates did not show any delamination under both static tension and compression until final failure.

The $[\pm 45/90]_s$ laminate is much stronger in compression than in tension as predicted by failure analysis. In the $[0/45/90/-45]_{2s}$ laminate, the tensile and compressive strengths are practically identical. A considerable scatter is indicated in the tensile strength of the $[\pm 45/0/90]_s$ for both reinforced and unreinforced specimens. The tensile strength was increased by approximately 20% with the reinforcement. This increase appears to be due mainly to eliminating free-edge delamination. The reinforced specimens did not show any delamination in both static and fatigue load. However, the effect of the reinforcement on the occurrence of transverse crack, such as the first ply failure, stress, and crack density appears to be negligible. In the unreinforced specimens, where fatigue stress is smaller than the stress level at onset of delamination, delamination occurred in the early fatigue cycle and extended rapidly to the middle of the specimen width as the fatigue cycle increased. Table 47 presents the summary of the fatigue data of the $[\pm 45/0/90]_s$ laminate. The fatigue life of the specimen was increased substantially by

TABLE 46
SUMMARY OF STATIC TEST RESULT

Laminate	Type of Loading	Mean Strength, ksi	Weibull Parameters $\hat{\alpha}$ $\hat{\beta}$	No. of Specimens Tested
[+45/90 ₂] _s	Tension	22.70	48 23.23	10
	Compression	40.23	24 41.18	10
[+45/0/90] _s	Tension	86.27	10 91.08	5
	Compression	73.07	16.4 75.11	5
Reinforced	Tension	72.25	8.7 76.801	5
Unreinforced	Tension	75.45	18.6 77.89	5
[0/+45/90/-45] _s	Tension	75.45	18.6 77.89	5
	Compression	73.07	16.4 75.11	5

TABLE 47

FATIGUE DATA FOR Gr/Ep [+45/0/90]_s

(a) Unreinforced Free-edges

S_{max} , Ksi	Cycle to Failure			Characteristic Life for Common $\hat{\sigma}_p=1.04$
60	570	10,930	210 120	2,710 3,007
50.8	181,380	83,040	158,040 184,030	107,990 143,139
45	3,148,910	2,144,980	1,384,910 1,076,210	3,124,280 2,182,883

(b) Reinforced Free-edges

S_{max} , Ksi	Cycle to Failure			Characteristic Life for Common $\hat{\sigma}_p=1.04$
60	24,450	47,700	730 1,590	22,090 19,671
50.8	451,420	557,430	134,390 206,640	1,022,760 478,611
45	5×10^6	5×10^6	5×10^6 5×10^6	2,881,220 -

* Indicates runout at the cycle

preventing the free-edge delamination. The S-N relation for the reinforced specimens is compared with that for the unreinforced specimens in Figure 25. The circles are characteristic life obtained by experiment and solid lines are eyeball fitting to the experimental data. The summary of T-T, C-C and T-C fatigue data for the $[\pm 45/90]_2$ laminate is presented in Table 48. The S-N relation of T-T fatigue is compared with that of C-C fatigue in Figure 26. The compressive fatigue strength is considerably greater than the tensile fatigue strength for this laminate as in static strength. Since it is known that the statically stronger specimen has the longer fatigue life, the fatigue stress was normalized with respect to mean static strength to obtain an S-N relation for the normalized fatigue stress. The difference between tension and compression in fatigue strength is reduced remarkably in the normalized S-N curve as shown in Figure 27. Considerable damage in the form of transverse crack was observed in T-T fatigue specimens but no damage was observed in C-C fatigue. This laminate does not exhibit any delamination in both T-T and C-C fatigue. Therefore, the transverse crack appears to be responsible for lower tensile fatigue strength of this laminate which has the matrix dominated failure mode. Table 48c presents the summary of the T-C fatigue data. The data indicates the pronounced effect of mean stress level on the fatigue life. For the identical peak stress in tension and compression, all the specimens reveal tension failure probably due to the lower strength in tension.

Table 49 presents the summary of fatigue data for the $[0/45/90/-45]_2$ laminate. Figure 28 shows the S-N curve of T-T and C-C fatigue. Although the compressive static strength is slightly smaller than the tensile static strength, the compressive fatigue strength is slightly stronger than tensile fatigue strength as shown in Figure 28. The damage incurred during fatigue load was examined using a microscope and x-ray. The x-ray of typical specimens fatigued up to one million cycles are shown in Figure 29 for T-T fatigue and Figure 30 for C-C fatigue. In T-T fatigue specimen, extensive delamination and

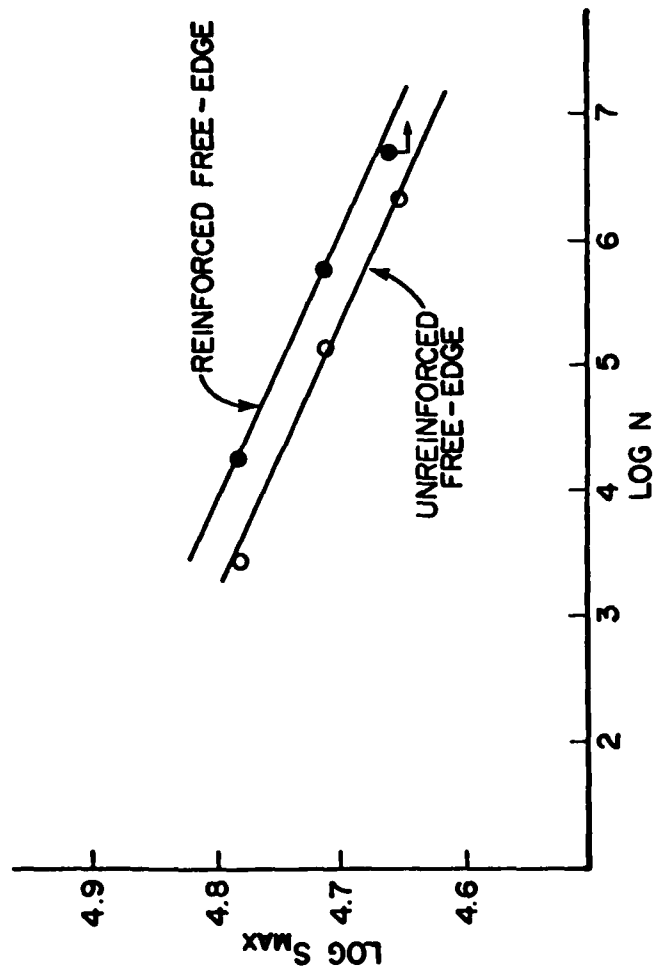


Figure 25. S-N Curve for [+45/0/90]_s.

TABLE 48
FATIGUE DATA FOR Gr/Ep [+45/90₂]

(a) Tension-Tension

S _{max} , Ksi	Cycle to Failure					Characteristic Life for Common $\hat{\alpha}_p = 5.1$
18.4	2,950	1,230	2,460	2,180	2,270	2,436
16.5	9,430	8,250	10,470	7,150	9,410	9,214
13.6	165,370	118,750	107,690	65,110	146,360	35,964
12.5	570,110	1,028,040	754,760	722,420	602,460	10,000
11.0	All five specimens ran out at 5×10^6 cycle					

(b) Compression-Compression

S _{max} , Ksi	Cycles to Failure					Characteristic Life for Common $\hat{\alpha}_p = 1.77$
32.2	8,030	1,230	4,690	1,970	930	4,109
28.00	17,670	16,350	13,170	49,190	33,990	28,665
24.10	455,070	309,140	311,690	324,710	543,750	397,578
22.00	469,890	3,365,760	771,970	1,175,280	934,850	1,615,236
20.00	All five specimens ran out at 5×10^6 cycle					

(c) Tension-Compression

Stress Range, Ksi			Cycles to Failure				Weibull Parameter	
S _{max}	S _{min}						$\hat{\alpha}$	$\hat{\beta}$
12.5	-22	3,410	4,210	2,830(T)	2,900(?)	3,740(T)	7.2	3,644
17.5	-17	600(T)	910(T)	2,720(T)	530(T)		1.5	1,340
7.5	-27	1,430(C)	2,250(T)	3,910(T)	1,090(C)		2.2	2,477
7.5	-22.5	7,880(T)						
10	-10	67,550(T)						
12.5	-12.5	20,340(T)						

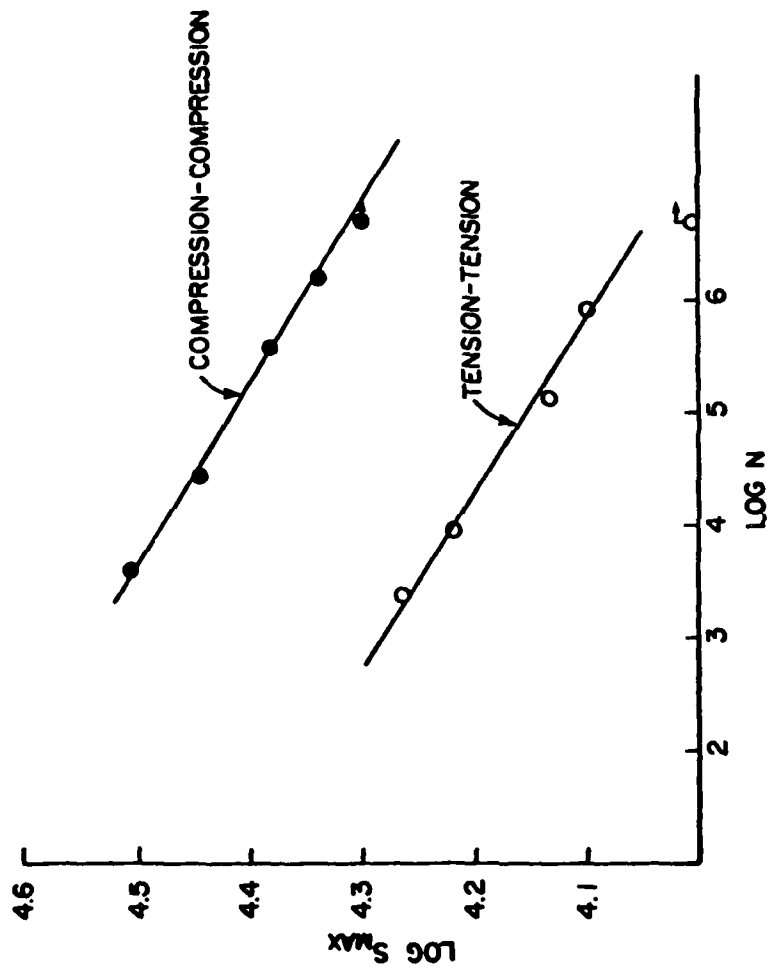


Figure 26. S-N Curve for [+45/90]_s.

AS/3502 Gr/Ep
[+45/90₂]_s

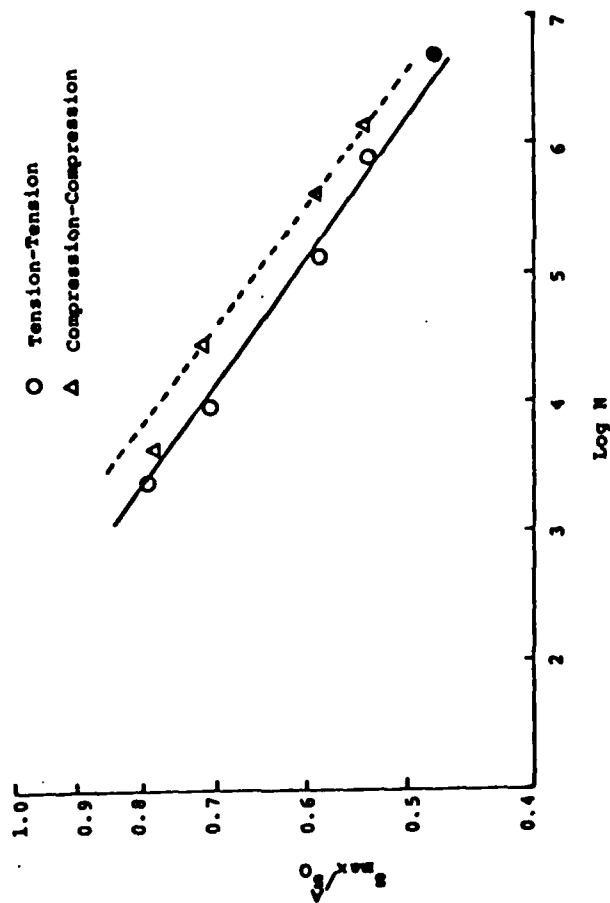


Figure 27. S-N Curve for [+45/90₂]_s.

TABLE 49
FATIGUE DATA FOR Gr/Ep [0/+45/90/-45]_{2s}

(a) Tension-Tension

S _{max} , Ksi	Cycle to Failure				Characteristic Life for Common $\hat{\sigma}_p=2.81$
60	11,760	7,160	13,120	8,390	10,610
53	66,950	204,400	131,550	198,670	167,726
50	642,550	660,560	149,910	242,830	516,237
48	186,030	278,470	*1x10 ⁶	*1x10 ⁶	-
45	729,840	*1x10 ⁶	*1x10 ⁶	*1x10 ⁶	-

(b) Compression-Compression

S _{max} , Ksi	Cycle to Failure				Characteristic Life for Common $\hat{\sigma}_p=1.1$
65	150	8,240	6,100	590	3,958
60	75,550	53,330	37,680	44,960	53,064
53	792,580	154,710	112,600	63,340	294,210
50	943,730	214,710	*1x10 ⁶	*1x10 ⁶	-
45	616,380	*1x10 ⁶	*1x10 ⁶	*1x10 ⁶	-

(c) Tension-Compression

Stress Range S _{max} , S _{min}	Cycle to Failure				-
27.5 -27.5	873,670	484,930	*1x10 ⁶	*1x10 ⁶	-
15 -40	663,760	387,640	740,720		-
10 -45	182,640	121,750			-
40 -15	769,150	820,990	*1x10 ⁶		
45 -10	268,900	638,050			

*Indicates runout at the cycle

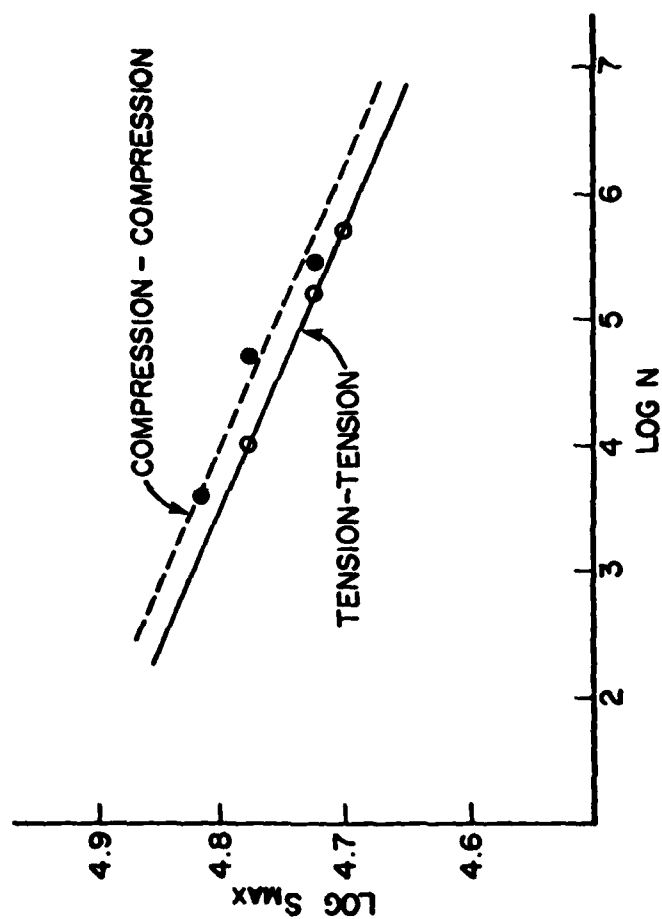







Figure 28. S-N Curve for [0/+45/90/-45]_{2s}.

	Specimen ID
	2-21-19
	2-21-20

(a) $S_R = .48$ to 48 ksi

	2-21-6
	2-21-8
	2-21-7
	2-21-26

(b) $S_R = .45$ to 45 ksi

Figure 29. X-ray Showing the Damage Incurred at One Million Cycles Under Tension-Tension Fatigue for $[0/45/90/-45]_{2s}$ Laminate.

Specimen
ID

2-21-71

2-21-76

(a) $S_R = -.50$ to -50 Ksi

2-21-77

2-21-78

2-21-76

(b) $S_R = -.45$ to -50 Ksi

2-21-80

2-21-81

2-21-89

2-21-82



(c) $S_R = -.40$ to -40 Ksi

Figure 30. X-ray Showing the Damage Incurred at One Million Cycles Under Compression-Compression Fatigue for $[0/45/0/-45]_s$ Laminates.

and transverse cracks were developed as shown in Figure 29. However, in the C-C fatigue specimen no damage was observed except for the case of 50 Ksi of fatigue stress. A limited local delamination near the endtab area occurred in the case of 50 Ksi as seen in Figure 30a. In this specimen no transverse crack was found. In the T-C fatigue specimen, extensive transverse crack occurred and delamination is rather moderate as shown in Figure 31. Tensile load is mainly responsible for all the damage in T-C fatigue.

All survived specimens were subjected to residual strength test and the result is summarized in Table 50. All the specimens fatigued under tension-tension load show the substantial decrease in both tensile and compressive strength. The reduction of static strength in tension and compression is approximately 23% in tension and 60% in compression. A considerable specimen buckling occurred in the compressive residual strength test because of the extensive delamination, and resulted in very low compressive residual strength. On the other hand, all the survived specimens in compression-compression fatigue load show a slight increase in both tensile and compressive residual strength. In tension-compression fatigue load, the reduction of tensile strength appears too insignificant, but the reduction in compressive strength is appreciable. The limited local delamination appears to be responsible for the lower compressive residual strength. The damage incurred during the tension-compression fatigue with various stress ratios is being reduced.

A series of fatigue tests was conducted to determine the effect of fatigue load frequency on fatigue life under tension-tension cyclic load. The material system used in this test was T300/5208 graphite/epoxy with $[0/90/+45]_s$ orientation. Four frequencies considered are one, five, ten and 20 Hz at 60 Ksi of maximum fatigue stress level. A tensile coupon 3/4 in. wide was tested until final failure. A thermocouple was instrumented on the surface of two specimens for each frequency. The temperature rise during the entire fatigue life was continuously

	Specimen ID
	2-21-39
	2-21-38

$S_R = 27.5 \text{ to } -27.5$

Figure 31. X-ray Showing the Damage Incurred at One Million Cycles Under Tension-Compression Fatigue for $[0/45/90/-45]_{2s}$ Laminates.

TABLE 50
SUMMARY OF RESIDUAL STRENGTH DATA
FOR [0/45/90/-45]_{2s} AT 1x10⁶ CYCLE

Fatigue Load	Specimen ID	S _{max} , Ksi	R	Residual Strength, Ksi Tension Compression	Modulus 10 ⁶ psi
Tension-Tension	2-21-19	48	0.1	51.21	4.22
	2-21-20	48	0.1	-29.03	4.97
	2-21-6	45	0.1	63.96	
	2-21-8	45	0.1	59.42	
	2-21-7	45	0.1	-32.93	
	2-21-26	45	0.1	-27.55	
Compression - Compression	2-21-71	-50	10	76.46	
	2-21-76	-50	10	-80.76	
	2-21-77	-45	10	87.59	
	2-21-78	-45	10	84.41	8.01
	2-21-76	-45	10	-83.55	
	2-21-80	-40	10	83.72	
Tension - Compression	2-21-81	-40	10	86.10	
	2-21-79	-40	10	-84.73	
	2-21-82	-40	10	-81.07	
	2-21-39	27.5	-1	73.33	6.55
	2-21-38	27.5	-1	-62.11	6.26

monitored using a strip chart recorder. A total of 62 specimens with 15 to 16 replicas were tested during the current reporting period. Weibull parameters were estimated for each frequency by using the maximum likelihood method, and the common shape parameter was obtained by pooling all the data. Figure 32 shows the distribution of fatigue data with common shape parameters. The various symbols represent the experimental data for each frequency. Table 51 presents a summary of the test results. The frequency effect on fatigue life appears to be insignificant for this laminate in the frequency range considered. Figure 33 shows the temperature rise with cycles endured. The temperature rise is substantial in 10 and 20 Hz compared with one and five Hz.

This test will be extended to the laminate having a notch and matrix dominated failure mode. The frequency of zero, one Hz will be included in this test.

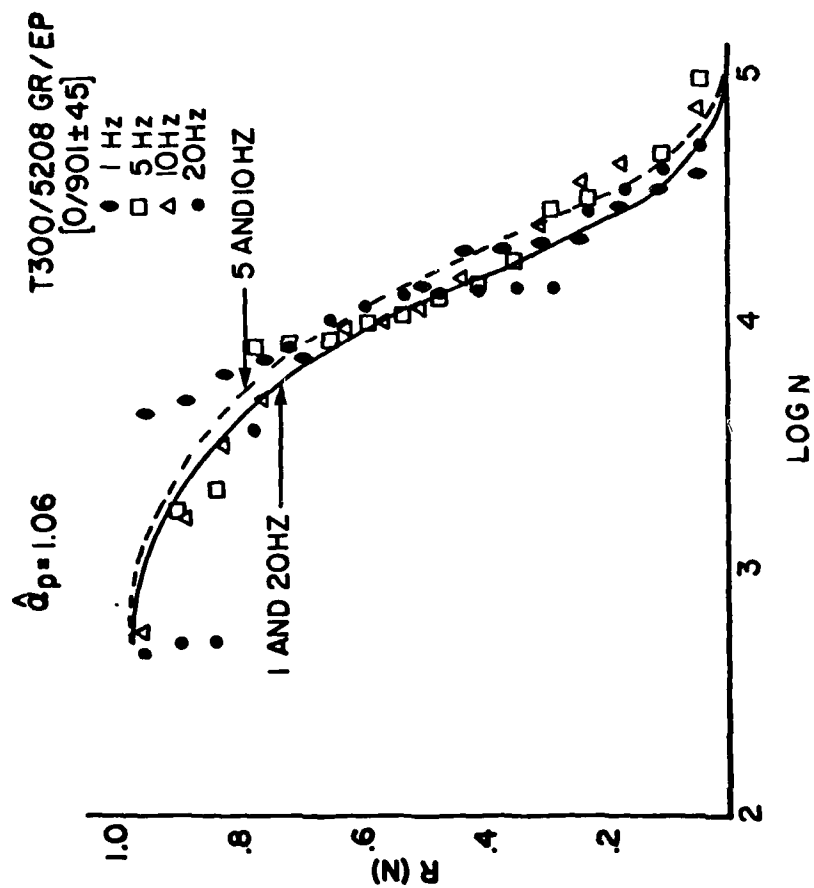


Figure 32. Weibull Distribution of Fatigue Data.

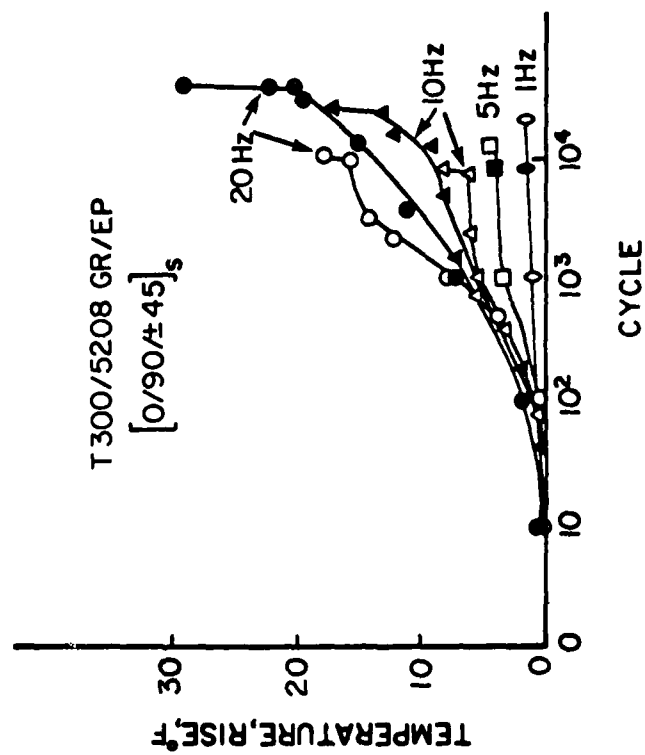


Figure 33. Temperature Rise as Function of Frequency.

TABLE 51
SUMMARY OF FATIGUE RESULTS

T300/5208 Gr/Ep [0/90/+45]_s $S_{\max} = 60 \text{ ksi}$

Frequency	No. of Specimen	Weibull $\hat{\alpha}$	Weibull $\hat{\beta}$	Pooled $\hat{\sigma}_p = 1.06$
1	15	1.59	18,800	17,010
5	16	0.90	18,741	21,312
10	15	0.98	20,474	21,176
20	16	0.95	16,677	17,408

Static Strength = 84 ksi

$$S_{\max}/S_o \approx .71$$

REFERENCES

1. Improved Materials for Composites and Adhesives, Final Report, AFWAL-TR-81-4154.
2. Hercules, Inc., Wilmington, Delaware.
3. Ashland Chemical Co., Columbus, Ohio 43216.
4. G.E. Hammer and L.T. Drzal, App. Surf. Sci., 4, 340, 1980.
5. Improved Materials for Composites and Adhesive Joints, Quarterly Progress Reports UDR-NM-QPR-81-29, UDR-NM-QPR-82-05, and UDR-NM-QPR-82-10.
6. Tecam Instruments, Techne (Princeton) Limited, Princeton, N.J.
7. J.W. Hitchon and D.C. Phillips, Fiber Science and Technology, 12, 217, 1979.
8. L.T. Drzal, et. al., Proc. 35th Reinforced Plastics/Composites Conf. Paper 20C, 1980.
9. N.J. Pagano, Stress Fields in Composite Laminates, AFML-TR-77-114, Wright-Patterson AFB, August 1977. Also, Int. J. Solids Structures 14, 385 (1978).
10. M.E. Gurtin, Continuum Theory of Fracture, Mechanics of Composites Review, Bergamo Center, Dayton, Ohio, 83(1977).
11. A.S.D. Wang and F.W. Crossman, Some New Results on Edge Effect in Symmetric Composite Laminates. J. Composite Mat. 11, 92(1977).
12. E.L. Stanton, L.M. Crain and T.F. Neu, A Parametric Cubic Modelling System for General Solids of Composite Material. Int. J. Num. Meth. Engg. 11, 653(1977).
13. N.J. Pagano, Exact Moduli of Anisotropic Laminates. In Composite Materials, Mechanics of Composite Materials (Edited by G.P. Sendeckyj, Vol. 2, pp. 23-44. Academic Press, New York (1974).
14. J.M. Whitney and C.T. Sun, A Higher Order Theory for Extensional Motion of Laminated Composites. J. Sound and Vibration, 30, 85(1973).
15. N.J. Pagano, On the Calculation of Interlaminar Normal Stress in Composite Laminate, J. Composite Mat. 8, 65(1974).

REFERENCES (CONTINUED)

16. N.J. Solomon, An Assessment of the Interlaminar Stress Problem in Laminated Composites. J. Composite Matl. Supplement 14, 177(1980).
17. R.L. Spilker and T.C.T. Ting, Stress Analysis of Composites. Army Materials and Mechanics Research Center, Watertown, Mass. Technical Report # AMMRC-TR-81-5(1981).
18. I.S. Raju, J.D. Whitcomb and J.G. Goree, A New Look at Numerical Analyses of Free Edge Stresses in Composite Laminates. NASA Tech. Paper 1751 (1981).
19. N.N. Blumberg and V.P. Tamuzh, Edge Effects and Stress Concentrations in Multilaminate Composite Plates. Mechanics of Composite Materials, 298-307(1980). Translated from Russian JI. Mekh. Kompositn. Mater. 3, 424(1980).
20. V.V. Partsevskii, Approximate Analysis of Mechanisms of Fracture of Laminated Composites at a Free Edge. Mechanics of Composite Materials, 179-185(1980). Translation of Russian JI. Mekh. Kompositn. Mater. 2, 246(1980).
21. N.J. Pagano and R.B. Pipes, Some Observations on the Interlaminar Strength of Composite Laminates. Int. Mech. Sci. 15, 679(1973).
22. S.R. Soni and N.J. Pagano, Global-Local Laminate Variational Model, AFWAL-TR-82-4028.
23. R.Y. Kim and S.R. Soni, Initiation of Delamination of Composite Laminates, 1982 SETA/JSME Joint Conference on Experimental Mechanics, Oahu-Maui, Hawaii, May 23-28, 1982.
24. S.R. Soni, Stress and Strength Analysis of Composite Laminates at Delamination, International Conference on Composite Materials-IV, Tokyo, Japan, Oct. 25-28, 1982.
25. S.R. Soni and N.J. Pagano, Elastic Response of Composite Laminates, Proceedings of IUTAM Symposium on Mechanics of Composite Materials, Blacksburg, Virginia, August 16-19, 1982.
26. M. Knight, The Determination of Interlaminar Moduli of Graphite/Epoxy Composites, Mechanics of Composite Review, AFWAL/Materials Laboratory, Dayton, Ohio, Oct. 1981.
27. S.W. Tsai, Mechanics of Composite Materials, Part II-Theoretical Aspects, AFML-TR-66-149 Part II, 1966.

REFERENCES (CONCLUDED)

28. R.J. Nuismer and J.M. Whitney, Uniaxial Failure of Composite Laminates Containing Stress Concentrations, ASTM STP 593, 1974.
29. J.M. Whitney, A Residual Strength Degradation Model for Competing Failure Modes, Symposium on Long-Term Behavior of Composites, ASTM, Williamsburg, Va, March 1982.

APPENDIX A
PUBLICATIONS AND PRESENTATIONS

PUBLICATIONS AND PRESENTATIONS

The following presentations and publications cover work carried out under this contract. They were either prepared or appeared publicly during this reporting period.

PUBLICATIONS

1. M. Rich, P. Lloyd, and L. Drzal, "The Effect of Adhesion on the Interfacial Fracture Mode in Graphite Fiber-Epoxy Composites," Proceedings of the 5th Annual Adhesion Society Conference, Mobile, Alabama, February 1982.
2. R. Kim, "In-Plane Tensile Strength of Multidirectional Composite Laminates," UDR-TR-81-84, October 1981.
3. M. Rich, L. Drzal, and P. Lloyd, "Interphase Effects on Fiber-Matrix Adhesion," Polymer Preprints, American Chemical Society 22, 2 (1981).
4. S. Soni and R. Kim, "Stress and Failure Analysis of An Adhesively Bonded Scarf Joint - Failure Prevention and Reliability - 1981," The American Society of Mechanical Engineers (1981).

PRESENTATIONS

5. R. Kim and S. Soni, "Initiation of Delamination of Composite Laminates," Society of Stress Analysis Spring Meeting, Honolulu, Hawaii, May 1982.
6. R. Kim, "Matrix Damage in Composite Laminates, Eleventh Southeastern Conference on Theoretical and Applied Mechanics, Huntsville, Alabama, April 1982.
7. R. Kim, "Moisture Absorption and Swelling of Composite," University of Florida, Gainesville, Florida, April 1982.
8. J. Hartness, "Thermoplastic Polyester Matrix Composites," 11th National SAMPE Technical Conference, Mt. Pocono, Pennsylvania, October 1981.
9. R. Kim, "A Technique to Prevent Delamination," Mechanics of Composite Review, Dayton, Ohio, October 1981.
10. R. Kim and S. Soni, "Stress and Failure Analysis of Adhesively Bonded Scarf Joint," 1981 Failure Prevention and Reliability Conference, Hartford, Connecticut, September 1981.

PRESENTATIONS (CONCLUDED)

11. S. Soni, "Stress and Strength Analysis of Bolted Joints in Composite Laminates," International Conference on Composite Structures, Paisley College of Technology, Paisley, Scotland, September 1981.

